

DOKUZ EYLÜL UNIVERSITY
GRADUATE SCHOOL OF NATURAL AND APPLIED
SCIENCES

ANALYSIS OF BISTABILITY BEHAVIOUR OF
LAC OPERON BY USING SYSTEMS THEORY

by
Neslihan AVCU

February, 2013
İZMİR

ANALYSIS OF BISTABILITY BEHAVIOUR OF LAC OPERON BY USING SYSTEMS THEORY

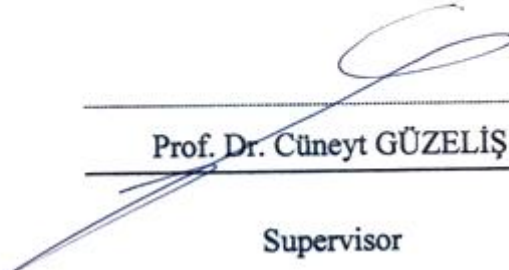
**A Thesis Submitted to the
Graduate School of Natural and Applied Sciences of Dokuz Eylül University
In Partial Fulfillment of the Requirements for
the Degree of Doctor of Philosophy in Electrical & Electronics Engineering,
Electrical & Electronics Engineering Program**

**by
Neslihan AVCU**


**February, 2013
İZMİR**

Ph.D. THESIS EXAMINATION RESULT FORM

We have read the thesis entitled “ANALYSIS OF BISTABILITY BEHAVIOUR OF LAC OPERON BY USING SYSTEMS THEORY” completed by NESLİHAN AVCU under supervision of PROF. DR. CÜNEYT GÜZELİŞ and we certify that in our opinion it is fully adequate, in scope and in quality, as a thesis for the degree of Doctor of Philosophy.


Prof. Dr. Cüneyt GÜZELİŞ

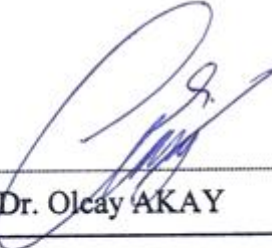
Supervisor


Yrd. Doç.Dr. Güleser KALAYCI DEMİR

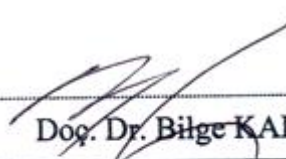
Thesis Committee Member


Doç. Dr. Levent ÇAVAŞ

Thesis Committee Member


Doç. Dr. Olcay AKAY

Examining Committee Member


Doç. Dr. Bilge KARAÇALI

Examining Committee Member


Prof. Dr. Mustafa SABUNCU

Director

Graduate School of Natural and Applied Sciences

ACKNOWLEDGEMENTS

I would like to express my appreciation to my advisor Prof. Dr. Cüneyt GÜZELİŞ for his advices, guidance, and encouragement during my thesis.

I would like to thank Asst. Prof. Dr. Güleser KALAYCI DEMİR and Assoc. Prof. Dr. Levent ÇAVAŞ as the members of my thesis examination committee for their contribution, guidance and support.

I would like to thank my family for their love, support, and persistent confidence in me.

I have been supported by Turkish Scientific and Technological Research Council in the framework of BIDEB scholarship program. The thesis studies have been supported by Turkish Scientific and Technological Research Council and CNRS (FRANCE) as a PIA BOSPHORUS joint research project with grant number 111E082.

Neslihan AVCU

ANALYSIS OF BISTABILITY BEHAVIOUR OF LAC OPERON BY USING SYSTEMS THEORY

ABSTRACT

This thesis presents the original results of theoretical and numerical studies on the analysis of bistable behavior of the most studied gene regulatory network “lac operon” in terms of the model parameters. In the study, two different lac operon models, one that ignores the transacetylase effect while the other takes it into account, are analyzed. The lac operon models assume methyl-1-thio- β -D-galactoside as the artificial inducer. The bistability regions in the parameter space for both of the models are thoroughly determined by newly introduced discriminant and root locus based methods. The developed methods not only identify the ranges of the physical parameters ensuring the bistable behavior of the lac operon models, but also provide a way of tackling the problem of model analysis for this gene regulatory network under parameter uncertainties.

For the lac operon model with no transacetylase effect, the boundedness of the state variables are demonstrated, the parameter values providing the existence of the multiple equilibria, thus the bistable behavior, are determined by the discriminant and root locus based analyses and a local stability analysis of the equilibria is performed. All these studies for the lac operon model with no transacetylase effect are performed in algebraic, graphical and numerical ways all supporting to each other. It is observed along the studies that, as in the lac operon model considering the transacetylase effect, the algebraic and graphical methods may get stuck for models yielding greater than third order polynomial equilibrium equations, and that the developed root locus based method provides an efficient numerical tool for any kind of gene regulatory and metabolic networks model given in a state equation form with rational right-hand side, derived based on enzyme kinetics employing Hill and Michaelis-Menten approaches.

Keywords: Lac operon, bistability, root locus, discriminant, gene regulatory networks, TMG, transacetylase.

SİSTEM KURAMI İLE LAK OPERONUN ÇİFT KARARLI ÇALIŞMASININ İNCELENMESİ

ÖZ

Bu tez, bilimsel yazında en çok incelenen gen düzenleyici ağ olan lak operonun çift kararlı çalışmasının model parametreleri cinsinden kuramsal ve sayısal analizi ile ilgili özgün sonuçlar sunmaktadır. Çalışmada, biri transasetilaz enziminin etkisini göz ardı eden diğeri bu etkiyi göz önüne alan temel olarak iki farklı model analiz edilmiştir. Lak operon modelleri yapay uyarıcı olarak metil-1-tio-β-D-galaktosid'i kabul etmektedir. Her iki model için parametre uzayındaki çift kararlı çalışma bölgeleri, yeni ortaya konan diskriminant ve köklerin geometrik yerine dayalı yöntemler ile tam olarak belirlenmiştir. Geliştirilen yöntemler, sadece lak operon modellerinin çift kararlı çalışmasını garanti eden parametre değerlerini tanılamada değil, en azından bu gen düzenleyici ağ için parametre belirsizliği altında model analizi problemine çözüm getirir.

Transasetilaz etkisinin göz önüne alınmadığı lak operon modeli için, durum değişkenlerinin sınırlılığı gösterilmiş, çoklu denge noktalarının varlığı ve dolayısıyla çift kararlı çalışmayı sağlayan parametre değerleri diskriminant ve köklerin geometrik yerine dayalı incelemelerle belirlenmiş ve denge noktalarının yerel kararlılık incelemesi yapılmıştır. Transasetilaz etkisinin göz önüne alınmadığı lak operon modeli için yapılan incelemeler birbirini destekleyen cebrik, çizgesel ve sayısal yöntemlerle gerçekleştirilmiştir. Çalışmalarda, transasetilaz etkisini göz önüne alan lak operon modelinde olduğu gibi cebrik ve çizgesel yöntemlerin üçten büyük dereceli polinomsal denge denklemleri veren modeller için etkin olmadıkları gözlemlenmiştir. Köklerin geometrik yeri tabanlı yöntemin, Hill ve Michaelis-Menten yaklaşımları uyarınca enzim kinetiğine dayalı olarak türetilen rasyonel sağ yanlı durum denklemleri ile verilen herhangi türden gen düzenleyici veya metabolik ağ modeli için etkin sayısal bir yöntem olduğu görülmüştür.

Anahtar sözcükler: Lak operon, çift kararlılık, köklerin geometrik yeri, diskriminant, gen düzenleyici ağlar, TMG, transasetilaz.

CONTENTS

	Page
Ph.D. THESIS EXAMINATION RESULT FORM	ii
ACKNOWLEDGEMENTS	iii
ABSTRACT	iv
ÖZ	vi
CHAPTER ONE - INTRODUCTION	1
CHAPTER TWO - BIOLOGICAL AND MATHEMATICAL LAC OPERON MODELS	7
2.1 A Biological Lac Operon Model	7
2.2 A Mathematical Lac Operon Model	9
CHAPTER THREE -BOUNDEDNESS OF THE STATE VARIABLES AND A LOCAL STABILITY ANALYSIS OF THE LAC OPERON MODEL.....	12
3.1 Boundedness of the State Variables	12
3.2 Existence of Multiple Equilibria	14
3.3 Local Stability Analysis	17
CHAPTER FOUR - DISCRIMINANT BASED BISTABILITY ANALYSIS OF THE LAC OPERON MODEL WITHOUT TRANSACETYLAASE EFFECT ...	20
CHAPTER FIVE - ROOT LOCUS BASED BISTABILITY ANALYSIS OF THE LAC OPERON MODEL WITHOUT TRANSACETYLAASE EFFECT ...	24
5.1 Root Locus for p Parameter	25

5.2 Root Locus for K Parameter	29
5.3 Root Locus for K_1 Parameter	35
5.4 Integration of One-Parameter Root Locus Analysis Results.....	39
5.5 Interpretation of the Bistability Interval for p in Terms of Physical Model Parameters	43
 CHAPTER SIX - ROOT LOCUS BASED BISTABILITY ANALYSIS OF THE LAC OPERON MODEL WITH TRANSACETYLASE EFFECT	 45
6.1 A Mathematical Model with Transacetylase Effect	45
6.2 Root Locus Analysis	50
6.2.1 Root Locus for K Parameter	50
6.2.2 Root Locus for p Parameter.....	68
6.2.3 Root locus for K_1 Parameter	85
6.3 Interpretation of the Bistability Interval for p with Transacetylase Effect	110
 CHAPTER SEVEN - CONCLUSION	 113
 REFERENCES.....	 115

CHAPTER ONE

INTRODUCTION

The lactose operon, abbreviated as lac operon, of *Escherichia coli* (*E. coli*) which is responsible for controlling the lactose metabolism operates as a bi-stable hysteretic switch under glucose starvation. This bistable behavior of lac operon has been investigated by many researchers in the literature (Novick & Weiner, 1957; Cohn & Horibata, 1959; Yıldırım & Mackey, 2003; van Hoek & Hogeweg, 2006; Özbudak, Thattai, Lim, Shraiman & Van Oudenaarden, 2009; Danchin, 2009). The main aim in this research field aims to explain and then control the behaviors of other more complex biological switches which are assumed to play key roles in the regulatory mechanisms of gene networks (Fell, 1992; de Jong, 2002; de Jong, Geiselman, Hernandez & Page, 2003). This thesis is another step in this direction: It introduces new methods for identifying exact parameter ranges ensuring the bistable behavior of two considered lac operon models. The results obtained in this thesis are expected to be useful to reveal the causes of variations in the presence of the bistable behavior of the lac operon. In other words, the determined bistability ranges can provide a quantitative explanation of the observed behavioral heterogeneity of biological lac operons across the population, across the species and also across the experiments (de Jong, Gouze, Hernandez, Page, Sari & Geiselman, 2004; Batt, Belta & Weiss, 2008).

Lac operon is the gene region which is responsible for the synthesis of the enzymes to metabolize lactose as energy source under glucose starvation (Novick & Weiner, 1957; Özbudak et al., 2009). Lac operon consists of three structural genes; namely, *LacZ*, *LacY*, and *LacA*. *LacZ*, *LacY*, and *LacA* gene produces, respectively, permease, β -galactosidase and transacetylase enzyme. The first one, permease, provides the transportation of external lactose into the cell through the cell membrane. The second one, β -galactosidase, is responsible for the conversion of the internal lactose to the allolactose while the third one, transacetylase, is involved in the sugar metabolism and acetylation reaction. The regulatory gene *LacI*, controls the operation mode of the lac operon: The repressor protein LacI prevents the expression

of gene products by binding to the promotor part of the lac operon when the glucose is present, so the lactose is not used as a carbon and energy source (Jacob, Perrin, Sanchez & Monod; 1960, Novick & Weiner, 1957).

The small amounts of permease and β -galactosidase enzymes are always available at the cell because of the basal activity due to the life period of gene products. These two enzymes at the basal levels provide the transport of the lactose from medium into the cell and the conversion of the internal lactose to the allolactose in the absence of glucose and the existence of lactose in the intracellular medium. The allolactose binds to the LacI repressor protein and causes a conformational change in the repressor, inhibiting the repressor by dissociating it from the promoter region. Then, the RNA polymerase enzyme starts the transcription of mRNA for inducing the three structural genes. By the explained process, the permease and the β -galactosidase concentrations increase rapidly from the basal levels to much higher levels, elevating the concentrations of the internal lactose and allolactose. This mutual amplification of the allolactose and mRNA concentration implies a positive feedback in the lactose metabolism. The positive feedback is known to be a source of unstable dynamics in general. Indeed, the mRNA concentration is bounded from below and above respectively by the basal and saturation activities, preventing unstable dynamics and yielding bounded trajectories settling down to one of two stable equilibria if not started at the third equilibrium which is unstable. One of the stable equilibrium is at a low level concentration corresponding to the uninduced state for lac operon and the other is at a high level concentration corresponding to the induced state. The coexistence of these induced and uninduced stable states which has been observed in the experimental studies provides a bistable behavior for lac operon (Jacob et al., 1960).

In experimental studies, it is generally preferred to use lactose analogs such as methyl-1-thio- β -D-galactoside (TMG) and isopropyl β -D-1-thiogalactopyranoside (IPTG) instead of natural inducer lactose (van Hoek & Hogeweg, 2006; Özbudak et al., 2004). These artificial inducers are not metabolized and do not interact with β -galactosidase enzyme. Therefore, the β -galactosidase enzyme concentration becomes

an irrelevant variable in the response of lac operon to artificial inducers. However, similar to the allolactose, the artificial inducers inhibit the LacI repressor, leading to the transcription of the mRNA and consequently to the production of permease at higher levels of concentrations. These features make the artificial inducers efficient means for experimental studies on the bistable dynamics of lac operon. In this thesis, lac operon models which assume TMG as the artificial inducer are studied only due to the availability of the related literature reporting the real measurement values of the physical parameters such as reaction and degradation rates (Özbudak et al., 2004; Yagil & Yagil, 1971).

Lac operon is the most studied gene regulatory mechanism in *E. coli* since its discovery by Novick & Weiner (1957). Discovery of the lactose regulation system of the *E. coli* has not only provided the understanding of gene regulation at glucose starvation in the existence of lactose but also has become a milestone for other gene regulatory mechanisms in other organisms. In other words, understanding of the behavior of lac operon as a biological switch is important as much to understand further complicated gene regulatory networks in higher organisms and also some metabolic disorders such as cancer (Murray, 2002; Kitano, 2004; Kitano, 2007). Therefore, many efforts have been attempted to analyze the bistable behavior of lac operon models. Wong et al. (1997) constructed a general mathematical model including the catabolite repression and inducer exclusion on the lac operon mechanism. The results of this study confirm the effect of the changes of the external glucose level on the lactose transport and cyclic AMP level. By parameter sensitivity analysis, the transformation process by β -galactosidase and the glucose concentration level that have effect on catabolite repression and inducer exclusion are defined as key parameters in lac operon. Yildirim & Mackey (2003) developed a mathematical model based on ordinary differential equations (ODEs) to explain the bi-directional transport of lactose through cell membrane via permease, conversion of lactose to glucose and galactose by β -galactosidase, inhibition of lac repressor by allolactose and synthesis of mRNA to produce gene products of lac operon. In contrast to the estimation of the model parameter from the results of three different experiments, the mathematical model shows the bistable behavior for realistic values of the external lactose and the bacterial growth rate. This model was simplified in another study by

Yıldırım et al. (2004) by assuming the permease concentration as constant. The authors investigated whether the β -galactosidase regulatory pathway is the most important component for the bistable behavior or not. Santillan & Mackey (2004) proposed a mathematical model which includes catabolite repression, inducer exclusion, and time delays associated to transcription and translation. The special attention was paid in this model to the effect of external glucose and inducer exclusion mechanisms on the bistability dynamics. van Hoek & Hogeweg (2006) studied the bistability of the lac operon induced with lactose and also with an artificial inducer in another case. According to the theoretical and also numerical results of van Hoek & Hogeweg (2006), although the bistability could be observed for artificial inducers, it was not easily observed in the case of lactose in their model. Santillan et al. (2007) presented a mathematical model for the utilization of lactose versus external glucose. In their study, bistability was demonstrated as an important factor in consumption of lactose and glucose efficiently by the cell. In another study of Santillan & Mackey (2008), cooperative interaction between Catabolite Activator Protein (CAP) molecule and operator 3 was added to their previously developed model (Santillan et al., 2007). Effect of growth rate was also studied in the new version of the model. Özbudak et al. (2004) presented the phase diagram of the bistability observed in lac operon dependent on sugar uptake and transcriptional regulation. They argued that this phase diagram could be used as a sensitive probe of molecular interactions. Moreover, they used green fluorescent proteins to show the bistability behavior of the lac operon for the first time *in vivo*.

In the literature, the behavior of the lac operon is generally modeled by using ordinary differential equations, ODEs, derived from enzyme kinetics (Özbudak et al., 2004; Yıldırım et al., 2004; van Hoek & Hogeweg, 2006). Besides, the delay-time ODE systems and stochastic models are also presented in the literature (Julius, Halasz, Sakar, Harvey & Pappas, 2008). In the deterministic models, the reaction rates are expressed as the time derivatives of molecule concentrations. The resulting systems of ordinary differential equations defining the lac operon become nonlinear, more precisely rational functions of molecule concentrations when Michealis-Menten and/or Hill approaches are used to model enzyme kinetics (Özbudak et al.,

2004; Yıldırım et al., 2004; van Hoek & Hogeweg, 2006). Although they are nonlinear, ODE models are more efficient for numerical and also theoretical analyses. The stochastic models which are introduced for low molecule concentrations, are derived usually either by choosing reaction rates as random variables in terms of the numbers of molecules or by introducing a noise term to the ODE models (Julius et al., 2008). The stochastic models suffer from high computational cost however they can be preferred especially for modeling the spontaneous transitions between the induced and uninduced states.

Although many efforts have been attempted to analyze the bistability behavior of lac operon, the ranges of the parameters originated from enzyme kinetics ensuring the bistability are not completely determined yet and the reasons for the variations in the appearance of bistability across different inducer, i.e. lactose, TMG, IPTG etc., across the population of *E. coli* and across different experimental settings (Batt, Ropers, de Jong, Geiselmann, Mateescu, Page & Schneider, 2005; Ropers, de Jong, Page, Schneider & Geiselmann, 2006; Batt, Belta & Weiss, 2008; Avcu, Demir, Pekergin, Alyürük, Çavaş & Güzeliş, 2012).

The main aim of this thesis is to derive the parameter ranges ensuring the bistability for lac operon. Two different lac operon models derived from enzyme kinetics, one takes into account the transacetylase enzyme effect and the other does not, are considered in the thesis. The bistability analysis is performed by two newly introduced methods, one is based on discriminant and the other is based on the root locus which is a well-known tool of control theory. The obtained parametric conditions on the bistability of the TMG induced lac operon model confirm and further extend the results available in the literature. For the sake of establishing a thorough bistability analysis in the thesis, equilibrium analysis realized by applying discriminant and root locus based methods on the polynomial equilibrium equations are supported by a complementary study on the boundedness of the state variables together with the local stability of the equilibrium points.

Chapter 2 of the thesis presents biological and mathematical lac operon models considered. The analysis results on the boundedness of the trajectories and local stability of the equilibrium points of the lac operon model with no transacetylase effect are given in Chapter 3. The discriminant based analysis method and the obtained results for determining parameter regions for the bistability of the lac operon model with no transacetylase effect are presented in Chapter 4. The root locus based method and the related results for determining the bistability regions are given in Chapter 5 and, respectively, in Chapter 6 for the lac operon model with transacetylase effect. The summary of all these analyses are compiled in Chapter 7.

CHAPTER TWO

BIOLOGICAL AND MATHEMATICAL LAC OPERON MODELS

This chapter presents a biological lac operon model and a mathematical model derived based on enzyme kinetics. There is no unique biological lac operon model in the literature. Depending on the used inducer such as lactose, TMG, or IPTG, and depending on the included biochemical interactions such as the efflux of TMG across the membrane, there correspond different biological and so mathematical models. For the sake of simplicity, a minimal set of biochemical interactions known to be involved in the lactose metabolism are considered in the biological model and its associated mathematical model given in this chapter. For the same reason, the acetylation effect of β -thiogalactoside transacetylase (GAT) is not considered in this chapter but it will be studied in Chapter 6 for demonstrating the capability of the root locus based analysis in revealing possible effects of a specific interaction, herein the acetylation.

2.1 A Biological Lac Operon Model

The lac operon is a genetic switching mechanism by which *E. coli* utilizes the lactose as a nutrient source under glucose starvation. Lac operon has three structural genes; namely, LacZ, LacY, and LacA genes. LacZ, LacY, and LacA produces, respectively, β -galactosidase, permease, and transacetylase enzyme. The permease enzyme is responsible for transporting the external lactose into the cell. The β -galactosidase enzyme provides the cleavage of the internal lactose to the allolactose and also the cleavage of the allolactose and internal lactose to the glucose and galactose. The transacetylase enzyme, usually ignored in the lactose utilization mechanism, is involved with the sugar metabolism and acetylation reaction. The main carbon source of *E. coli* is the glucose. In the absence of glucose, the existence of lactose leads the lac operon to be induced for catabolizing the lactose. The lac operon is induced through the following process: First, the lactose enters the cell by means of the permease which is always available as a consequence of the basal activity providing a small amount of mRNA. Second, the lactose entered to the cell is

converted to the allolactose by the basal β -galactosidase concentration. Third, the allolactose binds to the LacI repressor protein and causes a conformational change in the repressor, so inhibiting the repressor by dissociating it from the promoter region. Then, the RNA polymerase enzyme starts the transcription of mRNA for inducing the three structural genes. By the explained process, the permease and the β -galactosidase concentrations increase rapidly from the basal levels to much higher levels, so elevating the concentrations of the internal lactose and allolactose. The mutual amplification of the allolactose and mRNA concentration implies a positive feedback in the lactose metabolism. The positive feedback is known to be a source of unstable dynamics. Indeed, the mRNA concentration is bounded below and above, respectively, by the basal and saturation activities which provide two stable equilibria: One at a low level concentration corresponding to the uninduced state for lac operon and the other at a high level concentration corresponding to the induced state. The coexistence of these induced and uninduced stable states which has been observed in the experimental studies provides a bistable behavior for lac operon.

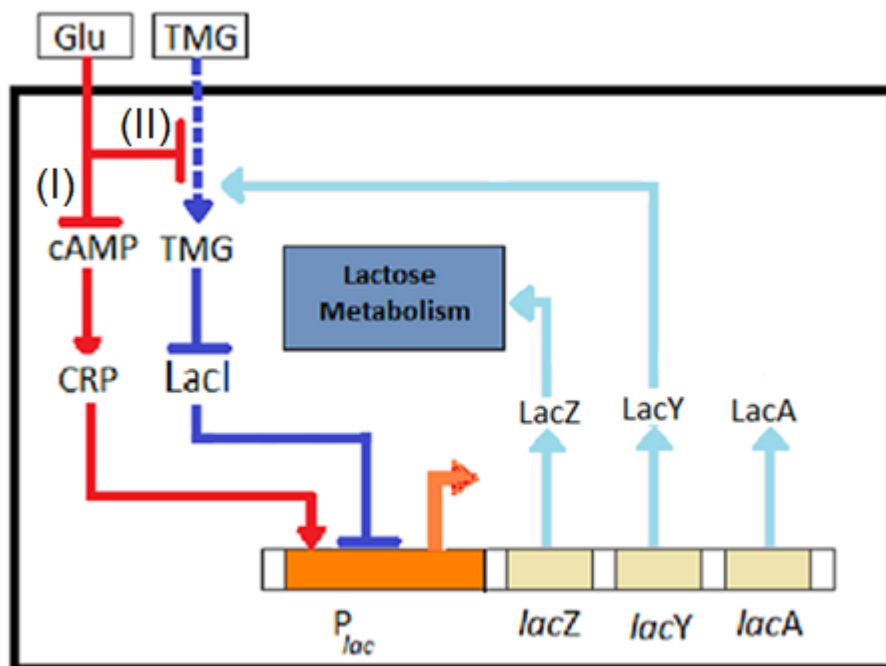


Figure 2.1 Lac operon gene regulatory network

The glucose when it exists suppresses the operation of the lac operon via two different pathways. By one of the pathways, called inducer exclusion as path (II) in

Figure 2.1, the glucose inhibits the transport of the external lactose into the cell by interfering with the permease activity leading to the exclusion of the inducer, i.e. lactose. In the second pathway, called catabolite repression as path (I) in Figure 2.1, the presence of glucose yields to decrease cAMP concentration. The decrease in cAMP concentration lacks of binding cAMP to CRP, i.e. cAMP receptor protein, to form CAP complex. Hence, mRNA transcription can not be induced due to the lack of CAP complex. This means the glucose leads the lac operon to the uninduced state.

2.2 A Mathematical Lac Operon Model

The thesis considers a simple yet sufficient ODE model in which an artificial inducer, TMG, is used. The mathematical model consists of three ordinary differential equations with the mRNA, permease and TMG concentration as state variables. The considered model includes i) the catabolite repression and inducer exclusion of the extracellular glucose, ii) the transcription of mRNA by TMG, iii) the production of permease, iv) the transportation of TMG via permease and v) the degradations of TMG, mRNA and permease as shown in Figure 2.1. It is assumed that there are no translational and transcriptional delays in the lac operon mechanism. As will be seen in the sequel, this model is very suitable for analyzing the hysteretic bistable behavior of lac operon.

The mathematical model is described by the following state model which is composed of three first order differential equations representing the reaction rates in terms of the mRNA, permease and internal TMG concentrations:

$$\frac{dM}{dt} = \alpha_M f_{M,T}(T) f_{M,Ge}(Ge) - \gamma_M M \quad (1)$$

$$\frac{dP}{dt} = \alpha_P M - \gamma_P P \quad (2)$$

$$\frac{dT}{dt} = \alpha_T f_{T,Te}(Te) f_{T,Ge}(Ge) P - \gamma_T T \quad (3)$$

where, state variable M , P and T stands for the mRNA, permease and internal TMG concentration, respectively. The input T_e and G_e is, respectively, external TMG and external glucose concentration. The parameters γ_i with $i \in \{M, P, T\}$ represent the loss constants for M , P , and T . The γ_i is indeed the composition of the active degradation, $\bar{\gamma}_i$, and the dilution due to growth rate, μ_i . The parameters α_i with $i \in \{M, P, T\}$ denote the production constants of the gene products. $f_{M,T}(T)$ and $f_{M,Ge}(Ge)$ expresses the positive effect of the internal TMG and the negative effect of the external glucose on the synthesis of mRNA, respectively. Similarly, $f_{T,Te}(Te)$ and $f_{T,Ge}(Ge)$ express the positive effect of external TMG and negative effect of external glucose on the TMG uptake into the cell. Here, $f_{M,Ge}(Ge)$ and $f_{T,Ge}(Ge)$ are decreasing functions of external glucose, the former describes the catabolite repression while the latter describes the inducer exclusion.

In the model, the temporal change of the mRNA concentration is defined in (1) as the difference between the production depending on the internal TMG concentration under the catabolite repression effect of external glucose and the losses due to active degradation and growth. The equation (2) gives the change of the permease concentration in terms of the synthesized permease and the losses. Similarly, the change of the internal TMG concentration is expressed in (3) where the increase is due to the import of the external TMG under the reduction effect of inducer exclusion and the decrease is due to the degradation and dilution.

Assuming the production of mRNA under TMG as an allosteric interaction similar to the allolactose case, $f_{M,T}(T)$ can be chosen as the following modified Hill function (Yagil & Yagil, 1971).

$$f_{M,T}(T) = \frac{1 + K_1 T^n}{K + K_1 T^n} \quad (4)$$

where, n is the number of TMG required to inactivate a repressor protein, K_1 is the equilibrium constant of TMG-repressor protein interaction, and K^{-1} is the basal level

of mRNA transcription in *E. coli*. For the inhibition of repressor protein, at least two TMG molecules have to bind the repressor. n is taken as 2 in our analysis throughout the study.

The transport of T_e into the cell by the permease can be modeled via Michaelis-Menten kinetics as follows:

$$f_{T,T_e}(T_e) = \frac{T_e}{K_{T_e} + T_e} \quad (5)$$

where, K_{T_e} is the Michaelis constant. The monotonically decreasing functions of G_e for describing the catabolite repression and inducer exclusion are chosen as follows:

$$f_{M,G_e}(G_e) = \frac{K_{M,G_e,1} + G_e^m}{K_{M,G_e,2} + K_{M,G_e,2}G_e^m} \quad (6)$$

$$f_{T,G_e}(G_e) = 1 - \beta_{T,G_e} \frac{G_e}{K_{T,G_e} + G_e} \quad (7)$$

Where, $K_{M,G_e,1}$, $K_{M,G_e,2}$, $K_{M,G_e,3}$, and m are catabolite repression parameters and β_{T,G_e} is inducer exclusion parameter (Santillan et al., 2007).

CHAPTER THREE
BOUNDEDNESS OF THE STATE VARIABLES AND A LOCAL
STABILITY ANALYSIS OF THE LAC OPERON MODEL

The previous models (Wong et al., 1997; Özbudak et al., 2004; Yıldırım et al., 2004) confirm the bistable behavior of lac operon observed in experimental studies. A bistable dynamics for a system is defined by the existence of two (locally) asymptotically stable equilibria such that any trajectory of the system tends to one of these equilibria depending on the initial condition if not starting at a possible unstable equilibrium. This implies the boundedness of the state variables of the system dynamics and also excludes the other kinds of dynamics such as limit cycle and chaos.

This chapter describes that the considered model in (1)-(3) has bounded dynamics, multiple equilibria, and presents a local stability analysis of the equilibria of the model (1)-(3).

3.1 Boundedness of the State Variables

The loss terms in (1)-(3) are linear. So, considering the (nonlinear) production terms as inputs for first order linear differential equations, one can obtain an analytical expression for each of the state variables of the model (1)-(3):

$$M(t) = e^{-\gamma_M(t-t_0)}M(t_0) + \int_{t_0}^t e^{-\gamma_M(t-\tau)} \alpha_M f_{M,T}(T(\tau)) f_{M,G_e}(G_e) d\tau \quad (8)$$

$$P(t) = e^{-\gamma_P(t-t_0)}P(t_0) + \int_{t_0}^t e^{-\gamma_P(t-\tau)} \alpha_P M(\tau) d\tau \quad (9)$$

$$T(t) = e^{-\gamma_T(t-t_0)}T(t_0) + \int_{t_0}^t e^{-\gamma_T(t-\tau)} \alpha_T f_{T,T_e}(T_e) f_{T,G_e}(G_e) P(\tau) d\tau \quad (10)$$

As expressed in (4) and (6), the production function of the mRNA and the catabolite repression effect of the G_e are bounded above.

$$|f_{M,T}(T)| = \left| \frac{1 + K_1 T^2}{K + K_1 T^1} \right| < 1 \quad \text{for } K > 1 \quad (11)$$

$$|f_{M,G_e}(G_e)| = \left| \frac{K_{M,G_e,1} + G_e^m}{K_{M,G_e,2} + K_{M,G_e,2} G_e^m} \right| \leq \frac{K_{M,G_e,1}}{K_{M,G_e,2}} \quad (12)$$

Note that $K > 1$ is always true as observed from the experimental studies. Then, an upper bound for the mRNA concentration is obtained as follows:

$$|M(t)| \leq e^{-\gamma_M(t-t_0)} M(t_0) + \frac{\alpha_M K_{M,G_e,1}}{\gamma_M K_{M,G_e,2}} [1 - e^{-\gamma_M(t-\tau)}] \quad (13)$$

The following upper bound for the permease concentration is found in a similar way.

$$|P(t)| \leq e^{-\gamma_P(t-t_0)} P(t_0) + \frac{\alpha_P}{\gamma_P} |M(t)| [1 - e^{-\gamma_P(t-\tau)}] \quad (14)$$

Considering the following bounds for $f_{T,T_e}(T_e)$ and $f_{T,G_e}(G_e)$,

$$|f_{T,T_e}(T_e)| = \left| \frac{T_e}{K_{T_e} + T_e} \right| \leq 1 \quad (15)$$

$$|f_{T,G_e}(G_e)| = \left| 1 - \beta_{T,G_e} \frac{G_e}{K_{T,G_e} + G_e} \right| \leq 1 \quad (16)$$

an upper bound for the internal TMG concentration is derived as:

$$|T(t)| \leq e^{-\gamma_T(t-t_0)} T(t_0) + \frac{\alpha_T}{\gamma_T} |P(t)| [1 - e^{-\gamma_T(t-\tau)}] \quad (17)$$

The expressions given in (13), (14), and (17) show the boundedness of the state variables $M(t)$, $P(t)$, and $T(t)$. As can be seen from the limits of the upper bounds given in (18), (19), and (20), the model (1)-(3) is indeed eventually uniformly bounded (Vidyasagar, 1972).

$$\exists t_M > 0 \ni |M(t)| \leq \frac{\alpha_M K_{M,Ge,1}}{\gamma_M K_{M,Ge,2}} \quad \forall t \geq t_M \quad (18)$$

$$\exists t_P > 0 \ni |P(t)| \leq \frac{\alpha_P \alpha_M K_{M,Ge,1}}{\gamma_P \gamma_M K_{M,Ge,2}} \quad \forall t \geq t_P \quad (19)$$

$$\exists t_T > 0 \ni |T(t)| \leq \frac{\alpha_T \alpha_P \alpha_M K_{M,Ge,1}}{\gamma_T \gamma_P \gamma_M K_{M,Ge,2}} \quad \forall t \geq t_T \quad (20)$$

Since the functions in (12), (15) and (16) are continuous functions of the lac operon inputs (i.e external glucose and external TMG) so are the upper bounds of the states. Then, the lac operon defined by (1)-(3) is concluded to be Bounded Input Bounded State (BIBS) stable (Vidyasagar, 1972).

3.2 Existence of Multiple Equilibria

In this subsection, it will be shown that the considered model has either one or three equilibrium points depending on the model parameters. Setting the state variables M , P , and T constant and then eliminating the equilibrium concentrations M and P , the equilibrium equation for T can be obtained as:

$$p f_{M,T}(T) - T = p \frac{1 + K_1 T^2}{K + K_1 T^2} - T = 0 \quad (21)$$

where

$$p \triangleq \frac{\alpha_T \alpha_P \alpha_M}{\gamma_T \gamma_P \gamma_M} f_{T,T_e}(T_e) f_{T,G_e}(G_e) f_{M,G_e}(G_e) \quad (22)$$

As illustrated in Figure 3.1, the production function $f_{M,T}(T)$ of mRNA starts at $1/K$ and tends asymptotically to 1 irrespective of the parameters K and K_1 . $1/K > 0$ and the continuity of $f_{M,T}(T)$ together with the saturation characteristic imply that the graph of $p f_{M,T}(T)$ intersects the unity slope line corresponding to the second term

T in (21). This proves the existence of at least one equilibrium point. Further, $f_{M,T}(T)$ is a monotonically increasing function since its derivative,

$$\frac{d}{dT} f_{M,T}(T) = \frac{d}{dT} \left\{ \frac{1 + K_1 T^2}{K + K_1 T^2} \right\} = \frac{2K_1 T(K - 1)}{(K + K_1 T^2)^2} \quad (23)$$

is positive for $K > 1$ that is always true. However, the derivative of $pf_{M,T}(T)$ is not monotonic and is less than 1 for sufficiently small and large T values and greater than 1 for intermediate T values. Depending on the value of the parameter p , the graphs of the first and second terms in (21) may have three intersection points as shown in Figure 3.1 which means there are three equilibria for the considered model.

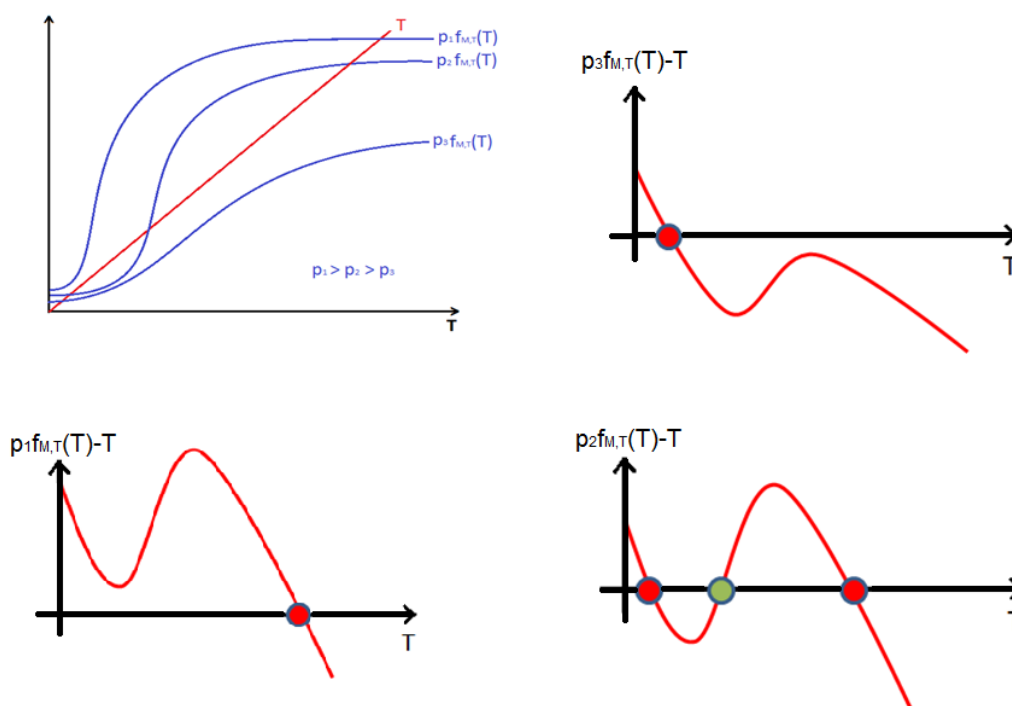


Figure 3.1 Geometric Analysis of the Equilibria

The above graphical analysis provides an insight on the appearance of bistability which requires the existence of three equilibria, two of them are stable. However, determining the ranges of the parameters ensuring the existence of multiple equilibria needs a rigorous analysis. Considering the availability of well established methods

for the parametric studies of the roots of polynomial equations, it is convenient to rearrange the equilibrium equation (21) into the following polynomial form.

$$K_1T^3 + pK_1T^2 + KT - p = 0 \quad (24)$$

It is obvious that, irrespective of the values of the parameters, there is always a real root of (24), indicating the existence of at least one equilibrium point. The remaining two roots of (24) are either complex conjugate pair or real. In the case of three real roots, there are three different possibilities: A triple root, two roots such that one of them is double, and three different roots. The bistable behaviour occurs when there exist three equilibria corresponding to the three different real roots of (24). Then, to determine the ranges of the parameters ensuring the existence of three real roots, the parameter values at which the complex roots turn to the real ones could be identified. These turning points in the parameter space can be found by obtaining the conditions for the presence of repeated roots.

As also exploited in the literature for different lac operon models the conditions for a triple root of the polynomial equation in (24) can be derived by considering the fact that the polynomial itself, its first and second derivatives simultaneously vanish at a triple root (Özbudak et al., 2004; van Hoek & Hogeweg, 2006):

$$K_1T^3 + pK_1T^2 + KT - p = 0 \quad (25)$$

$$3K_1T^2 + 2pK_1T + K = 0 \quad (26)$$

$$6K_1 + 2pK_1 = 0 \quad (27)$$

The above equations show that a triple root appears at $T = p/3$ when $K = 9$ and $K_1 = 27/p^2$. It is interesting to note that $K > 9$ is derived in the literature as the bistability condition for different lac operon models (Özbudak et al., 2004; van Hoek & Hogeweg, 2006). By this derivation, one can conclude that $K = 9$ is a boundary of the bistability interval for K when only the parameters K_1 and p satisfy $K_1 = 27/p^2$.

As will be seen in the discriminant and root locus analyses employed in Chapter 4 and Chapter 5, a bistability condition other than $K > 9$ becomes valid when $K_1 > 27/p^2$. For these cases, the boundary for the bistability region is derived by considering the two real roots such that one of them is double. This derivation will be performed in Chapter 4 by calculating the discriminant of the polynomial in (24) and also in Chapter 5 by applying the root locus method.

3.3 Local Stability Analysis

Local stability analysis of the state model (1)-(3) for constant G_e and T_e inputs can be realized by determining the location of the eigenvalues of the Jacobian matrix in the framework of Lyapunov's first method (Vidyasagar, 1972). For the sake of simplicity, one can transform (1)-(3) into the following form:

$$\frac{1}{\gamma_M} \frac{dM}{dt} = \frac{\alpha_M}{\gamma_M} f_{M,T}(T) f_{M,Ge}(Ge) - M \quad (28)$$

$$\frac{1}{\gamma_P} \frac{dP}{dt} = \frac{\alpha_P}{\gamma_P} M - P \quad (29)$$

$$\frac{1}{\gamma_T} \frac{dT}{dt} = \frac{\alpha_T}{\gamma_T} f_{T,Te}(Te) f_{T,Ge}(Ge) P - T \quad (30)$$

By this transformation, the locations of the eigenvalues of the Jacobian matrix remain in the same half-plane of the complex plane. This fact can be seen from (31), showing that the eigenvalues λ of the Jacobian matrix related to the transformed model in (28)-(30) are just the scaled versions of the eigenvalues $\hat{\lambda}$ for the original model (1)-(3), namely $\lambda = \frac{\hat{\lambda}}{\gamma_i}$ with $\gamma_i > 0$.

$$\det(\hat{\lambda}I - \hat{f}) = \det(\hat{\lambda}I - \text{diag}(\gamma_M, \gamma_P, \gamma_T)J) = \gamma_M \gamma_P \gamma_T \det(\lambda I - J) = 0 \quad (31)$$

where, \hat{f} and J is the Jacobian matrix at a certain equilibrium point T^* for the original and the transformed model, respectively. The eigenvalues of the transformed model are determined by finding the roots of the characteristic equation given in (32).

$$\det(\lambda I - J) = \begin{vmatrix} \lambda + 1 & 0 & -\frac{\alpha_M}{\gamma_M} f_{M,G_e}(G_e) \frac{d}{dT} f_{M,T}(T^*) \\ -\frac{\alpha_P}{\gamma_P} & \lambda + 1 & 0 \\ 0 & -\frac{\alpha_T}{\gamma_T} f_{T,T_e}(T_e) f_{T,G_e}(G_e) & \lambda + 1 \end{vmatrix}$$

$$= \lambda^3 + 3\lambda^2 + 3\lambda + 1 - p \frac{d}{dT} f_{M,T}(T^*) \quad (32)$$

To apply the Routh-Hurwitz test for deciding if there exists any eigenvalue in the right-halfplane for the equilibrium point T^* , the Routh array is constructed in Table 3.1. Since $f_{M,T}(T)$ is monotonically increasing, then the third term in the first column is always strictly positive. Therefore, the sign change in the first column can occur only when $p \frac{d}{dT} f_{M,T}(T^*) > 1$. It can be seen from the equilibrium equation $p f_{M,T}(T) - T = 0$ together with the positiveness of the initial value $1/K$ of the monotonically increasing function $f_{M,T}(T)$ that, for the three different equilibria case, the smallest and also the largest equilibrium point arise when $p \frac{d}{dT} f_{M,T}(T^*) < 1$ and the middle equilibrium point arises when $p \frac{d}{dT} f_{M,T}(T)^* > 1$. Therefore, the middle equilibrium point is seen to be unstable while the other two ones stable. It can be concluded that the parameter region ensuring the existence of three different equilibria is indeed the bistability region of the lac operon model in (1)-(3). This bistability region in the p-K-K_1 parameter space will be characterized by two different methods in Chapter 4 and Chapter 5.

Table 3.1 Routh array for the characteristic equation of the transformed model

$$\begin{array}{c}
 \lambda^3 \\
 \lambda^2 \\
 \lambda^1 \\
 \lambda^0
 \end{array}
 \left| \begin{array}{cc}
 1 & 3 \\
 3 & 1 - p \frac{d}{dT} f_{M,T}(T) \\
 \frac{1}{3} \left(8 + p \frac{d}{dT} f_{M,T}(T) \right) & \\
 1 - p \frac{d}{dT} f_{M,T}(T) &
 \end{array} \right.$$

CHAPTER FOUR
DISCRIMINANT BASED BISTABILITY ANALYSIS OF THE LAC OPERON
MODEL WITHOUT TRANSACETYLASE EFFECT

The discriminant Δ of (24) is given by:

$$\Delta = -4K_1^3 p^4 + (18K_1^2 K - 27K_1^2 + K_1^2 K)p^2 - 4K_1 K^3 \quad (33)$$

Since the discriminant of a polynomial is proportional to the product of the squares of pairwise differences between its roots, then Δ becomes zero when there exists a double or triple root. Positive values of Δ correspond to the case of three different real roots of the equilibrium equation in (24). To obtain the conditions on the parameters, the discriminant equation, *i.e.* $\Delta = 0$, can be solved in terms of one of the parameters while holding the others fixed. In order to determine the range of p , one can find the p values satisfying $\Delta = 0$ as follows:

$$p^{(1,2)} = \sqrt{\frac{a \pm \sqrt{b}}{8K_1}} \quad (34)$$

$$p^{(3,4)} = -\sqrt{\frac{a \pm \sqrt{b}}{8K_1}} \quad (35)$$

where,

$$a \triangleq K^2 + 18K - 27 \quad (36)$$

$$b \triangleq K^4 - 28K^3 + 270K^2 - 972K + 729 \quad (37)$$

To identify the interval of p where $\Delta > 0$, one can first find the real p roots of $\Delta = 0$. When the inequality in (38) is not satisfied, $\Delta = 0$ has 4 complex roots, hence there is

no any p value yielding $\Delta > 0$ since $-4K^3$ which is the greatest power of p in (33) is always negative due to the positiveness of the biological parameter K_1 .

$$K^4 - 28K^3 + 270K^2 - 972K + 729 = (K - 1)(K - 9)^3 \geq 0 \quad (38)$$

Therefore, it can be concluded that K values with $1 < K < 9$ does not provide bistability. One can observe the following relation.

$$\begin{aligned} a^2 - b^2 &= (K^2 + 18K - 27)^2 - (K^4 - 28K^3 + 270K^2 - 972K + 729) \\ &= 64K^3 > 0 \end{aligned} \quad (39)$$

The relation (39) implies that a is, in magnitude, greater than \sqrt{b} . Then, $a > 0$ becomes a necessary condition for the bistability since its violation leads all of $p^{(i)}$'s roots in (34)-(35) to be complex, so there is no any p value yielding $\Delta > 0$. Observing $a < 0$ for K values with $0 < K < 1$, all $p^{(i)}$'s in (34)-(35) become real only when $K > 9$. In the case of real $p^{(1)}$, $p^{(2)}$, $p^{(3)}$ and $p^{(4)}$, $\Delta > 0$ is obtained for p values lying in the intervals of $(p^{(1)}, p^{(2)})$ and $(p^{(3)}, p^{(4)})$. The latter interval is not valid due to the positiveness of the biological parameter p . Hence, the above analysis considering the discriminant $\Delta(p, K, K_1)$ as a function of p provides $p^{(1)} < p < p^{(2)}$, $K > 9$, and $K_1 > 0$ constraints as necessary conditions defining the following region \mathfrak{R}_{bi}^p .

$$\mathfrak{R}_{bi}^p \triangleq \{ (p, K, K_1) \in \mathbb{R}^3 \mid p^{(1)} < p < p^{(2)}, K > 9, K_1 > 0 \} \quad (40)$$

Repeating the above derivations now for considering the dependence of $\Delta(p, K, K_1)$ on K_1 and K , the whole set of bistability conditions are obtained in the sequel. The roots of $\Delta(p, K, K_1) = 0$ in terms of K_1 which are obtained as $K_1^{(1)} = 0$ and $K_1^{(2,3)} = \frac{a \pm \sqrt{b}}{8p^2}$ define the region $\mathfrak{R}_{bi}^{K_1}$ where $K > 9$ and $p > 0$ are required for having real $K_1^{(2,3)}$ roots.

$$\mathfrak{R}_{bi}^{K_1} \triangleq \left\{ (p, K, K_1) \in \mathbb{R}^3 \mid K_1^{(2)} < K_1 < K_1^{(3)}, \quad K > 9, \quad p > 0 \right\} \quad (41)$$

Similarly, the roots of $\Delta(p, K, K_1) = 0$ by taking K as the variable are obtained as:

$$K^{(1)} = \frac{Kp^2}{12} + \frac{c}{12d} + \frac{1}{12}d \quad (42)$$

$$K^{(2,3)} = \frac{1}{24} \left(2K_1p^2 - \frac{(1 \mp i\sqrt{3})c}{d} - (1 \mp i\sqrt{3})d \right) \quad (43)$$

where, c and d are given below.

$$c = K_1p^2(216 + K_1p^2) \quad (44)$$

$$d = \left(5832K_1p^2 - 540(K_1p^2)^2 + (K_1p^2)^3 + 24\sqrt{3}\sqrt{-(-27 + K_1p^2)^3(K_1p^2)^2} \right)^{1/3} \quad (45)$$

Note that $K^{(1)}$, $K^{(2)}$, and $K^{(3)}$ are functions of K_1p^2 and their highly nonlinear dependency on K_1p^2 can be visualized as follows.

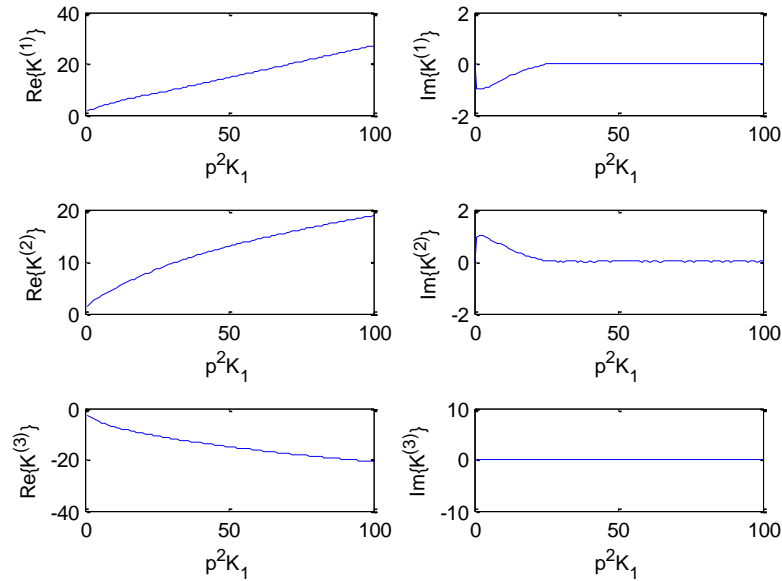


Figure 4.1 The $K^{(1,2,3)}$ values for different p^2K_1 .

Then, the region \mathfrak{R}_{bi}^K is defined with the positive and real roots $K^{(1)}$ and $K^{(3)}$ under the condition of $K_1 p^2 > 27$ since $K^{(2)}$ is always a negative real number independent from K_1 and p .

$$\mathfrak{R}_{bi}^K \triangleq \{ (p, K, K_1) \in \mathbb{R}^3 \mid K^{(1)} < K < K^{(3)}, K_1 p^2 > 27 \} \quad (46)$$

The above discriminant based analysis is concluded by defining the bistability region \mathfrak{R}_{bi} in the $p - K - K_1$ parameter space as the intersection of the derived \mathfrak{R}_{bi}^p , \mathfrak{R}_{bi}^K and $\mathfrak{R}_{bi}^{K_1}$

$$\mathfrak{R}_{bi} \triangleq \{ (p, K, K_1) \in \mathbb{R}^3 \mid p^{(1)} < p < p^{(2)}, K^{(1)} < K < K^{(3)}, K_1^{(2)} < K_1 < K_1^{(3)}, K_1 p^2 > 27, p > 0, K > 9, K_1 > 0 \} \quad (47)$$

Note that $K > 9$ is reported as the bistability condition in the literature (Özbudak et al., 2004; van Hoek & Hogeweg, 2006). However, the above analysis shows that not all K values greater than 9 imply the existence of triple equilibria but for K values larger than 9 there is always a p value in the interval of $(p^{(1)}, p^{(2)})$ ensuring the existence of triple equilibria. Further note that the $(p^{(1)}, p^{(2)})$ interval actually depends on K and K_1 parameters such that small K_1 and large K values result in large $(p^{(1)}, p^{(2)})$ interval shifted to the right hand side, on the contrary large K_1 and small K values result in small $(p^{(1)}, p^{(2)})$ interval shifted to the left-hand side. As will also be shown in Chapter 5 by employing the root locus method, each of p , K , and K_1 parameters ensuring bistability should lie in finite intervals whose upper and lower bounds and also lengths depend on the other two parameters.

CHAPTER FIVE
ROOT LOCUS BASED BISTABILITY ANALYSIS OF THE LAC OPERON
MODEL WITHOUT TRANSACETYLASE EFFECT

It is seen in Chapter 4, the discriminant of a polynomial equation, herein the equilibrium equation, can be used for studying the change of the number of real roots depending on the parameters defining the coefficients of the polynomial. Such a discriminant based method requires employment of a symbolic analysis for deriving parametric representations of the roots of high order discriminant equations. That method may get stuck even when the equilibrium equation is of order 4 or when an interdependency exists among the coefficients of an equilibrium equation of order 3. The root locus method which is a well-known method used for controller design in electrical engineering to determine the changes in the location of closed-loop system poles as a function of the controller parameter is proposed in this paper to overcome the above mentioned drawbacks of the discriminant based method. It will be cleared in the sequel that the root locus method is an efficient method for studying the changes in the number of equilibria of the lac operon model which is defined by state equations with rational right-hand sides derived from enzyme kinetics. The root locus based approach allows the use of root locus tools of numerical software packages in specifying the boundary of the bistability region and it provides a graphical representation for understanding the qualitative changes depending on the model parameters.

The main concern in control applications employing root locus is to identify the controller parameters ensuring desired locations for the closed-loop poles such as the open left complex half plane to meet asymptotic stability. However, the concern of root locus based approach in the identification of the bistability region for lac operon is to determine the model parameters yielding the existence of multiple (positive) equilibria. The root locus is applied in this paper to the equilibrium equation which is a rational function of TMG concentration whereas in the control area it is applied to the (rational) characteristic equation in the Laplace domain.

To determine the bistability region the root locus method will be applied in the following steps:

1. For each parameter, the equilibrium equation (21) will be written in the usual characteristic equation form of $1 + q \frac{N(T, \bar{q})}{D(T, \bar{q})} = 0$ where $q \in \{p, K, K_1\}$ is the parameter under consideration, \bar{q} represents the rest of the parameters, the numerator N and denominator D are polynomial functions of T and \bar{q} .
2. Determine the roots of $N(T, \bar{q}) = 0$ and $D(T, \bar{q}) = 0$ for specific choices of \bar{q} . Then, draw the root-locus originating from the roots of $N(T, \bar{q}) = 0$ and ending at the roots of $D(T, \bar{q}) = 0$.
3. In order to identify the boundaries of the bistability region, compute the break-in and break-away points where a pair of complex conjugate roots turn into a double real root and vice versa.

5.1 Root Locus for p Parameter

For p parameter, the equilibrium equation in (21) can be written in the characteristic equation form as:

$$1 - p \frac{1 + K_1 T^2}{T(K + K_1 T^2)} = 0 \quad (48)$$

The positive feedback in the above equation should be taken into account when drawing the root locus.

The general expression for the roots $T_N^{(1,2)}$ of the numerator and the roots $T_D^{(1,2,3)}$ of the denominator can be obtained as follows.

$$T_N^{(1,2)} = \pm j \sqrt{\frac{1}{K_1}} \quad (49)$$

$$T_D^{(1)} = 0 \quad (50)$$

$$T_D^{(2,3)} = \pm j \sqrt{\frac{K}{K_1}} \quad (51)$$

By finding the extrema of p with respect to T from

$$\frac{d}{dT} \left(\frac{T(K + K_1 T^2)}{1 + K_1 T^2} \right) = \frac{T^4(3K_1 - KK_1) + K_1^2 T + K}{(1 + K_1 T^2)^2} \quad (52)$$

the break-in and break-away points are obtained in terms of K and K_1 as

$$T^{(1,2,3,4)} = \pm \sqrt{\frac{(K - 3) \pm \sqrt{(K - 9)(K - 1)}}{2K_1}} \quad (53)$$

It should be noted that only real ones of $T^{(1,2,3,4)}$ correspond to the break-in and breakaway points. Hence, $K > 9$ and $K_1 > 0$ are obtained as necessary conditions for the existence of bistability which coincide with the result of discriminant based analysis given in (40).

When considering $K = 167.1$ and $K_1 = 0.02$ values reported in some experimental studies on *E. coli* (Özbudak et al., 2004), the root locus diagram for the p parameter is drawn in Figure 5.1 by using Matlab numerical software. It is seen from the diagram that there is only one real root for small and large p values and three real roots exist for a bounded interval of p . By computing the break-in and break-away points, the bistability interval is determined as $p \in (182, 594)$ for the considered K and K_1 values.

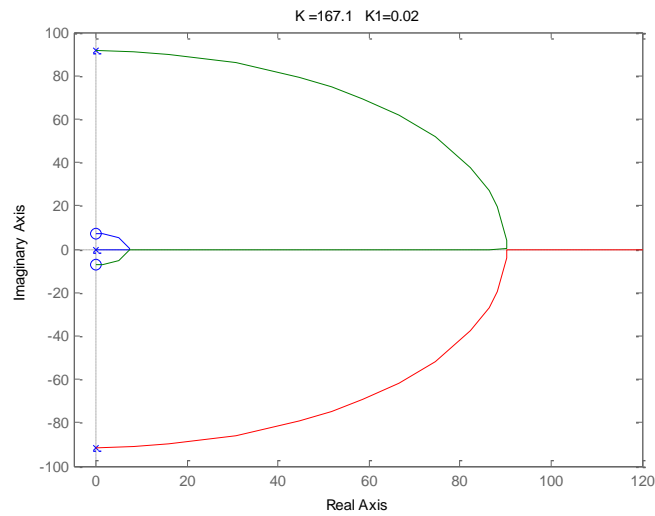


Figure 5.1 The root locus for p parameter when $K = 167.1$ and $K_1 = 0.02$.

The above bistability interval is derived for particular values of K and K_1 . The lower and upper limits and furthermore the existence of the bistability interval for p do indeed depend on K and K_1 values. The expression (53) of break-in and break-away points shows that the (positive) K_1 acts only as a scaling factor causing a quantitative change but not a qualitative change on the root locus drawn for p . To see the qualitative changes in the root locus and hence in the bistability interval for p , it is sufficient to consider different values of only K parameter.

A gallery of root locus diagrams obtained for different K values is given in Figure 5.2 where K_1 is held constant as 0.02.

Figure 5.2.a shows the case of only one real root for all p values, in other words, the case of the complex roots loci which never cross the real axis. Herein, K is taken equal to 2 as an example for K values less than 9 lacking the existence of break-in and break-away points. Figure 5.2.b corresponds to the limit case of $K = 9$ in which the break-in and break-away points coincide such that there is a triple real root for a specific p value but no other p value providing multiple real roots. In Figure 5.2.c-f obtained for four different K values greater than 9, three real roots exist for p values in non-empty and bounded intervals.

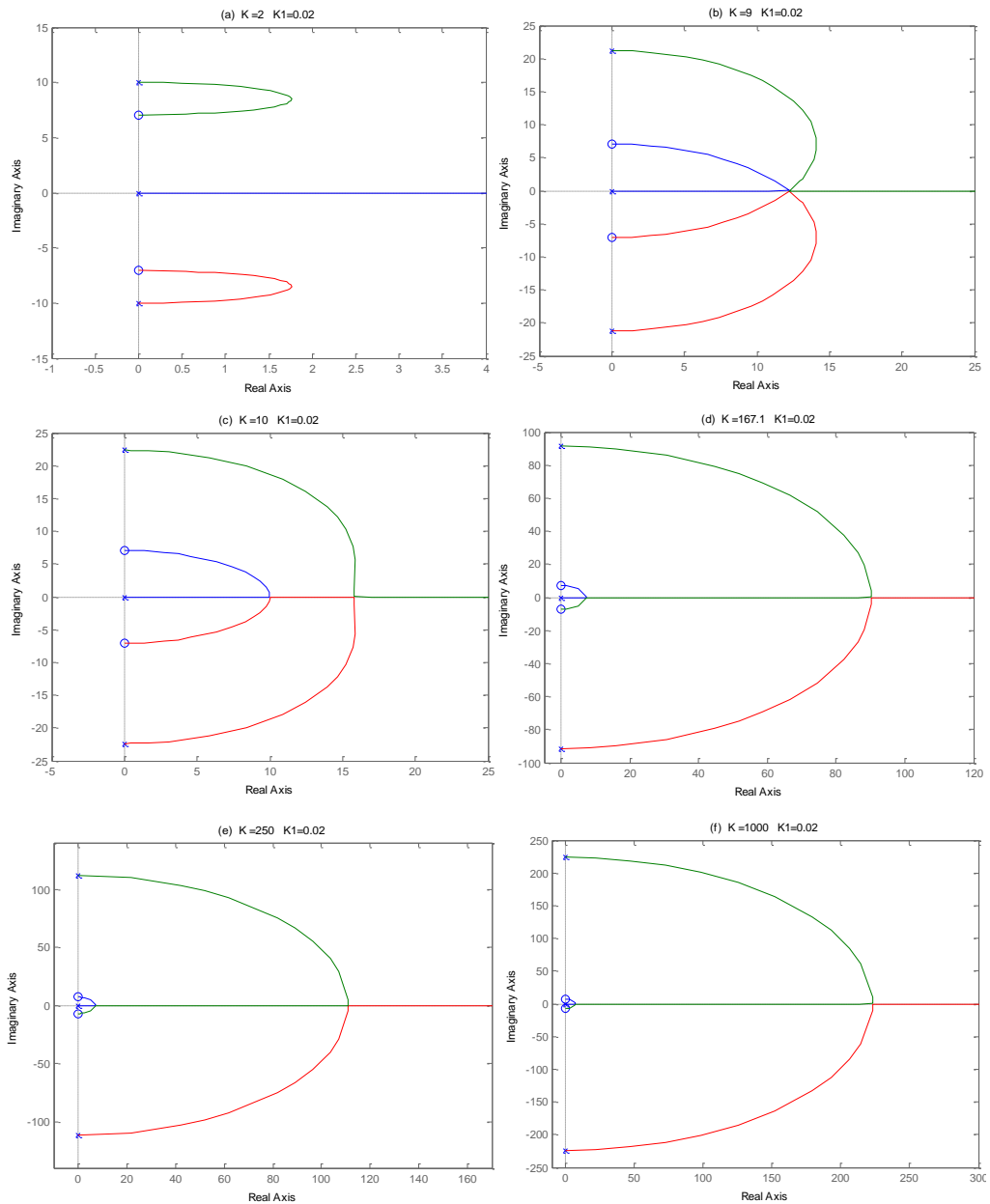


Figure 5.2 The root locus for p parameter with different K values when holding K_1 fixed as 0.02.

The lower p^l and the upper p^u limits of the bistability intervals for p parameter change with the K parameter such that the bigger the K , the larger the interval. The variations of p^l and p^u values with K can be expressed by determining the p values corresponding to the break-away and break-in points already found in (53) using the rewritten equilibrium equation $p = \frac{T(K+K_1T^2)}{1+K_1T^2}$.

$$\begin{aligned}
p^l &= \frac{\sqrt{\frac{(K-3) + \sqrt{(K-9)(K-1)}}{2K_1}} \left(K + K_1 \left(\sqrt{\frac{(K-3) + \sqrt{(K-9)(K-1)}}{2K_1}} \right)^2 \right)}{1 + K_1 \left(\sqrt{\frac{(K-3) + \sqrt{(K-9)(K-1)}}{2K_1}} \right)^2} \\
&= \sqrt{\frac{(K-3) + \sqrt{(K-9)(K-1)}}{2K_1}} \left(\frac{3K-3 + \sqrt{(K-9)(K-1)}}{K-1 + \sqrt{(K-9)(K-1)}} \right) \quad (54)
\end{aligned}$$

$$\begin{aligned}
p^u &= \frac{\sqrt{\frac{(K-3) - \sqrt{(K-9)(K-1)}}{2K_1}} \left(K + K_1 \left(\sqrt{\frac{(K-3) - \sqrt{(K-9)(K-1)}}{2K_1}} \right)^2 \right)}{1 + K_1 \left(\sqrt{\frac{(K-3) - \sqrt{(K-9)(K-1)}}{2K_1}} \right)^2} \\
&= \sqrt{\frac{(K-3) - \sqrt{(K-9)(K-1)}}{2K_1}} \left(\frac{3K-3 - \sqrt{(K-9)(K-1)}}{K-1 - \sqrt{(K-9)(K-1)}} \right) \quad (55)
\end{aligned}$$

Note that the real and positive T values used above in finding p^l and p^u are the only break-away and break-in points under the condition of $K > 9$ and $K_1 > 0$ since T representing TMG concentration can take non-negative values only.

5.2 Root Locus for K Parameter

The equilibrium equation in Equation (24) can be rewritten into the following characteristic equation form to repeat the analysis of Chapter 5.1 for the K parameter.

$$1 + K \frac{T}{K_1 T^3 - p K_1 T^2 - p} = 0 \quad (56)$$

Both of the discriminant based analysis of Chapter 4 and the root locus with respect to p parameter in Chapter 5.1 shows that $K > 9$ seems to be the only

condition necessary for the bistability. However, as given in Figure 5.3 the root locus with respect to the K parameter by considering $K_1 = 0.02$ and $p = 250$ reveals that, to have the bistability, K must not be bounded below only, but also bounded above. The lower and upper limits are actually the break-in and respectively break-away points.

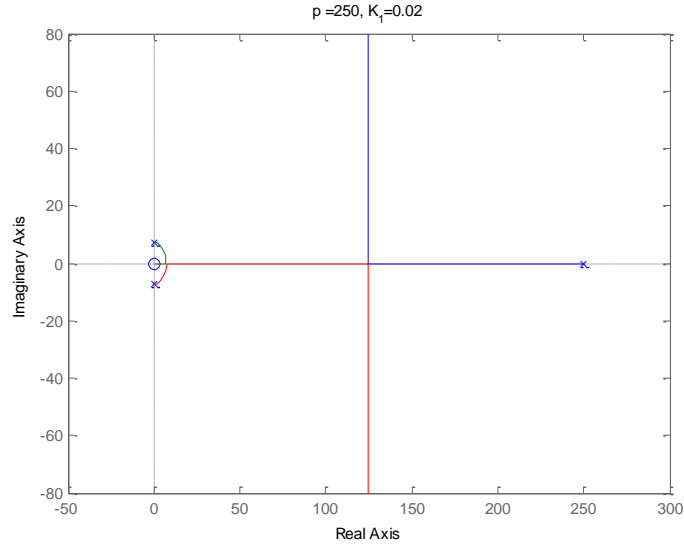


Figure 5.3 The root locus for K parameter.

The bistability conditions on K parameter are studied in the sequel by deriving the structural features of the root locus for K such as the break-in and break-away points in terms of p and K_1 .

The numerator T has a unique root at the origin. The roots of the denominator $K_1 T^3 - p K_1 T^2 - p$ can be obtained as in Equation (58)-(60) by using Cardano formula.

$$T_N^{(1)} = 0 \quad (57)$$

$$T_D^{(1)} = \frac{p}{3} - \frac{1}{3K_1} \sqrt[3]{\frac{1}{2}(r_1 + r_2)} - \frac{1}{3K_1} \sqrt[3]{\frac{1}{2}(r_1 - r_2)} \quad (58)$$

$$T_D^{(2)} = \frac{p}{3} + \frac{1 + i\sqrt{3}}{6K_1} \sqrt[3]{\frac{1}{2}(r_1 + r_2)} + \frac{1 - i\sqrt{3}}{3K_1} \sqrt[3]{\frac{1}{2}(r_1 - r_2)} \quad (59)$$

$$T_D^{(3)} = \frac{p}{3} + \frac{1 - i\sqrt{3}}{6K_1} \sqrt[3]{\frac{1}{2}(r_1 + r_2)} + \frac{1 + i\sqrt{3}}{3K_1} \sqrt[3]{\frac{1}{2}(r_1 - r_2)} \quad (60)$$

where, r_1 and r_2 variables are defined below.

$$r_1 = -pK_1^3(2p^2K_1 + 27) \quad (61)$$

$$r_2 = \sqrt{27p^2K_1^4(4p^2K_1 + 27)} \quad (62)$$

The break-in and break-away points are the roots of $2K_1T^3 - pK_1T^2 + p = 0$ since $\frac{dK}{dT} = 0$ can be obtained as:

$$\frac{dK}{dT} = \frac{d}{dT} \left\{ -\frac{K_1T^3 - pK_1T^2 - p}{T} \right\} = -\frac{2K_1T^3 - pK_1T^2 + p}{T^2} = 0 \quad (63)$$

The $T^{(1,2,3)}$ values in Equation (64)-(66) which are the roots of the numerator polynomial $2K_1T^3 - pK_1T^2 + p = 0$ of Equation (63) are the break-in and break-away points of the root locus.

$$T^{(1)} = \frac{p}{6} - \frac{1}{6K_1} \sqrt[3]{\frac{1}{2}(r_3 + r_4)} - \frac{1}{6K_1} \sqrt[3]{\frac{1}{2}(r_3 - r_4)} \quad (64)$$

$$T^{(2)} = \frac{p}{6} + \frac{1 + i\sqrt{3}}{12K_1} \sqrt[3]{\frac{1}{2}(r_3 + r_4)} + \frac{1 - i\sqrt{3}}{12K_1} \sqrt[3]{\frac{1}{2}(r_3 - r_4)} \quad (65)$$

$$T^{(3)} = \frac{p}{6} + \frac{1 - i\sqrt{3}}{12K_1} \sqrt[3]{\frac{1}{2}(r_3 + r_4)} + \frac{1 + i\sqrt{3}}{12K_1} \sqrt[3]{\frac{1}{2}(r_3 - r_4)} \quad (66)$$

where, r_1 and r_2 variables are defined below.

$$r_3 = 2pK_1^2(54 - p^2K_1) \quad (67)$$

$$r_4 = \sqrt{432p^2K_1^4(27 - p^2K_1)} \quad (68)$$

Note that break-in and break-away points $T^{(1)}$, $T^{(2)}$, and $T^{(3)}$ are functions of K_1p^2 and also p and K_1 parameters. To understand the highly nonlinear dependency of $T^{(1)}$, $T^{(2)}$, and $T^{(3)}$ on K_1p^2 , instead of $T^{(1)}$, $T^{(2)}$, and $T^{(3)}$ it would be better to draw the real and imaginary parts of the functions $\hat{T}^{(1)} \triangleq \frac{6K_1T^{(1)}}{\sqrt[3]{K_1p^2}}$, $\hat{T}^{(2)} \triangleq \frac{12K_1T^{(2)}}{\sqrt[3]{K_1p^2}}$ and $\hat{T}^{(3)} \triangleq \frac{12K_1T^{(3)}}{\sqrt[3]{K_1p^2}}$ as illustrated in Figure 5.4.

It is observed from Figure 5.4, $p^2K_1 > 27$ is obtained as necessary condition for the existence of bistability since only real and positive $T^{(1)}$, $T^{(2)}$, and $T^{(3)}$ values define break-in and break-away points. The condition $p^2K_1 > 27$ can be seen to coincide with the one obtained in the discriminant based analysis of Chapter 4.

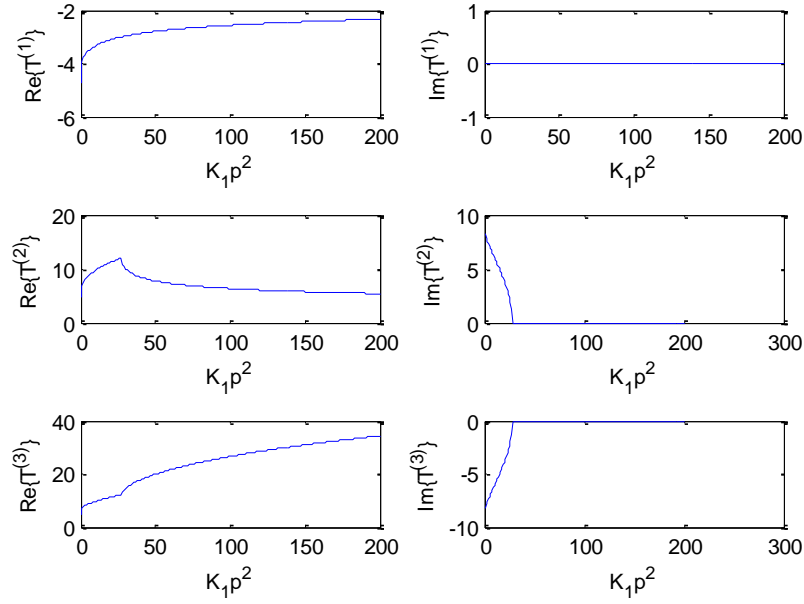


Figure 5.4 The real and imaginary parts of the scaled break-in and break-away points, $\hat{T}^{(1)}$, $\hat{T}^{(2)}$ and $\hat{T}^{(3)}$, for different p^2K_1 parameter.

The analytical expressions of the upper and lower limits of K , K^u and K^l respectively, derived by a similar procedure in Chapter 5.1 are given in Equation (69)-(70).

$$K^u = -\frac{K_1(T^{(2)})^3 - pK_1(T^{(2)})^2 - p}{T^{(2)}} \quad (69)$$

$$K^l = -\frac{K_1(T^{(3)})^3 - pK_1(T^{(3)})^2 - p}{T^{(3)}} \quad (70)$$

where $T^{(2)}$ and $T^{(3)}$ are defined in Equations (65)-(66).

A gallery of root locus diagrams obtained by Matlab for different K_1 and p values yielding the existence or non-existence of the break-in and break-away points are given in Figure 5.5. Figure 5.5.a-c correspond to the case of a constant $K_1 = 0.02$ and three different p values with $p^2K_1 < 27$, $p^2K_1 = 27$, and $p^2K_1 > 27$. Figure 5.5.d-f correspond to the case of a constant $p = 150$ and three different K_1 values

again with $p^2 K_1 < 27$, $p^2 K_1 = 27$, and $p^2 K_1 > 27$. Note that Figure 5.5.c and f only have an interval of K providing the bistability.

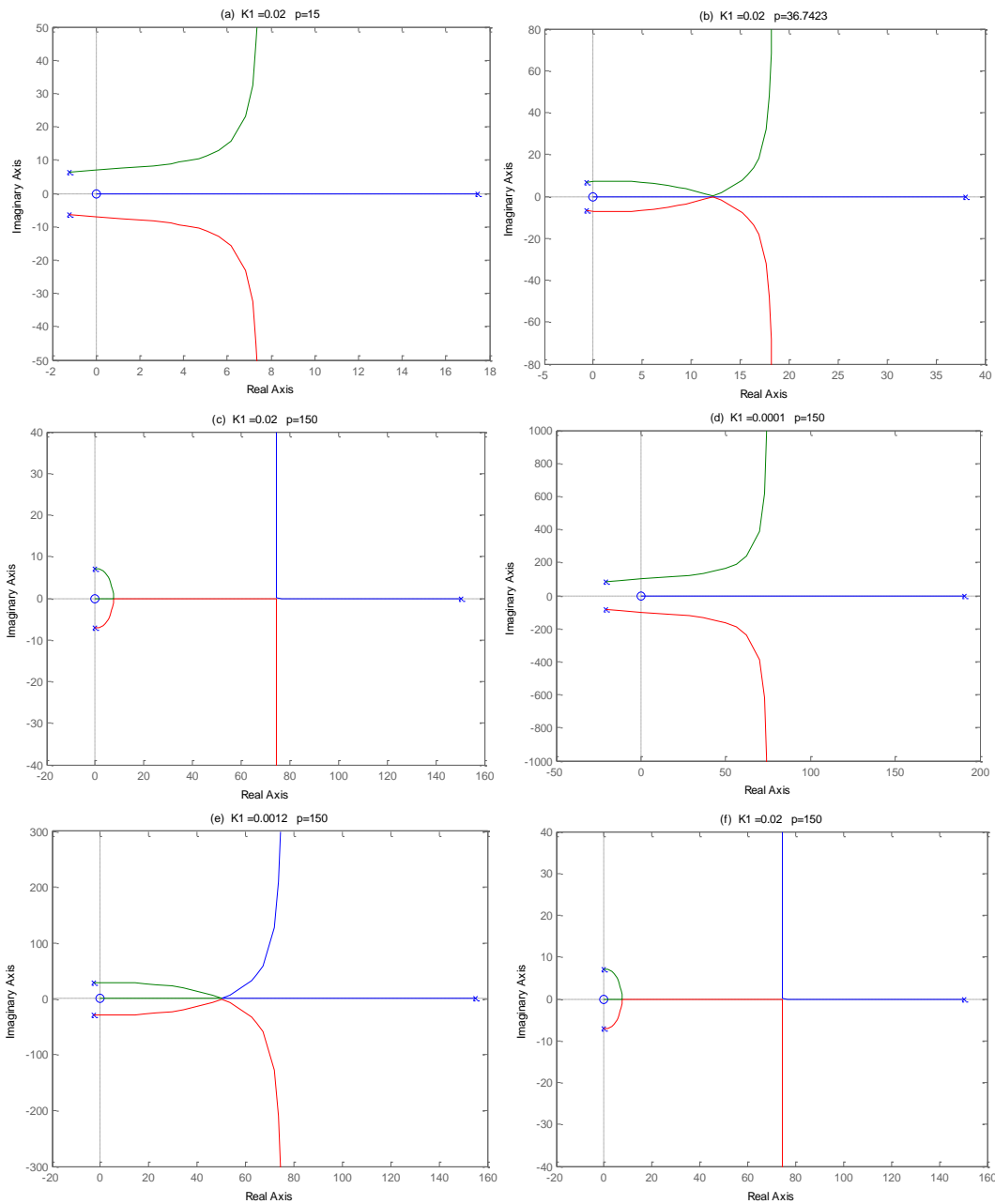


Figure 5.5 The root locus for K parameter with different $p^2 K_1$ values

5.3 Root Locus for K_1 Parameter

Chapter 5.3 provides the root locus analysis now for K_1 parameter. For this purpose, the equilibrium equation in (24) is rewritten in the characteristic equation form with respect to K_1 in Equation (71):

$$1 + K_1 \frac{T^3 - pT^2}{KT - p} = 0 \quad (71)$$

The numerator has a double root at $T = 0$ and a real root at $T = p$. However, the denominator has only one real root which is at $T = \frac{p}{K}$ whereas the numerator has three real roots.

$$T_N^{(1,2)} = 0 \quad (72)$$

$$T_N^{(3)} = p \quad (73)$$

$$T_D^{(1)} = \frac{p}{K} \quad (74)$$

The break-in and break-away points which are the extrema of K_1 with respect to T can be calculated in terms K and p parameters as follows.

$$\frac{d}{dT} \left\{ \frac{p - KT}{T^3 - pT^2} \right\} = \frac{T(2KT^2 - pT(3 + K) + 2p^2)}{(T^3 - pT^2)^2} = 0 \quad (75)$$

The first break-in / break-away point in Equation (76) is equal to zero. The other two break-in / break-away points in Equation (77) are the roots of the second order numerator polynomial equation $2KT^2 - pT(3 + K) + 2p^2 = 0$.

$$T^{(1)} = 0 \quad (76)$$

$$\begin{aligned}
T^{(2,3)} &= \frac{p(3+K) \pm \sqrt{p^2(3+K)^2 - 16p^2K}}{8K} = \frac{p(3+K) \pm p\sqrt{K^2 - 10K + 9}}{8K} \\
&= \frac{p(3+K) \pm p\sqrt{(K-9)(K-1)}}{8K} \tag{77}
\end{aligned}$$

To have real $T^{(2,3)}$ defining the break-in / break-away points and the bistability interval of K_1 , $(K-9)(K-1)$ should be strictly positive. Hence, $K > 9$ is obtained again as a necessary condition for bistability. The second possibility $0 < K < 1$ does not belong to the bistability region for K_1 since such K values yield negative K_1 values in Equations (78)-(79) at the break-in / break-away points. Hence, K_1^l and K_1^u represent the upper and lower limits of the bistability interval for K_1 parameter. K_1^l and K_1^u are obtained by substituting $T^{(2)}$ and $T^{(3)}$ in the equation $K_1 = \frac{p-KT}{T^3-pT^2}$ as given below.

$$\begin{aligned}
K_1^l &= \frac{p - K \frac{p(3+K) - p\sqrt{(K-9)(K-1)}}{8K}}{\left(\frac{p(3+K) - p\sqrt{(K-9)(K-1)}}{8K}\right)^2 \left(\frac{p(3+K) - p\sqrt{(K-9)(K-1)}}{8K} - p\right)} \\
&= \frac{64K^3}{p^2} \frac{5 - K + \sqrt{(K-9)(K-1)}}{(3+K - \sqrt{(K-9)(K-1)})^2 (3 - 7K - \sqrt{(K-9)(K-1)})} \tag{78}
\end{aligned}$$

$$\begin{aligned}
K_1^u &= \frac{p - K \frac{p(3+K) + p\sqrt{(K-9)(K-1)}}{8K}}{\left(\frac{p(3+K) + p\sqrt{(K-9)(K-1)}}{8K}\right)^2 \left(\frac{p(3+K) + p\sqrt{(K-9)(K-1)}}{8K} - p\right)} \\
&= \frac{64K^3}{p^2} \frac{5 - K - \sqrt{(K-9)(K-1)}}{(3+K + \sqrt{(K-9)(K-1)})^2 (3 - 7K + \sqrt{(K-9)(K-1)})} \tag{79}
\end{aligned}$$

Choosing $K = 167.1$ and $p = 250$ which are known to ensure the bistability at least for some specific K_1 value, for instance $K_1 = 0.02$, the root locus diagram for

the K_1 is drawn by using Matlab as in Figure 5.6. For these considered values of K and p parameters, the bistability region is determined as $K_1 \in (0.0106, 0.1130)$ from the root locus and also from Equations (78)-(79).

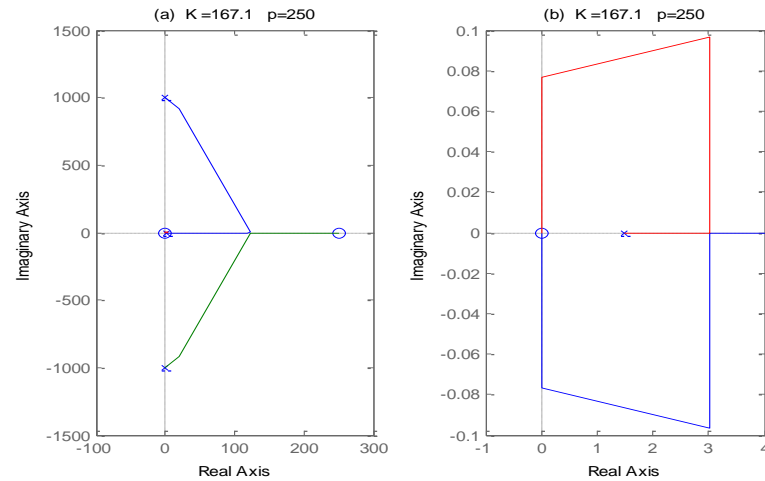
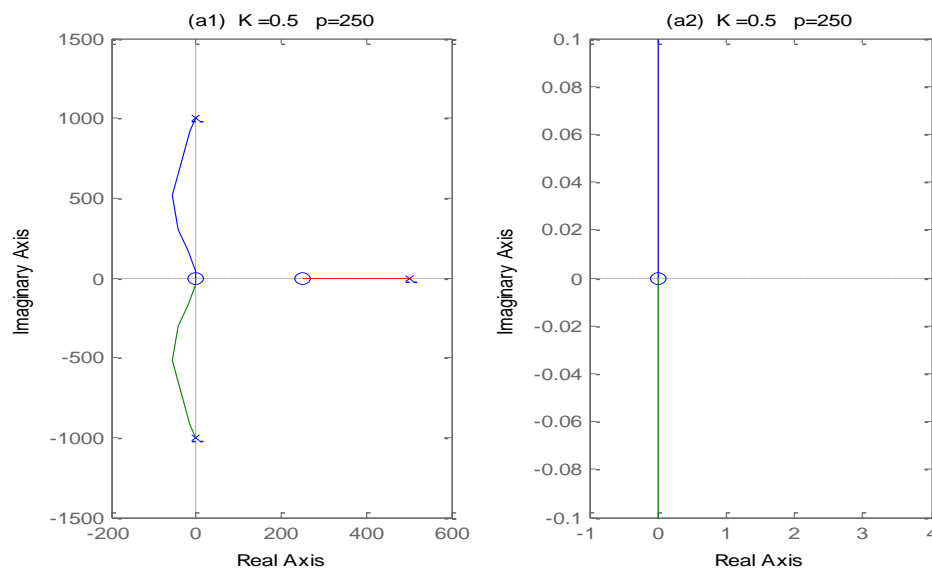


Figure 5.6 a. The root locus for K_1 parameter when $K = 167.1$ and $p = 250$, b. Zoomed in root locus visualizing the portion of the diagram around the break-away point.

A selection of root locus diagrams for K_1 obtained by Matlab with a fixed p and different K values yielding the existence or non-existence of the break-in and break-away points are given in Figure 5.7.



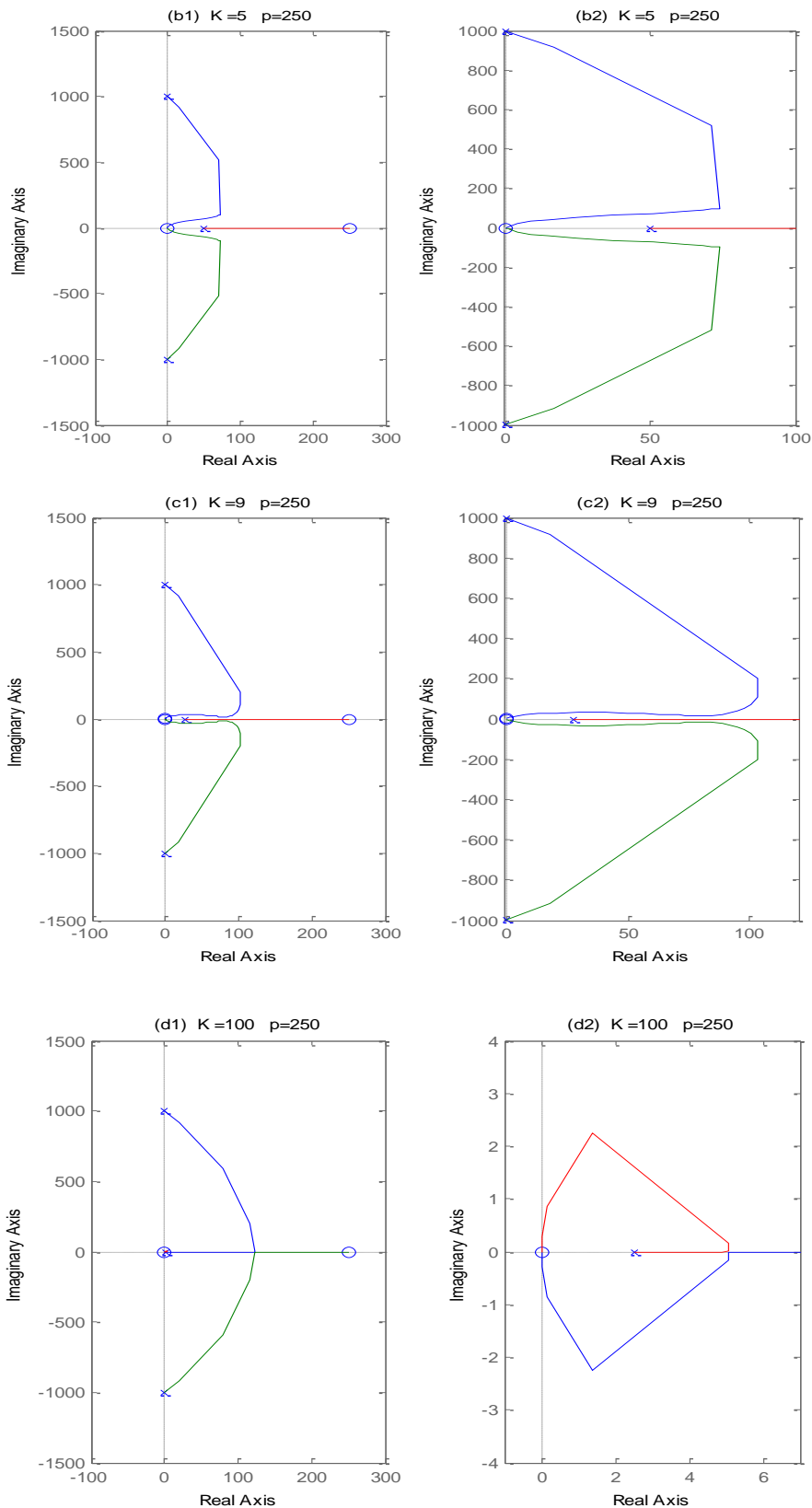


Figure 5.7 a., c., e., g. The root locus for K_1 with a fixed $p = 250$ and different K values b., d., f., h., Zoomed in versions of the root locus diagrams in a., c., e., and g.

5.4 Integration of One-Parameter Root Locus Analysis Results

The bistability conditions derived by root locus in Chapter 5.1-5.3, are obtained for one-parameter only, *i.e.* for $q \in \{p, K, K_1\}$. Each of these conditions defines actually a one-dimensional bistability region by considering one of the parameters as free and holding the other two fixed. The upper and lower limits of the bistability interval for a specific parameter are functions of the other two parameters. Considering the dependency of the limits of the bistability intervals associated with specific q parameters on the rest \bar{q} of the parameters and combining all of the obtained conditions, three-dimensional bistability region in $p - K - K_1$ space and also its two-dimensional intersections with certain planes determined by holding a parameter in \bar{q} as fixed can be constructed. With the integration of all bistability conditions, the complete bistability region is given algebraically as in Equation (80) and graphically as shown in Figure 5.8.

$$\widehat{\mathfrak{R}}_{bi} \triangleq \{(p, K, K_1) \in \mathbb{R}^3 | p^l < p < p^u, K_1^l < K_1 < K_1^u, K^l < K < K^u, p^2 K_1 > 27, p > 0, K > 9, K_1 > 0\} \quad (80)$$

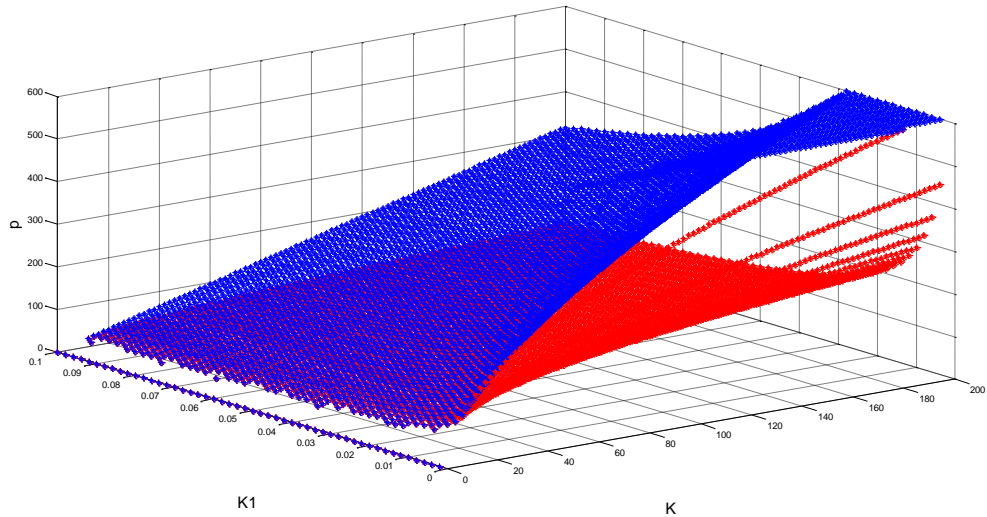


Figure 5.8 Bistability region in $p - K - K_1$ space.

Some two-dimensional intersections of the bistability region $\widehat{\mathfrak{R}}_{bi}$ with certain planes defined by keeping one of p , K , or K_1 are constant given in Figure 5.9 and Figure 5.10.

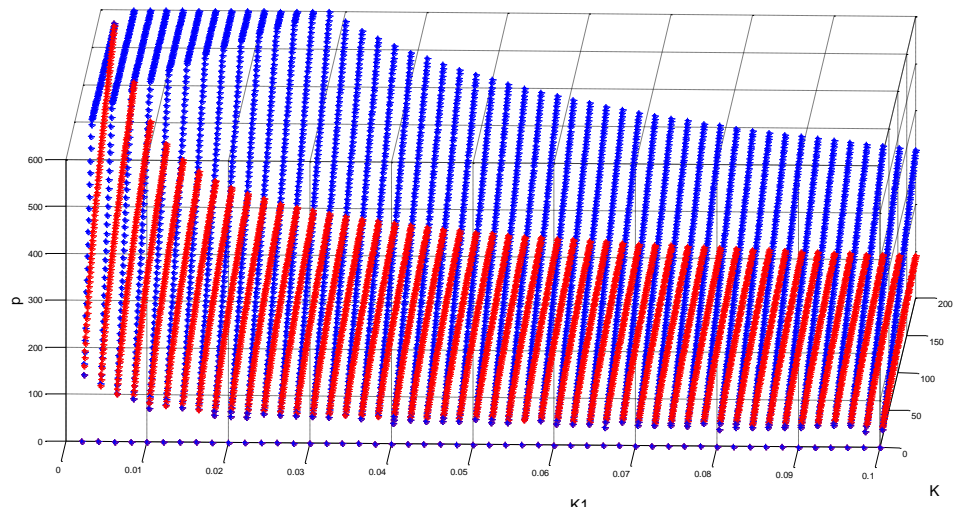


Figure 5.9 2D intersection of bistability region in $p - K - K_1$ space.

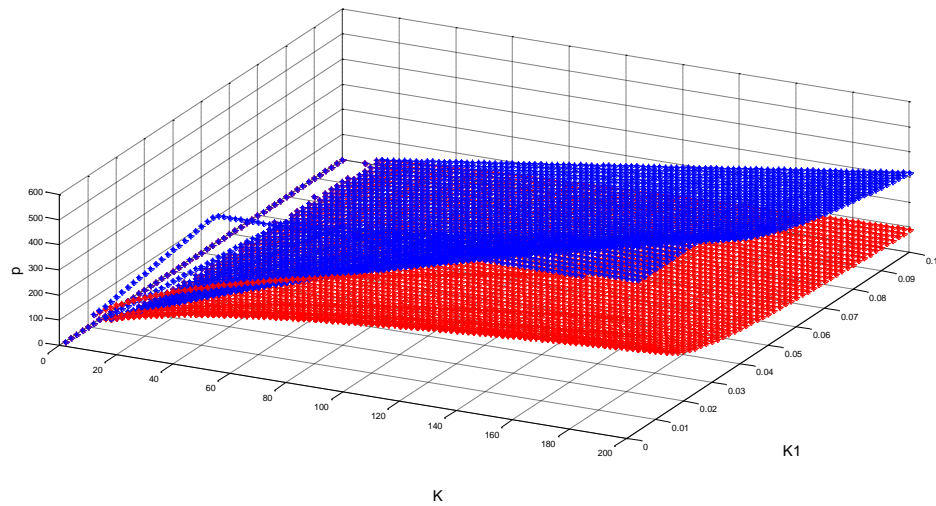


Figure 5.10 2D intersection of bistability region in $p - K - K_1$ space.

Using the expression of p^l and p^u given in (54)-(55), the bistability range of p parameter can be depicted as a function of K and K_1 parameters. For three specific values of K_1 such as 0.005, 0.02, and 0.05, the corresponding bistability regions in the two dimensional parameter space of $K - p$ are then shown as in Figure 5.11. Note that the larger the K_1 value, the smaller the upper limit p^u , the smaller the lower limit p^l and also the narrower the (p^l, p^u) interval of p parameter are obtained.

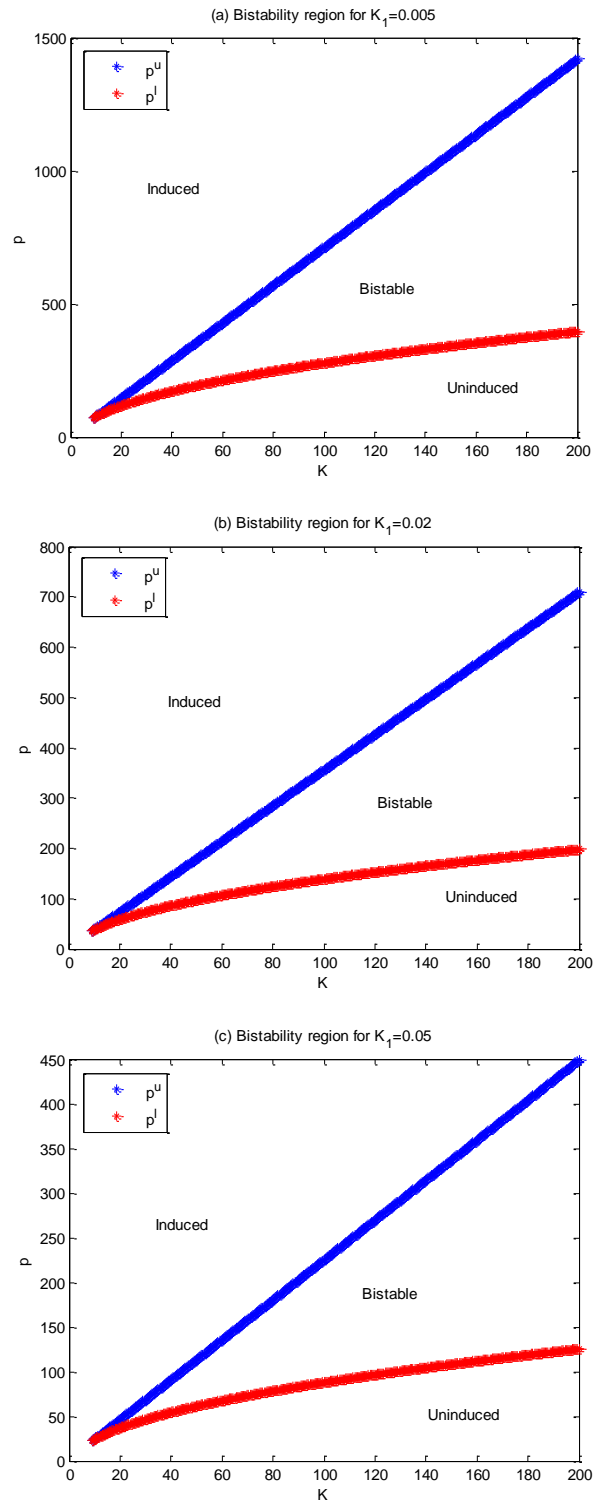


Figure 5.11 The bistability region in $p - K$ space for different K_1 values

Using the upper and lower limits of K_1 in (78)-(79), the bistability regions in $K - K_1$ plane for some p values such as 10, 150, and 300 are drawn in Figure 5.12. Note that the apex of the bistability region takes place at $K = 9$.

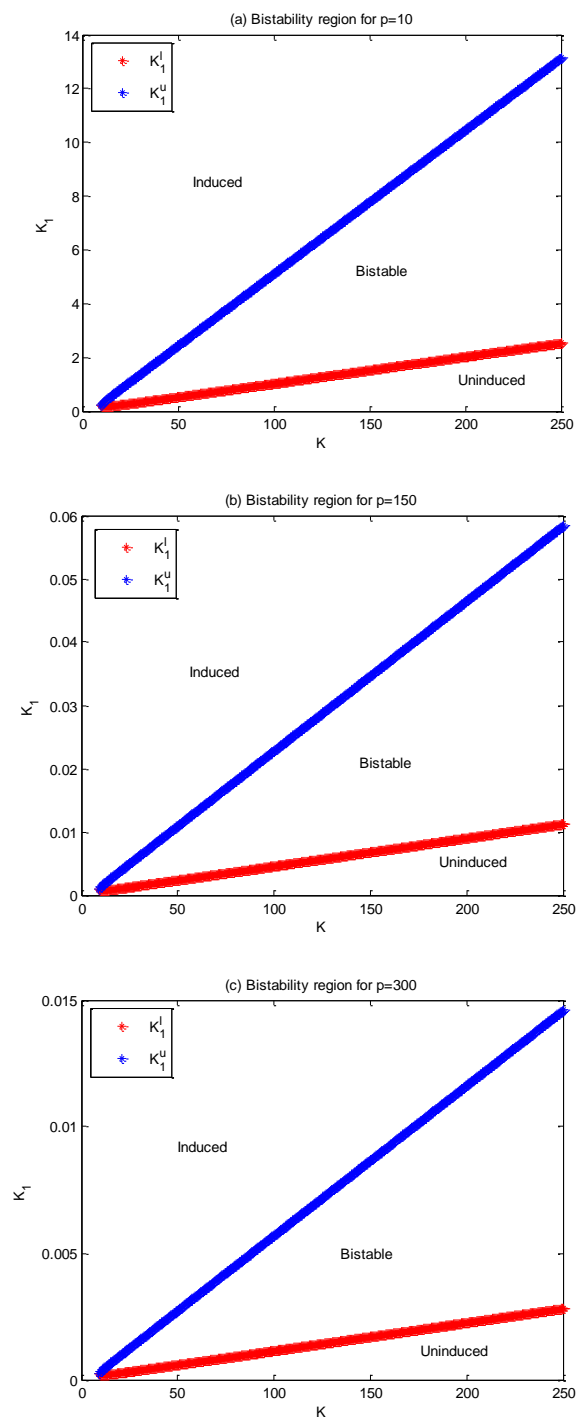


Figure 5.12 The bistability region in $K_1 - K$ space for different p values

5.5 Interpretation of the Bistability Interval for p in Terms of Physical Model Parameters

The analyses in previous chapters confirm the same bistability conditions. It is interesting to note that $K > 9$ is derived in the literature (Özbudak et al., 2004; van Hoek & Hogeweg, 2006) as the bistability condition for different lac operon models. As a result of both the discriminant and root-locus analysis employed, a bistability condition other than $K > 9$ becomes valid when only $p^2 K_1 > 27$. For these cases, the boundary for the bistability region is derived by considering the two real roots such that one of them is double. This derivation is performed in Chapter 4 by calculating the discriminant of the polynomial in (24) and also in Chapter 5 by applying the root locus method.

In the literature, the bistability region is given commonly in $G_e - T_e$ space, namely in terms of external glucose and TMG concentrations, not in the $p - K - K_1$ parameter space. Since p parameter is a function of G_e and T_e as expressed in Equation (81), then the bistability region in the $G_e - T_e$ space can be identified by determining the limits T_e^l and T_e^u corresponding to the p^l and p^u limits. Exploiting the invertibility of $f_{T,T_e}(T_e) = \frac{T_e}{K_{T_e} + T_e}$ for T_e , the T_e^l and T_e^u limits are derived as a function of G_e as in Equations (82)-(83).

$$p \triangleq \frac{\alpha_T}{\gamma_T} \frac{\alpha_P}{\gamma_P} \frac{\alpha_M}{\gamma_M} f_{T,T_e}(T_e) f_{T,G_e}(G_e) f_{M,G_e}(G_e) \quad (81)$$

$$T_e^u = K_{T_e} \frac{f_{T,T_e}^u(T_e)}{1 - f_{T,T_e}^u(T_e)} = \frac{p^u \gamma_T \gamma_P \gamma_M}{\alpha_T \alpha_P \alpha_M f_{T,G_e}(G_e) f_{M,G_e}(G_e) - p^u \gamma_T \gamma_P \gamma_M} \quad (82)$$

$$T_e^l = K_{T_e} \frac{f_{T,T_e}^l(T_e)}{1 - f_{T,T_e}^l(T_e)} = \frac{p^l \gamma_T \gamma_P \gamma_M}{\alpha_T \alpha_P \alpha_M f_{T,G_e}(G_e) f_{M,G_e}(G_e) - p^l \gamma_T \gamma_P \gamma_M} \quad (83)$$

Herein, the $G_e - T_e$ plot obtained by using Equations (82)-(83) is drawn in Figure 5.13 (Özbudak et al., 2004; Yıldırım et al., 2004).

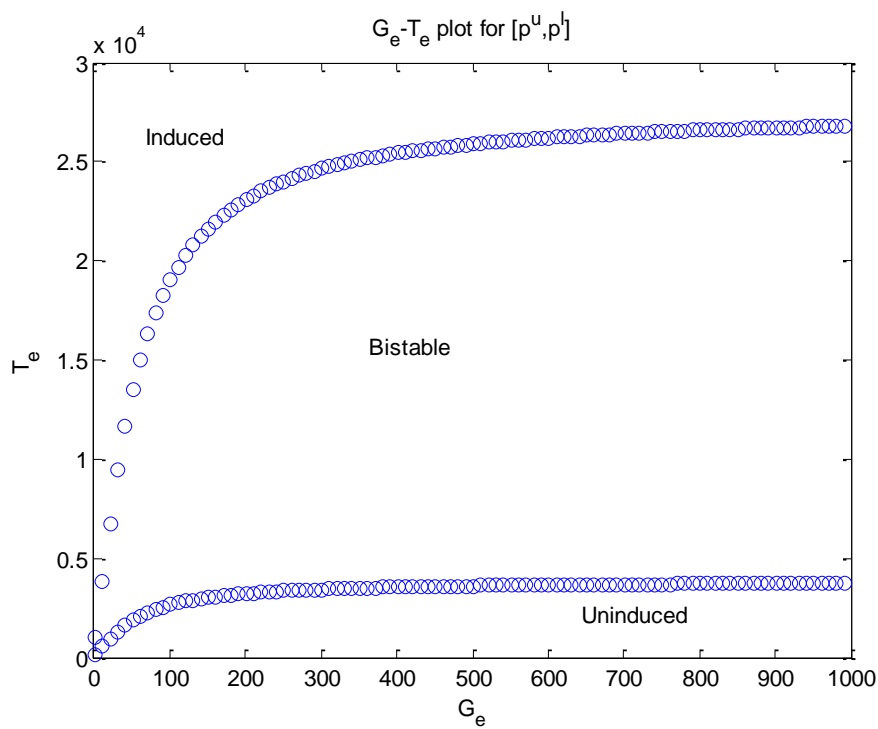


Figure 5.13 The bistability region in $G_e - T_e$ space

CHAPTER SIX
ROOT LOCUS BASED BISTABILITY ANALYSIS OF THE LAC OPERON
MODEL WITH TRANSACETYLASE EFFECT

The lac operon of *E. coli* is a well-studied transcriptional regulatory network in the systems biology. In the last decade, much attention has been given to the bistability behavior of the lac operon. Despite the fact that the operon consists of three structural genes, the mechanism of the lac operon is generally analyzed through only two of them. The gene product of lacA, GAT, has not been taken into consideration in the bistability studies. In the previous chapters, the effects of the GAT on the bistability behavior of lac operon is ignored. In Chapter 6, the effect of GAT on the bistability range of lac operon is examined by employing root locus analysis method to the higher order equilibrium equation. In the model with transacetylase effect, bi-bi ordered kinetics and also Michaelis-Menten kinetics were used for acetylation of the artificial inducer, (TMG), by GAT. The range of the unified parameters ensuring the bistable behavior of the lac operon was found to be slightly affected by the transacetylase.

6.1 A Mathematical Model with Transacetylase Effect

The mathematical model describing the regulation mechanism of the lac operon is developed in the presence of both glucose and TMG and in the absence of lactose to determine the effect of transacetylase to the bistability dynamics. The model in Chapter 6 consists of the terms related with the synthesis of the gene products, uptake of TMG into the cell, degradation / dilution of gene products. This model also includes the acetylation of TMG by β -galactosidase to determine the effect of the third enzyme of the lac operon. The catabolite repression and inducer exclusion effects of the external glucose, respectively, to the synthesis of mRNA and uptake of TMG by permease also are defined in the models. The model is composed of four differential equations that respectively account for the temporal changes on the concentration of mRNA (M), permease (P), transacetylase (G), and TMG (T).

$$\frac{dM}{dt} = \alpha_M f_{M,T}(T) f_{M,G_e}(G_e) - \gamma_M M \quad (84)$$

$$\frac{dP}{dt} = \alpha_P M - \gamma_P P \quad (85)$$

$$\frac{dG}{dt} = \alpha_G M - \gamma_G G \quad (86)$$

$$\frac{dT}{dt} = \alpha_T f_{T,T_e}(T_e) f_{T,G_e}(G_e) P - f_{T,G}(T) G - \gamma_T T \quad (87)$$

where $f_{M,T}(T)$, $f_{M,G_e}(G_e)$, $f_{T,T_e}(T_e)$, $f_{T,G_e}(G_e)$ are the same as in (1)-(3). Similar to the model in (1)-(3), the γ_i is the composition of the active degradation, $\bar{\gamma}_i$, and the dilution due to growth rate, μ_i . The parameters α_i with $i \in \{M, P, T\}$ denote the production constants of the gene products.

$f_{T,G}(T)$ is the acetylation of the artificial inducer TMG by GAT and bi-bi ordered kinetic is used to model this reaction as given below (Musso & Zabin, 1973).

$$f_{T,G}(T) = \frac{C_1 T - C_2}{C_3 + C_4 T} \quad (88)$$

At the steady-state which means the temporal changes on the concentration of M , P , G , and T are constant, it is known that $dM/dt = dP/dt = dG/dt = dT/dt = 0$. The equilibrium equations for three state variables of the lac operon model, M , P , and G , are derived in Equations (90), (92), and (94).

$$\frac{dM}{dt} = \alpha_M f_{M,T}(T) f_{M,G_e}(G_e) - \tilde{\gamma}_M M = 0 \quad (89)$$

$$M = \frac{\alpha_M}{\tilde{\gamma}_M} f_{M,T}(T) f_{M,G_e}(G_e) \quad (90)$$

$$\frac{dP}{dt} = \alpha_P M - \tilde{\gamma}_P P = 0 \quad (91)$$

$$P = \frac{\alpha_P}{\tilde{\gamma}_P} M = \frac{\alpha_P}{\tilde{\gamma}_P} \frac{\alpha_M}{\tilde{\gamma}_M} f_{M,T}(T) f_{M,G_e}(G_e) \quad (92)$$

$$\frac{dG}{dt} = \alpha_G M - \tilde{\gamma}_G G = 0 \quad (93)$$

$$G = \frac{\alpha_G}{\tilde{\gamma}_G} M = \frac{\alpha_G}{\tilde{\gamma}_G} \frac{\alpha_M}{\tilde{\gamma}_M} f_{M,T}(T) f_{M,G_e}(G_e) \quad (94)$$

Again, after setting the state variables M , P , G and T constant, the equilibrium equation of T can be obtained as given in Equation (96) by eliminating the equilibrium concentrations M , P , and G .

$$\frac{dT}{dt} = \alpha_T f_{T,T_e}(T_e) f_{T,G_e}(G_e) P - f_{T,G}(T) G - \tilde{\gamma}_T T = 0 \quad (95)$$

$$T^2 + \left(\frac{C_1}{C_4 \tilde{\gamma}_T} \frac{\alpha_G}{\tilde{\gamma}_G} \frac{\alpha_M}{\tilde{\gamma}_M} f_{M,G_e}(G_e) f_{M,T}(T) + \frac{C_3 \tilde{\gamma}_T}{C_4 \tilde{\gamma}_T} \right. \\ \left. - \frac{C_4}{C_4} \frac{\alpha_T}{\tilde{\gamma}_T} \frac{\alpha_P}{\tilde{\gamma}_P} \frac{\alpha_M}{\tilde{\gamma}_M} f_{T,T_e}(T_e) f_{T,G_e}(G_e) f_{M,G_e}(G_e) f_{M,T}(T) \right) T \\ - \frac{C_3}{C_4} \frac{\alpha_T}{\tilde{\gamma}_T} \frac{\alpha_P}{\tilde{\gamma}_P} \frac{\alpha_M}{\tilde{\gamma}_M} f_{T,T_e}(T_e) f_{T,G_e}(G_e) f_{M,G_e}(G_e) f_{M,T}(T) \\ - \frac{C_2}{C_4 \tilde{\gamma}_T} \frac{\alpha_G}{\tilde{\gamma}_G} \frac{\alpha_M}{\tilde{\gamma}_M} f_{M,G_e}(G_e) f_{M,T}(T) = 0 \quad (96)$$

When the state variables are constant, the equilibrium points characteristic equation is obtained to determine the equilibrium states of the system. In Equation (96), derived from Equations (84)-(87) at steady-state, some problems came up about the values of the unknown parameters. It is very difficult to define the exact parameter values due to the same reasons like the extensive experiment conditions and measurement inaccuracies. Because of these difficulties, the parameters are generally given in a range. To avoid the problems resulting from parameter uncertainty and simplify the equilibrium points characteristic equation, a new parameter, \hat{p} is defined in Equation (98) using the property that all the parameters in (96) are multipliers of each other. The p parameter includes the new \hat{p} parameter.

$$p \triangleq \frac{\alpha_T}{\tilde{\gamma}_T} \frac{\alpha_P}{\tilde{\gamma}_P} \frac{\alpha_M}{\tilde{\gamma}_M} f_{T,T_e}(T_e) f_{T,G_e}(G_e) f_{M,G_e}(G_e) \quad (97)$$

$$\hat{p} \triangleq \frac{\alpha_G \alpha_M}{\tilde{\gamma}_T \tilde{\gamma}_G \tilde{\gamma}_M} f_{M,G_e}(G_e) \quad (98)$$

The characteristic equilibrium equation is rewritten to obtain the simplest form as given below:

$$f_{M,T}(T) \left(\frac{C_1}{C_4} \hat{p} T - p T - \frac{C_3}{C_4} p - \frac{C_2}{C_4} \hat{p} \right) + T^2 + \frac{C_3}{C_4} T = 0 \quad (99)$$

where the function of mRNA transcription is given as $f_{M,T}(T) = \frac{1+K_1T^2}{K+K_1T^2}$. This function is substituted in (99).

$$\frac{1+K_1T^2}{K+K_1T^2} \left(\frac{C_1}{C_4} \hat{p} T - p T - \frac{C_3}{C_4} p - \frac{C_2}{C_4} \hat{p} \right) + T^2 + \frac{C_3}{C_4} T = 0 \quad (100)$$

As a result, the fourth order equilibrium equation is defined in Equation (101).

$$K_1 T^4 + \left(\frac{C_3}{C_4} K_1 + K_1 \frac{C_1 \hat{p} - C_4 p}{C_4} \right) T^3 + \left(K - \frac{C_3 p - C_2 \hat{p}}{C_4} K_1 \right) T^2 + \left(\frac{C_3}{C_4} K + \frac{C_1 \hat{p} - C_4 p}{C_4} \right) T - \frac{C_3 p - C_2 \hat{p}}{C_4} = 0 \quad (101)$$

To compare two different enzyme kinetics, the acetylation of the artificial inducer, (TMG), by GAT is rewritten in the form of Michaelis - Menten. The parameters are arranged as dual form in (102) and (103).

$$\frac{C_1 T - C_2}{C_3 + C_4 T} \Rightarrow \frac{\alpha_{TG} T}{K_{TG} + T} \quad (102)$$

$$\frac{C_1 T - C_2}{C_3 + C_4 T} \frac{1}{\frac{C_1}{C_4}} = \frac{\frac{C_1}{C_4} T - \frac{C_2}{C_4}}{\frac{C_3}{C_4} + T} \quad (103)$$

The parameters of two different acetylation reactions are derived as $C_2 = 0$, $\alpha_{TG} = \frac{C_1}{C_4}$, and $K_{TG} = \frac{C_3}{C_4}$. According to these equalities,

$$K_1 T^4 + \left(\frac{C_3}{C_4} K_1 + \left(\frac{C_1}{C_4} \hat{p} - p \right) K_1 \right) T^3 + \left(K - \left(\frac{C_3}{C_4} p - \frac{C_2}{C_4} \hat{p} \right) K_1 \right) T^2 + \left(\frac{C_3}{C_4} K + \frac{C_1}{C_4} \hat{p} - p \right) T - \left(\frac{C_3}{C_4} p - \frac{C_2}{C_4} \hat{p} \right) = 0 \quad (104)$$

When the acetylation of the artificial inducer, TMG, by GAT is defined as Michaelis - Menten form, the fourth order equilibrium points characteristic equation is defined in Equation (105).

$$K_1 T^4 + (K_1 + (\alpha_{TG} \hat{p} - p) K_1) T^3 + (K - p K_{TG} K_1) T^2 + (K_{TG} K + \alpha_{TG} \hat{p} - p) T - p K_{TG} = 0 \quad (105)$$

The model is also simplified as follows to determine the parameters for root locus analysis with Equation (106)-(110).

$$\alpha_T f_{T,T_e}(T_e) f_{T,G_e}(G_e) \underbrace{\frac{\alpha_P}{\tilde{Y}_P} M}_P - f_{T,G}(T) \underbrace{\frac{\alpha_G}{\tilde{Y}_G} M}_G - \tilde{Y}_T T = 0 \quad (106)$$

$$\left[\frac{\alpha_T \alpha_P}{\tilde{Y}_T \tilde{Y}_P} f_{T,T_e}(T_e) f_{T,G_e}(G_e) - f_{T,G}(T) \frac{\alpha_G}{\tilde{Y}_T \tilde{Y}_G} \right] \frac{\alpha_M}{\tilde{Y}_M} f_{M,G_e}(G_e) f_{M,T}(T) - T = 0 \quad (107)$$

$$[p - \hat{p} f_{T,G}(T)] f_{M,T}(T) - T = 0 \quad (108)$$

$$[p - \hat{p} f_{T,G}(T)] \frac{1 + K_1 T^2}{K + K_1 T^2} - T = 0 \quad (109)$$

$$K_1 T^4 + [K_1 \widehat{C}_3 + K_1 (\widehat{p} \widehat{C}_1 - p)] T^3 + [K - K_1 (p \widehat{C}_3 - \widehat{p} \widehat{C}_2)] T^2 + [K \widehat{C}_3 + \widehat{p} \widehat{C}_1 - p] T - [p \widehat{C}_3 - \widehat{p} \widehat{C}_2] = 0 \quad (110)$$

where, $\widehat{C}_1 = \frac{c_1}{c_4}$, $\widehat{C}_2 = \frac{c_2}{c_4}$ and $\widehat{C}_3 = \frac{c_3}{c_4}$. These parameter values are assumed as $\widehat{C}_1 = 31.5$, $\widehat{C}_2 = 0.7874$, and $\widehat{C}_3 = 7047$ (Musso & Zabin, 1973). The \widehat{p} is defined as equal to 80. It is chosen smaller than p parameter.

In the lac operon model with transacetylase effect, the parameters are defined as K_1 , K , \widehat{C}_1 , \widehat{C}_2 , \widehat{C}_3 , \widehat{p} , α_{TG} , and K_{TG} to define the bistability ranges by using root locus method. For the fourth order characteristic equilibrium equation, the discriminant analysis is not sufficient because the discriminant of the fourth order polynomial is the sixth order. There is no analytical formula for the roots of the sixth order polynomial. However, the root locus based bistability analysis method determines the bistability region of the parameter in a numerical way by using the break-in and break-away points.

6.2 Root Locus Analysis

In root locus analysis to determine the bistability ranges of parameter for the model with transacetylase effect, the characteristic equation is derived for bi-bi ordered reaction and Michaelis-Menten kinetics, respectively from Equation (110) and Equation (105). To define the differences on the bistability ranges for p , K and K_1 parameters, the bistability region are determined from the root locus plots for five different multiples of each new coefficients (between one percent to centuple). The changes are given in a tabular format for each parameter.

6.2.1 Root Locus for K Parameter

The root locus for K parameter is drawn for both of the acetylation kinetics to determine the effect of the tansacetylase in lac operon model.

In the root locus based bistability analysis, the characteristic equation of K parameter is defined as below for Michaelis-Menten kinetics.

$$1 + \frac{K(T^2 + K_{TG}T)}{K_1T^4 + K_1(K_{TG} - p + \alpha_{TG}\hat{p})T^3 - pK_1K_{TG}T^2 + (\alpha_{TG}\hat{p} - p)T - pK_{TG}} = 0 \quad (111)$$

The root locus of K parameter for the model without transacetylase effect is drawn in Figure 6.1 when $p = 250$ and $K_1 = 0.02$. Note that this p value is in the bistability region. To compare the bistability region of two models, the root locus of K parameter for the model with transacetylase effect is drawn when $p = 250$, $\hat{p} = 80$, $\alpha_{TG} = 120$, $K_{TG} = 1300000$, and $K_1 = 0.02$ in Figure 6.2. The third root locus plot of K parameter is drawn in Figure 6.3 for $p = 250$, $\hat{p} = 80$, $\alpha_{TG} = \widehat{C}_1$, $K_{TG} = \widehat{C}_3$, and $K_1 = 0.02$ to identify the changes on the bistability margins with respect to two different acetylation kinetics.

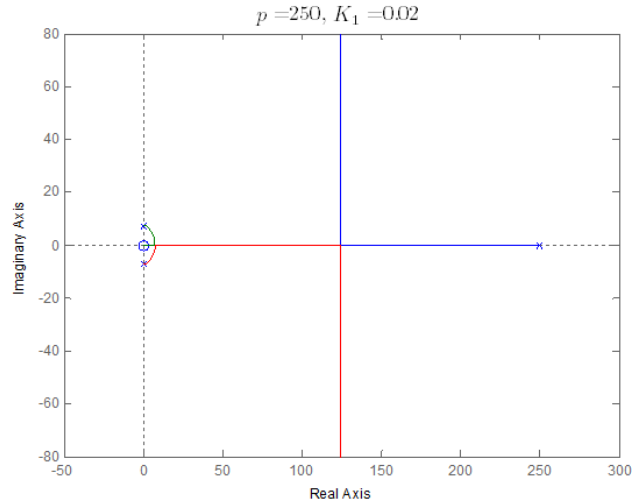


Figure 6.1 The root locus of K parameter for the model without transacetylase effect.

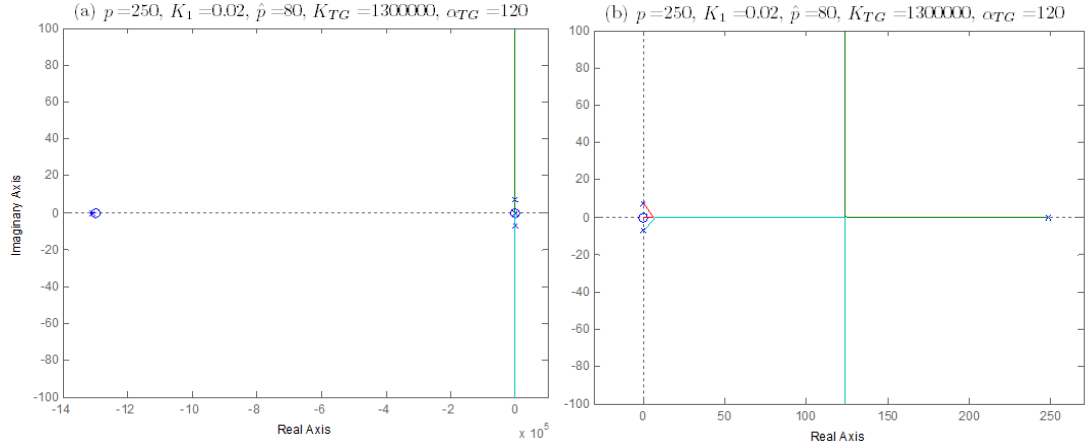


Figure 6.2 a. The root locus for K parameter when $p = 250$ and $K_1 = 0.02$ for Michaelis-Menten kinetics, b. Zoomed in root locus visualizing the portion of the diagram around the break-away point.

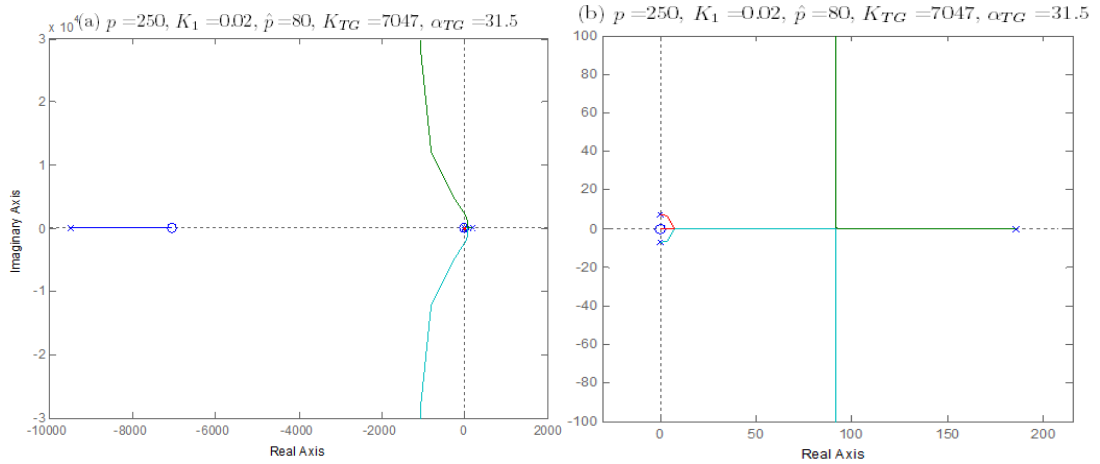


Figure 6.3 a. The root locus for K parameter when $p = 250$, $K_1 = 0.02$, $\hat{p} = 80$, $\alpha_{TG} = \widehat{C}_1$ and $K_{TG} = \widehat{C}_3$, b. Zoomed in root locus visualizing the portion of the diagram around the break-away point.

The bistability range for K parameter in the model without transacetylase effect when $p = 250$ and $K_1 = 0.02$ is determined as $K \in (69.8, 315)$ while this range is respectively $K \in (69.7, 312)$ and $K \in (68.9, 233)$ when $\alpha_{TG} = 120$, $K_{TG} = 1300000$ and $\alpha_{TG} = \widehat{C}_1$, $K_{TG} = \widehat{C}_3$.

The root locus for bi-bi ordered kinetics, the characteristic equation is defined in Equation (112). The root locus of K parameter in the model without transacetylase effect for bi-bi ordered acetylation kinetic is also drawn. In Figure 6.4, the

parameters have nominal values and in Figure 6.5, \widehat{C}_1 and \widehat{C}_3 have their nominal values but $\widehat{C}_2 = 0$ to compare the two different acetylation kinetics.

$$1 + \frac{K(T^2 + \widehat{C}_3 T)}{K_1 T^4 + K_1(\widehat{C}_3 - p + \widehat{p}\widehat{C}_1)T^3 - K_1(p\widehat{C}_3 + \widehat{p}\widehat{C}_2)T^2 + (\widehat{p}\widehat{C}_1 - p)T - (p\widehat{C}_3 + \widehat{p}\widehat{C}_2)} = 0 \quad (112)$$

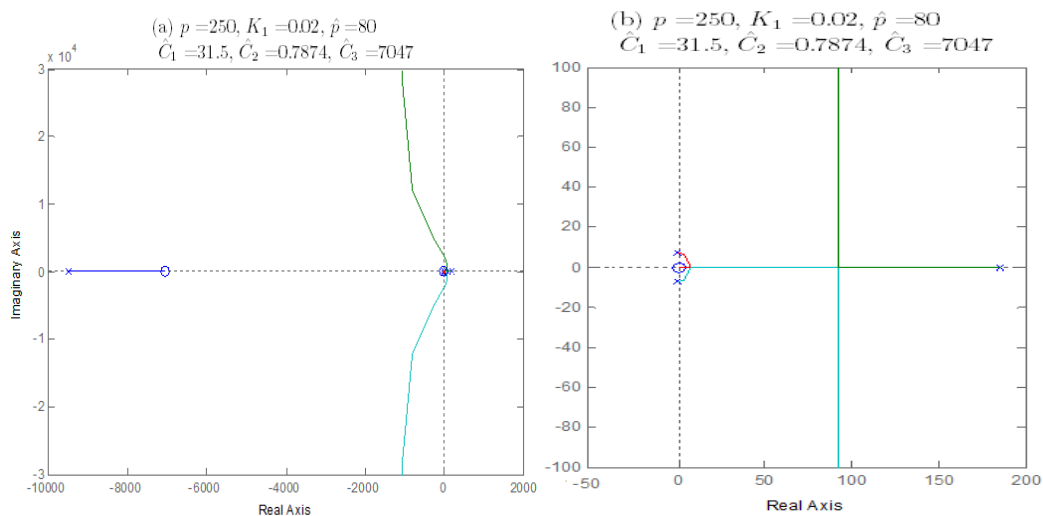


Figure 6.4 a. The root locus for K parameter when $p = 250$, $K_1 = 0.02$, $\widehat{p} = 80$, $\widehat{C}_1 = 31.5$, $\widehat{C}_2 = 0.7874$ and $\widehat{C}_3 = 7047$, b. Zoomed in root locus visualizing the portion of the diagram around the break-away point.

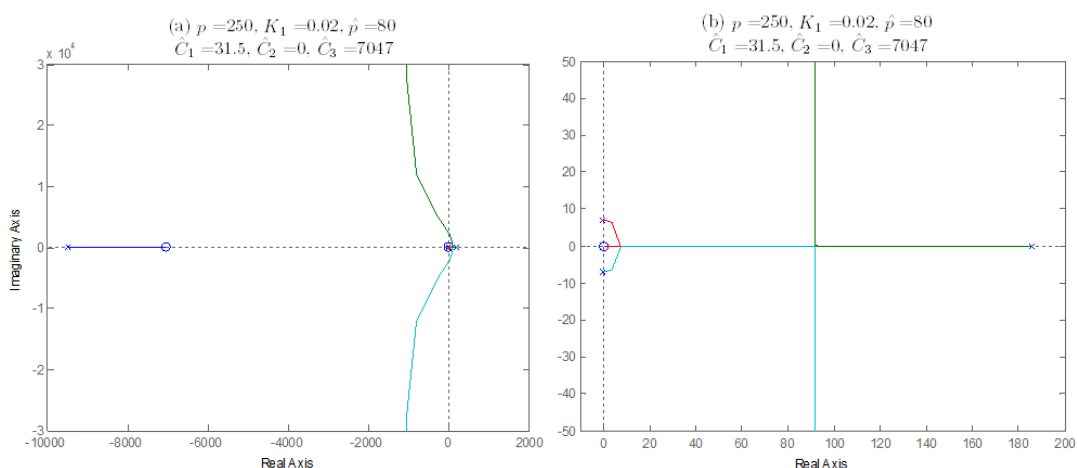


Figure 6.4 a. The root locus for K parameter when $p = 250$, $K_1 = 0.02$, $\widehat{p} = 80$, $\widehat{C}_1 = 31.5$, $\widehat{C}_2 = 0$ and $\widehat{C}_3 = 7047$, b. Zoomed in root locus visualizing the portion of the diagram around the break-away point.

The bistability ranges for K parameter in model with bi-bi ordered kinetic are determined as the same $K \in (68.9, 233)$ when $\widehat{C}_2 = 0.7874$ and $\widehat{C}_2 = 0$.

The root locus plots for five different multiples of each $\widehat{C}_1, \widehat{C}_2, \widehat{C}_3, \alpha_{TG}, K_{TG}$ and \hat{p} parameter are drawn and the K^l and K^u are determined as given below.

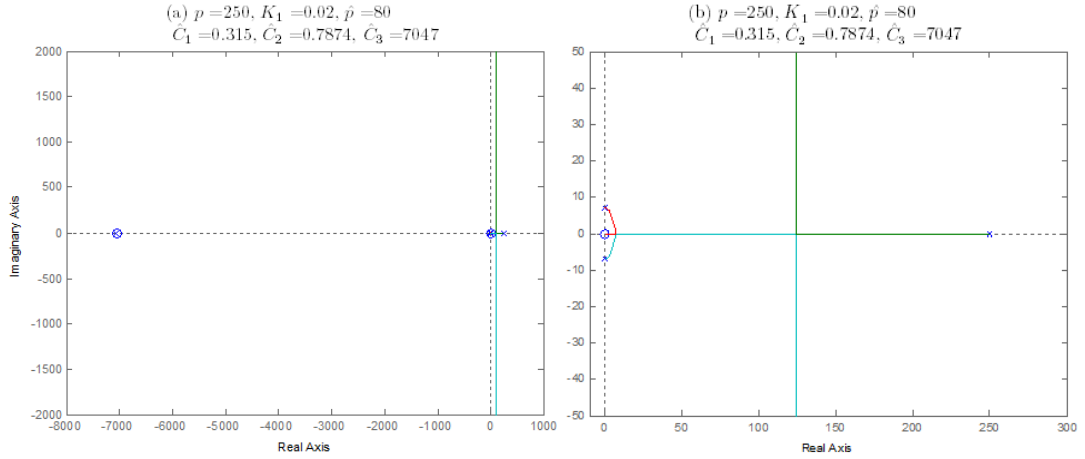


Figure 6.5 a. The root locus for K parameter when $p = 250, K_1 = 0.02, \hat{p} = 80, \widehat{C}_1 = 0.315, \widehat{C}_2 = 0.7874$ and $\widehat{C}_3 = 7047$, b. Zoomed in root locus visualizing the portion of the diagram around the break-away point.

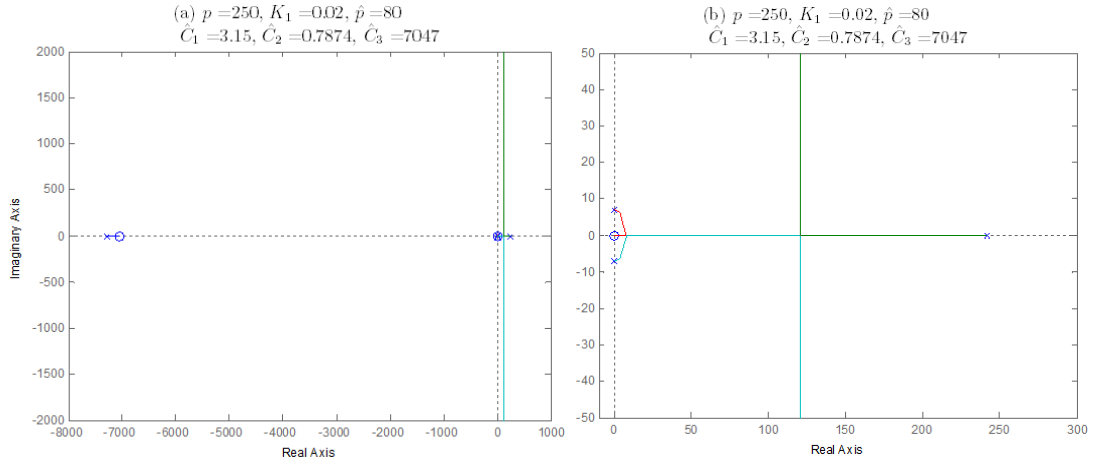


Figure 6.6 a. The root locus for K parameter when $p = 250, K_1 = 0.02, \hat{p} = 80, \widehat{C}_1 = 3.15, \widehat{C}_2 = 0.7874$ and $\widehat{C}_3 = 7047$, b. Zoomed in root locus visualizing the portion of the diagram around the break-away point.

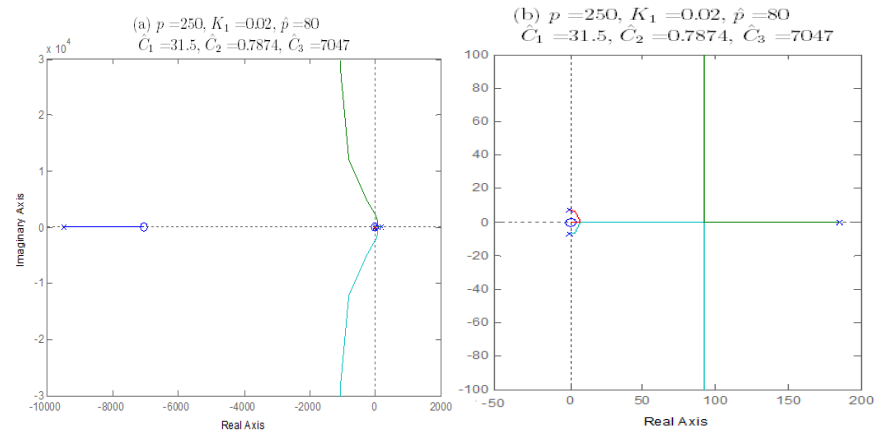


Figure 6.7 a. The root locus for K parameter when $p = 250, K_1 = 0.02, \hat{p} = 80, \widehat{C}_1 = 31.5, \widehat{C}_2 = 0.7874$ and $\widehat{C}_3 = 7047$, b. Zoomed in root locus visualizing the portion of the diagram around the break-away point.

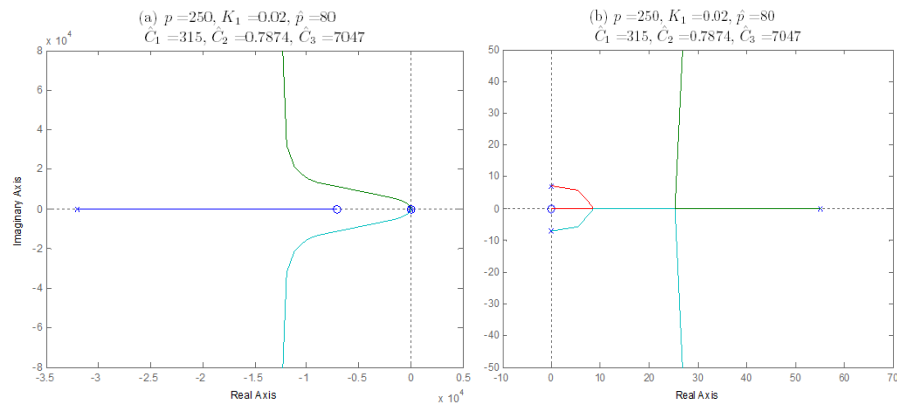


Figure 6.8 a. The root locus for K parameter when $p = 250, K_1 = 0.02, \hat{p} = 80, \widehat{C}_1 = 315, \widehat{C}_2 = 0.7874$ and $\widehat{C}_3 = 7047$, b. Zoomed in root locus visualizing the portion of the diagram around the break-away point.

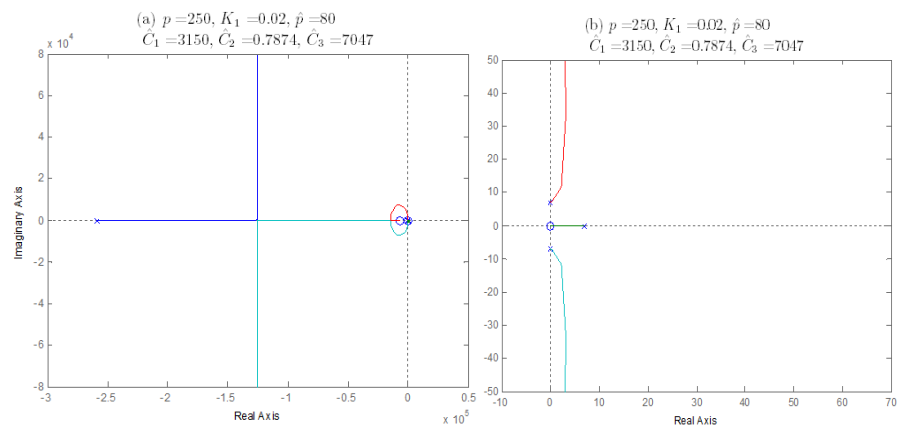


Figure 6.9 a. The root locus for K parameter when $p = 250, K_1 = 0.02, \hat{p} = 80, \widehat{C}_1 = 3150, \widehat{C}_2 = 0.7874$ and $\widehat{C}_3 = 7047$, b. Zoomed in root locus visualizing the portion of the diagram around the break-away point.

Table 6.1 The upper and lower limits of K parameter for different \widehat{C}_1 values

\widehat{C}_1	K^l	K^u
0.315	69.7	313
3.15	69.6	304
31.5	68.9	233
315	61.7	74.4
3150	No	No

While the upper limit of the K parameter is changing, the lower limit is almost constant.

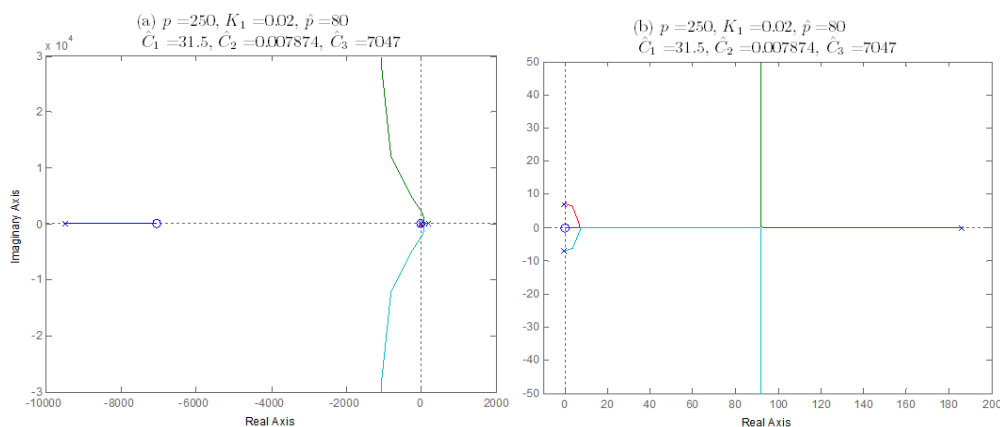


Figure 6.10 a. The root locus for K parameter when $\widehat{C}_2 = 0.007874$ the others are equal to nominal values, b. Zoomed in root locus visualizing the portion of the diagram around the break-away point.

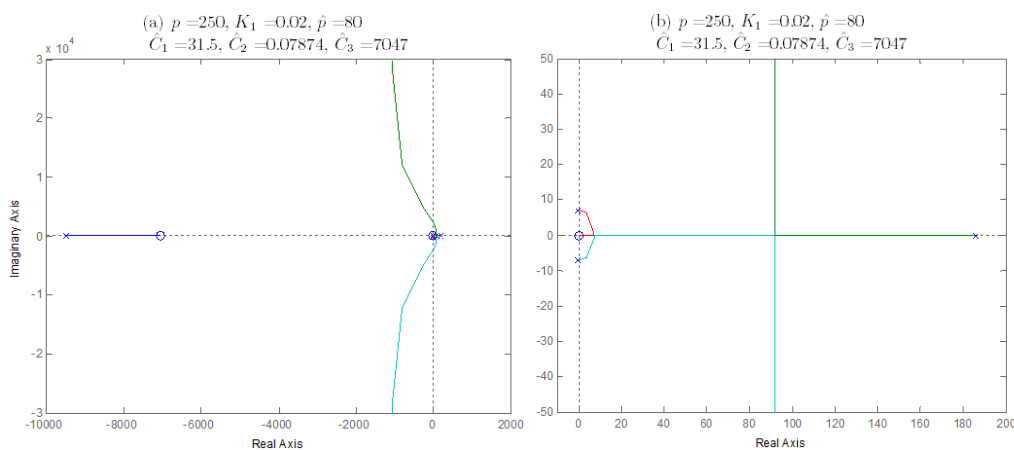


Figure 6.11 a. The root locus for K parameter when $p = 250$, $K_1 = 0.02$, $\hat{p} = 80$, $\widehat{C}_1 = 31.5$, $\widehat{C}_2 = 0.07874$ and $\widehat{C}_3 = 7047$, b. Zoomed in root locus visualizing the portion of the diagram around the break-away point.

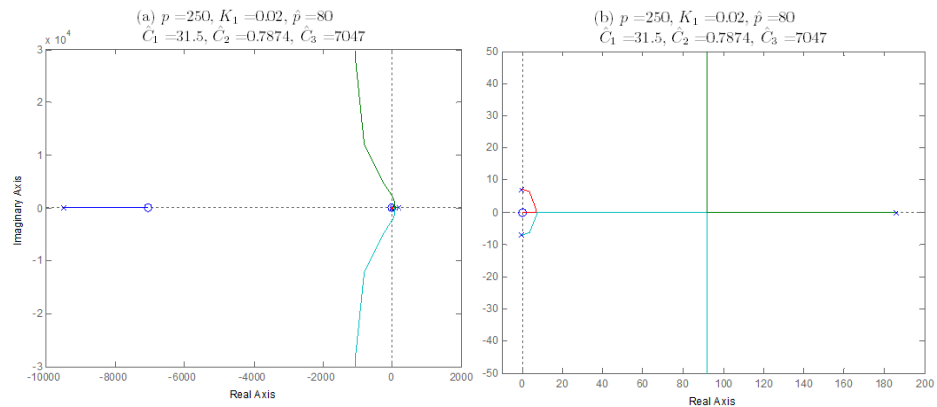


Figure 6.12 a. The root locus for K parameter when $p = 250, K_1 = 0.02, \hat{p} = 80, \widehat{C}_1 = 31.5, \widehat{C}_2 = 0.7874$ and $\widehat{C}_3 = 7047$, b. Zoomed in root locus visualizing the portion of the diagram around the break-away point.

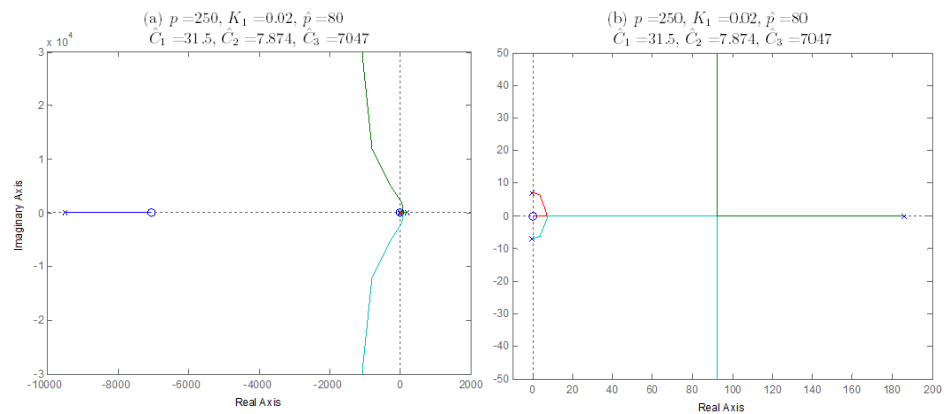


Figure 6.13 a. The root locus for K parameter when $p = 250, K_1 = 0.02, \hat{p} = 80, \widehat{C}_1 = 31.5, \widehat{C}_2 = 7.874$ and $\widehat{C}_3 = 7047$, b. Zoomed in root locus visualizing the portion of the diagram around the break-away point.

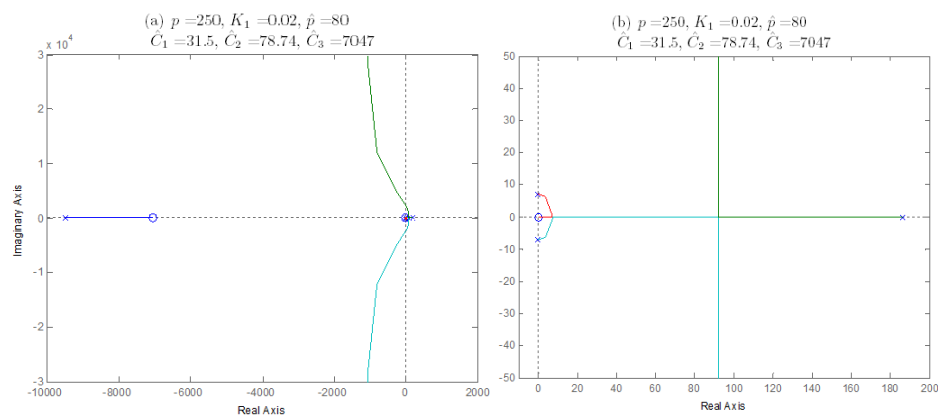


Figure 6.14 a. The root locus for K parameter when $p = 250, K_1 = 0.02, \hat{p} = 80, \widehat{C}_1 = 31.5, \widehat{C}_2 = 78.74$ and $\widehat{C}_3 = 7047$, b. Zoomed in root locus visualizing the portion of the diagram around the break-away point.

Table 6.2 The upper and lower limits of K parameter for different \widehat{C}_2 values

\widehat{C}_2	K^l	K^u
0.007874	68.9	233
0.07874	68.9	233
0.7874	68.9	233
7.874	69	233
78.74	69.2	235

While the upper limit of the K parameter almost constant, the lower limit changes a small amount for different \widehat{C}_2 values.

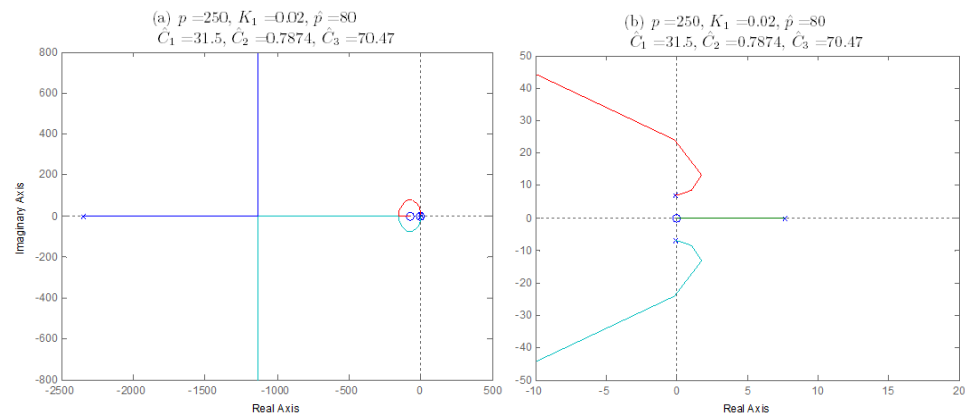


Figure 6.15 a. The root locus for K parameter when $p = 250$, $K_1 = 0.02$, $\hat{p} = 80$, $\widehat{C}_1 = 31.5$, $\widehat{C}_2 = 0.7874$ and $\widehat{C}_3 = 70.47$, b. Zoomed in root locus visualizing the portion of the diagram around the break-away point.

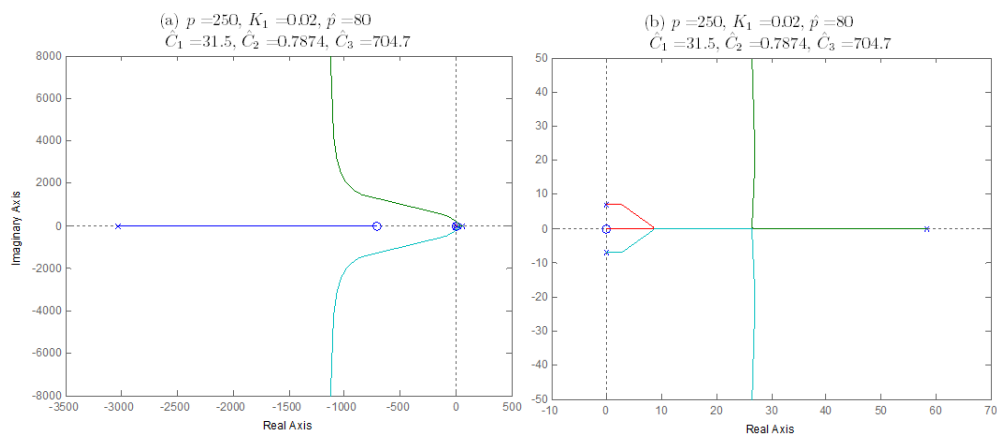


Figure 6.16 a. The root locus for K parameter when $p = 250$, $K_1 = 0.02$, $\hat{p} = 80$, $\widehat{C}_1 = 31.5$, $\widehat{C}_2 = 0.7874$ and $\widehat{C}_3 = 704.7$, b. Zoomed in root locus visualizing the portion of the diagram around the break-away point.

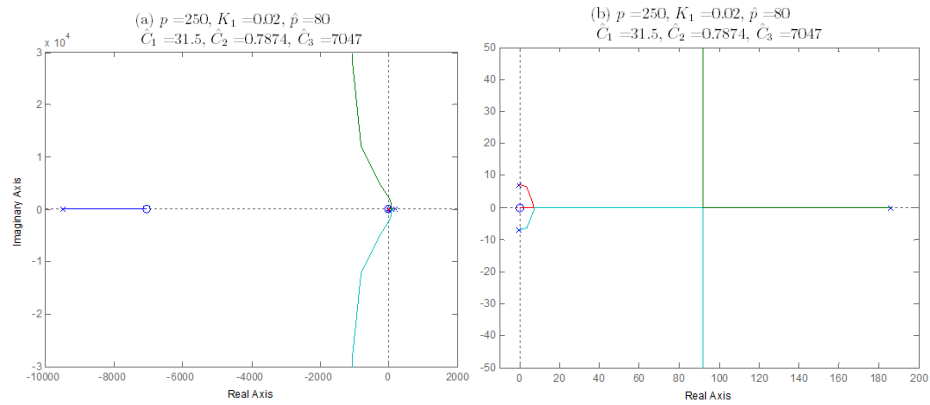


Figure 6.17 a. The root locus for K parameter when $p = 250, K_1 = 0.02, \hat{p} = 80, \hat{C}_1 = 31.5, \hat{C}_2 = 0.7874$ and $\hat{C}_3 = 7047$, b. Zoomed in root locus visualizing the portion of the diagram around the break-away point.

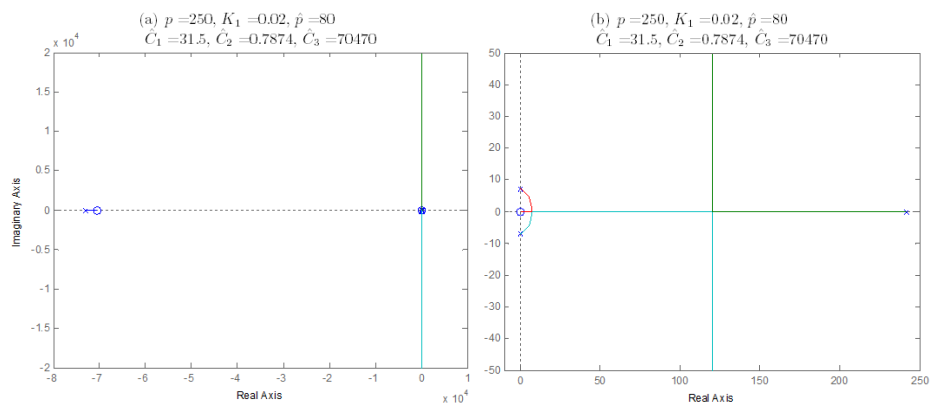


Figure 6.18 a. The root locus for K parameter when $p = 250, K_1 = 0.02, \hat{p} = 80, \hat{C}_1 = 31.5, \hat{C}_2 = 0.7874$ and $\hat{C}_3 = 70470$, b. Zoomed in root locus visualizing the portion of the diagram around the break-away point.

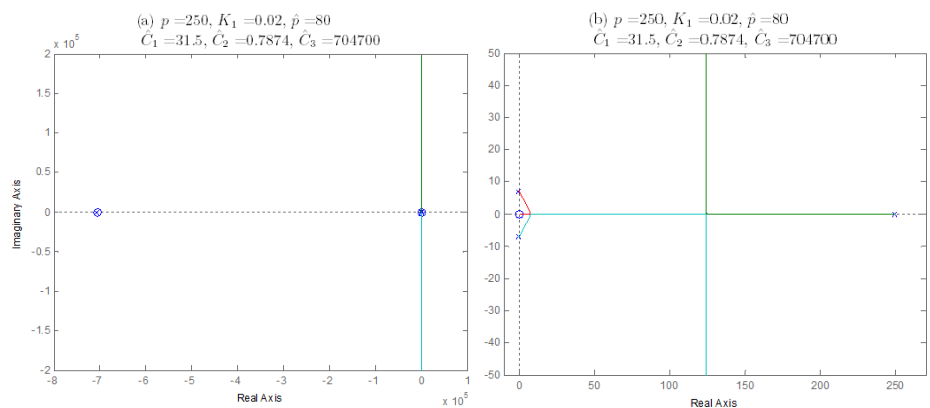


Figure 6.19 a. The root locus for K parameter when $p = 250, K_1 = 0.02, \hat{p} = 80, \hat{C}_1 = 31.5, \hat{C}_2 = 0.7874$ and $\hat{C}_3 = 704700$, b. Zoomed in root locus visualizing the portion of the diagram around the break-away point.

Table 6.3 The upper and lower limits of K parameter for different \widehat{C}_3 values

\widehat{C}_3	K^l	K^u
70.47	No	No
704.7	61.9	76.1
7047	68.9	233
70470	69.5	304
704700	69.7	313

In similar \widehat{C}_1 case, the upper limit changes in a large amount while lower one is almost constant.

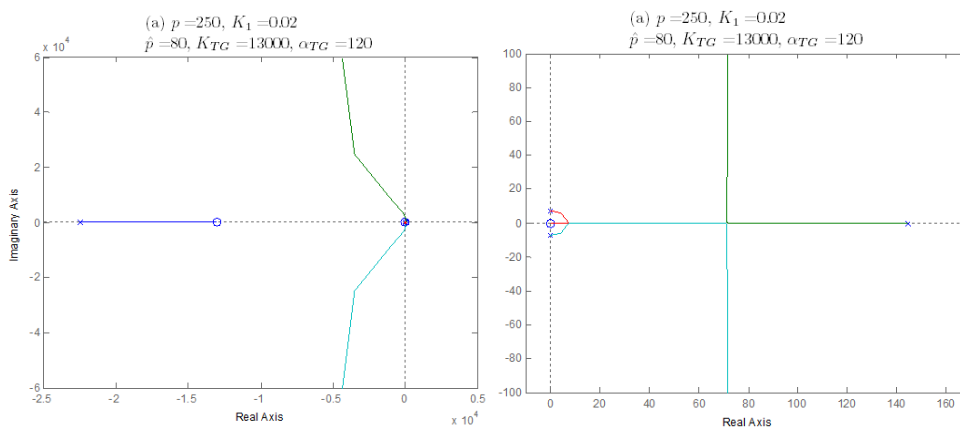


Figure 6.20 a. The root locus for K parameter when $p = 250$, $K_1 = 0.02$, $\hat{p} = 80$, $\alpha_{TG} = 120$ and $K_{TG} = 13000$, b. Zoomed in root locus visualizing the portion of the diagram around the break-away point.

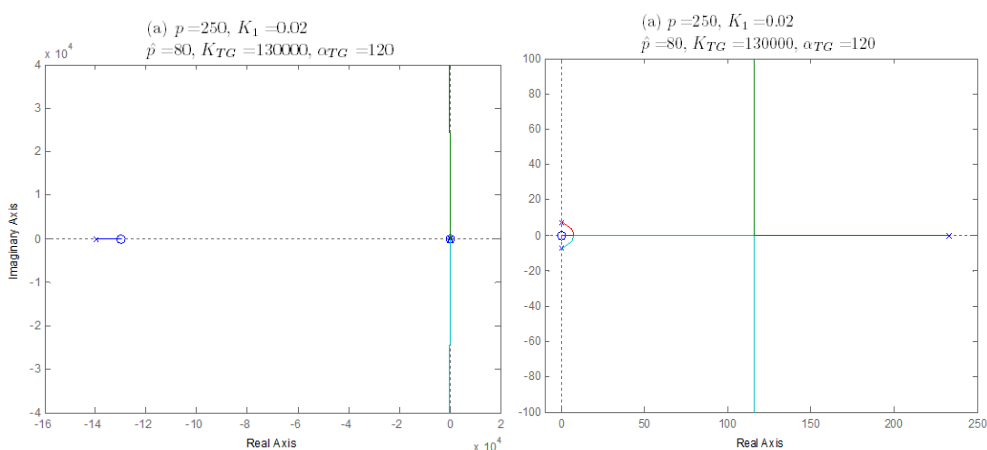


Figure 6.21 a. The root locus for K parameter when $p = 250$, $K_1 = 0.02$, $\hat{p} = 80$, $\alpha_{TG} = 120$ and $K_{TG} = 130000$, b. Zoomed in root locus visualizing the portion of the diagram around the break-away point.

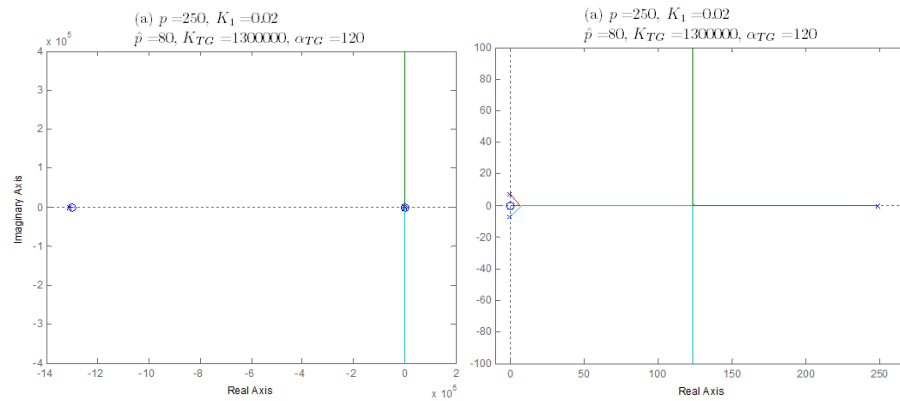


Figure 6.22 a. The root locus for K parameter when $p = 250, K_1 = 0.02, \hat{p} = 80, \alpha_{TC} = 120$ and $K_{TC} = 1300000$, b. Zoomed in root locus visualizing the portion of the diagram around the break-away point.

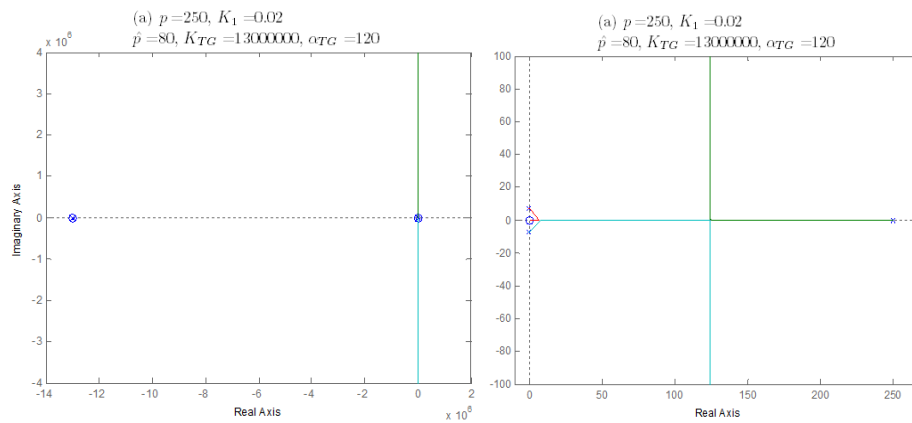


Figure 6.23 a. The root locus for K parameter when $p = 250, K_1 = 0.02, \hat{p} = 80, \alpha_{TC} = 120$ and $K_{TC} = 13000000$, b. Zoomed in root locus visualizing the portion of the diagram around the break-away point.

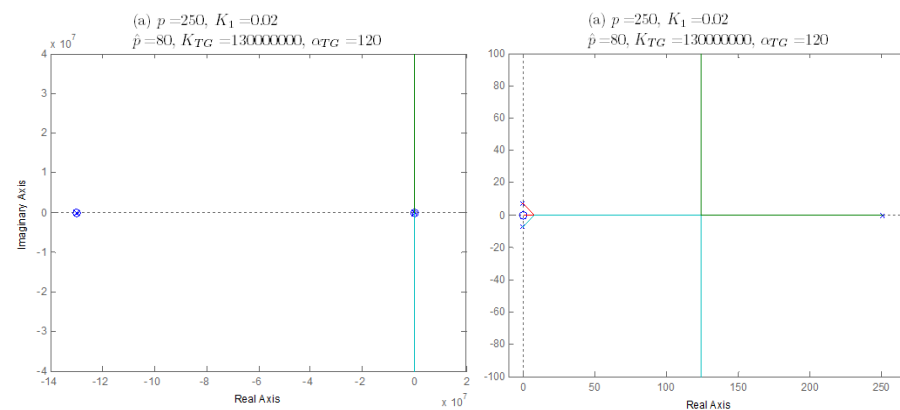


Figure 6.24 a. The root locus for K parameter when $p = 250, K_1 = 0.02, \hat{p} = 80, \alpha_{TC} = 120$ and $K_{TC} = 130000000$, b. Zoomed in root locus visualizing the portion of the diagram around the break-away point.

Table 6.4 The upper and lower limits of K parameter for different K_{TG} values

K_{TG}	K^l	K^u
13000	68.2	183
130000	69.5	293
1300000	69.7	312
13000000	69.7	314
130000000	69.7	314

The upper limit of the bistability range increases when K_{TG} increases however lower limit is almost constant.

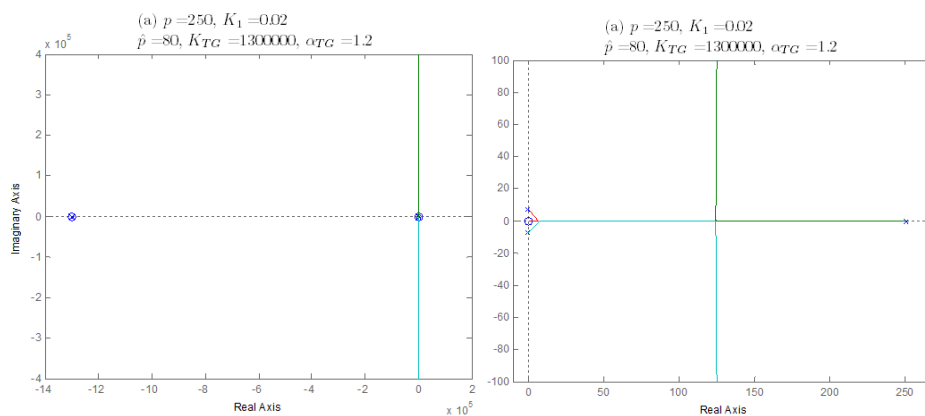


Figure 6.25 a. The root locus for K parameter when $p = 250$, $K_1 = 0.02$, $\hat{p} = 80$, $\alpha_{TG} = 1.2$ and $K_{TG} = 1300000$, b. Zoomed in root locus visualizing the portion of the diagram around the break-away point.

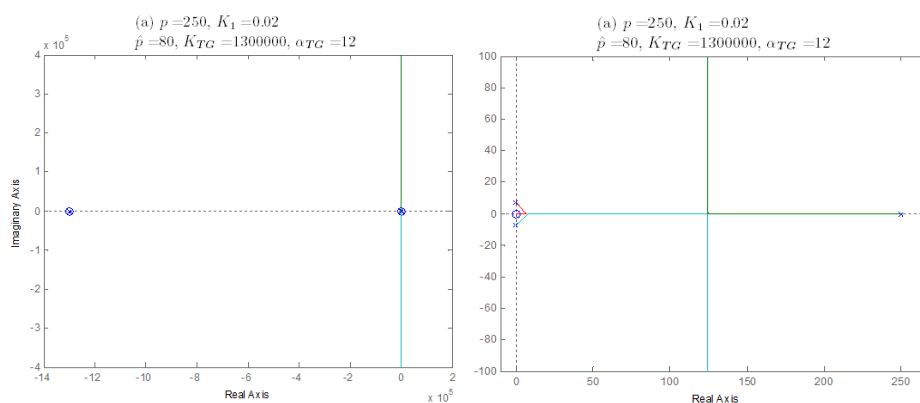


Figure 6.26 a. The root locus for K parameter when $p = 250$, $K_1 = 0.02$, $\hat{p} = 80$, $\alpha_{TG} = 12$ and $K_{TG} = 1300000$, b. Zoomed in root locus visualizing the portion of the diagram around the break-away point.

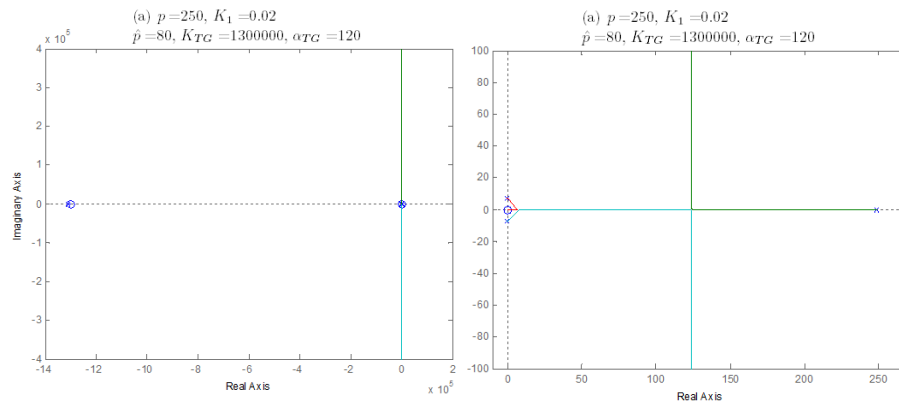


Figure 6.27 a. The root locus for K parameter when $p = 250$, $K_1 = 0.02$, $\hat{p} = 80$, $\alpha_{TG} = 120$ and $K_{TG} = 1300000$, b. Zoomed in root locus visualizing the portion of the diagram around the break-away point.

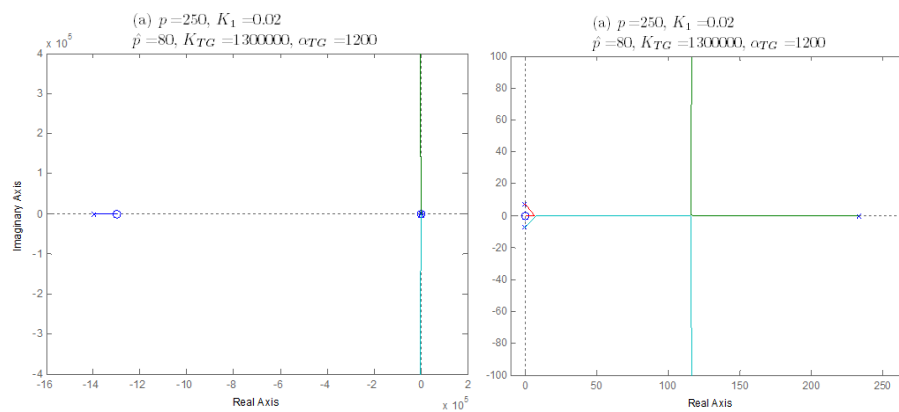


Figure 6.28 a. The root locus for K parameter when $p = 250$, $K_1 = 0.02$, $\hat{p} = 80$, $\alpha_{TG} = 1200$ and $K_{TG} = 1300000$, b. Zoomed in root locus visualizing the portion of the diagram around the break-away point.

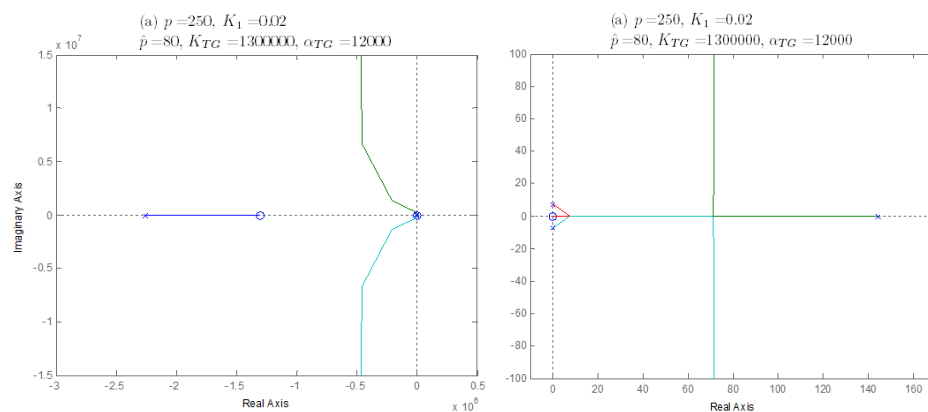


Figure 6.29 a. The root locus for K parameter when $p = 250$, $K_1 = 0.02$, $\hat{p} = 80$, $\alpha_{TG} = 12000$ and $K_{TG} = 1300000$, b. Zoomed in root locus visualizing the portion of the diagram around the break-away point.

Table 6.5 The upper and lower limits of K parameter for different α_{TG} values

α_{TG}	K^l	K^u
1.2	69.8	314
12	69.7	314
120	69.7	312
1200	69.5	293
12000	68.2	183

Opposite to K_{TG} parameter, the upper limit of bistability region of K parameter decreases when α_{TG} gets larger values. But again, the lower limit is almost constant.

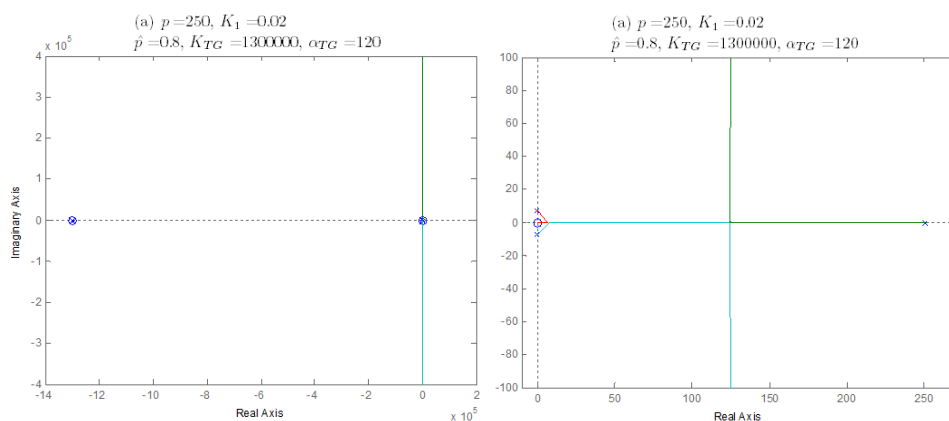


Figure 6.30 a. The root locus of K parameter when $p = 250$, $K_1 = 0.02$, $\hat{p} = 0.8$ and the nominal values of α_{TG} and K_{TG} in Michaelis-Menten kinetics, b. Zoomed in root locus visualizing the portion of the diagram around the break-away point.

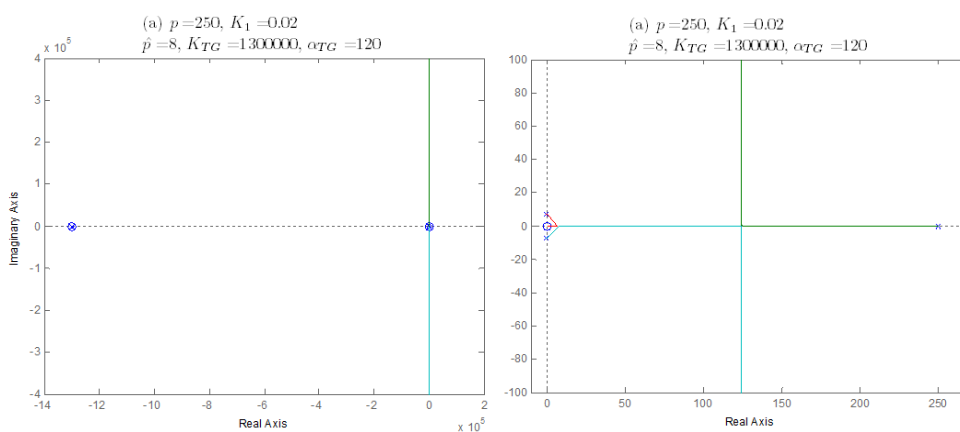


Figure 6.31 a. The root locus of K parameter when $p = 250$, $K_1 = 0.02$, $\hat{p} = 8$ and the nominal values of α_{TG} and K_{TG} in Michaelis-Menten kinetics, b. Zoomed in root locus visualizing the portion of the diagram around the break-away point.

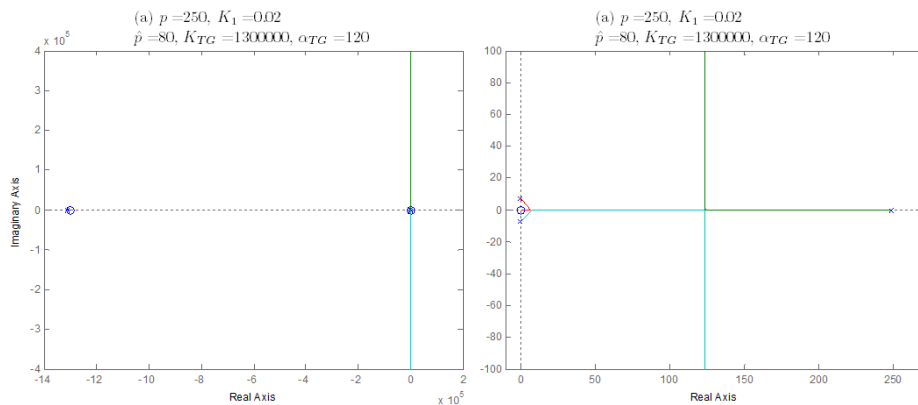


Figure 6.32 a. The root locus of K parameter when $p = 250$, $K_1 = 0.02$, $\hat{p} = 80$ and the nominal values of α_{TC} and K_{TC} in Michaelis-Menten kinetics, b. Zoomed in root locus visualizing the portion of the diagram around the break-away point.

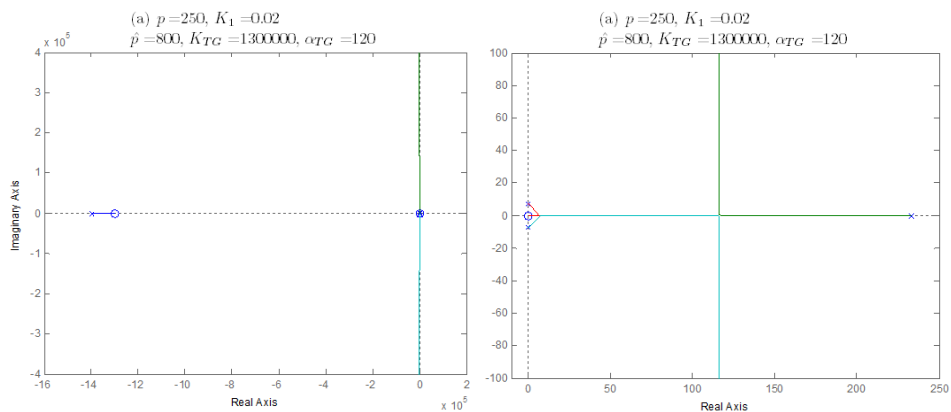


Figure 6.33 a. The root locus of K parameter when $p = 250$, $K_1 = 0.02$, $\hat{p} = 800$ and the nominal values of α_{TC} and K_{TC} in Michaelis-Menten kinetics, b. Zoomed in root locus visualizing the portion of the diagram around the break-away point.

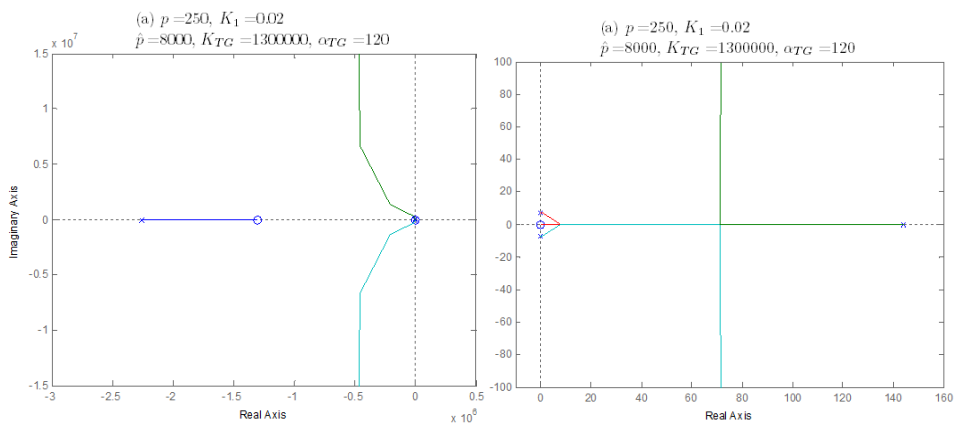


Figure 6.34 a. The root locus of K parameter when $p = 250$, $K_1 = 0.02$, $\hat{p} = 8000$ and the nominal values of α_{TC} and K_{TC} in Michaelis-Menten kinetics, b. Zoomed in root locus visualizing the portion of the diagram around the break-away point.

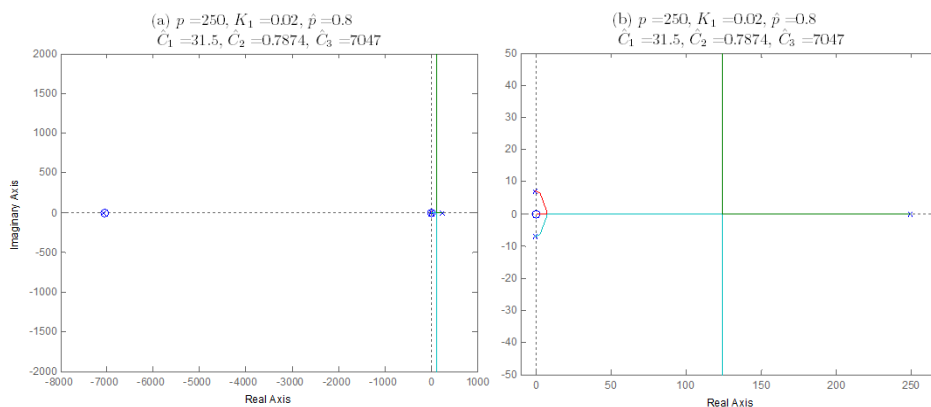


Figure 6.35 a. The root locus of K parameter when $p = 250, K_1 = 0.02, \hat{p} = 0.8$ and the nominal values of \hat{C}_1, \hat{C}_2 and \hat{C}_3 in bi-bi ordered kinetics, b. Zoomed in root locus visualizing the portion of the diagram around the break-away point.

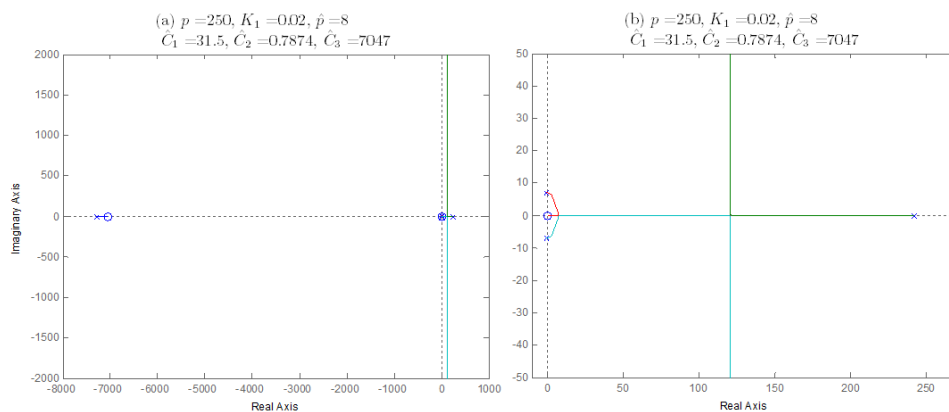


Figure 6.36 a. The root locus of K parameter when $p = 250, K_1 = 0.02, \hat{p} = 8$ and the nominal values of \hat{C}_1, \hat{C}_2 and \hat{C}_3 in bi-bi ordered kinetics, b. Zoomed in root locus visualizing the portion of the diagram around the break-away point.

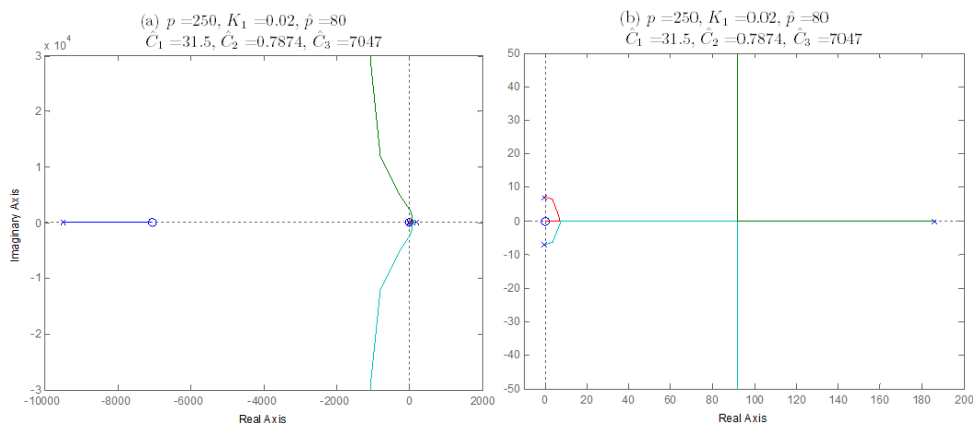


Figure 6.37 a. The root locus of K parameter when $p = 250, K_1 = 0.02, \hat{p} = 80$ and the nominal values of \hat{C}_1, \hat{C}_2 and \hat{C}_3 in bi-bi ordered kinetics, b. Zoomed in root locus visualizing the portion of the diagram around the break-away point.

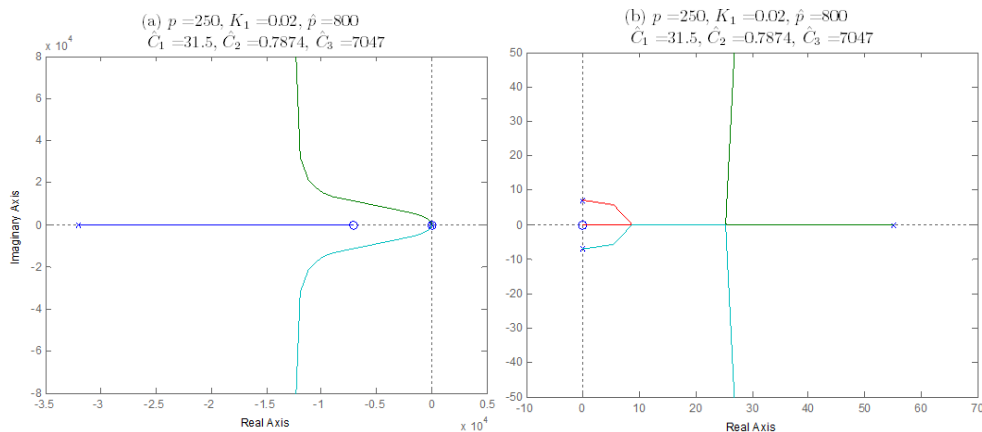


Figure 6.38 a. The root locus of K parameter when $p = 250$, $K_1 = 0.02$, $\hat{p} = 800$ and the nominal values of \hat{C}_1 , \hat{C}_2 and \hat{C}_3 in bi-bi ordered kinetics, b. Zoomed in root locus visualizing the portion of the diagram around the break-away point.

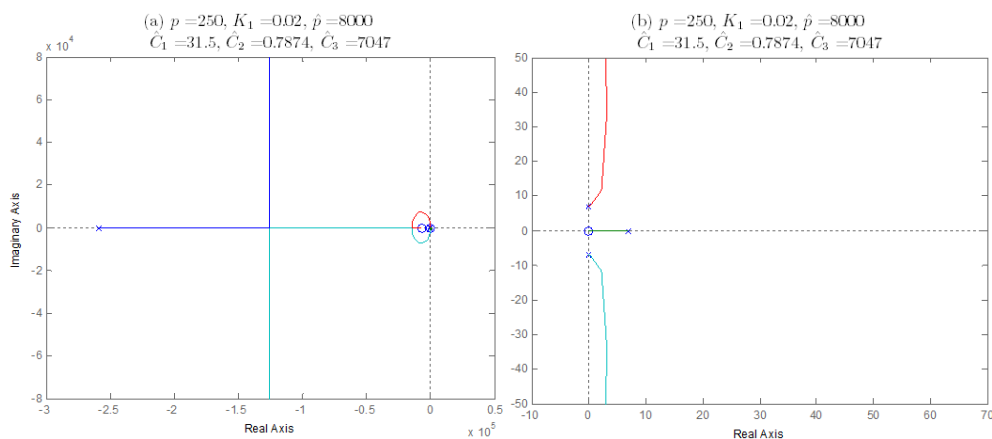


Figure 6.39 a. The root locus of K parameter when $p = 250$, $K_1 = 0.02$, $\hat{p} = 8000$ and the nominal values of \hat{C}_1 , \hat{C}_2 and \hat{C}_3 in bi-bi ordered kinetics, b. Zoomed in root locus visualizing the portion of the diagram around the break-away point.

Table 6.6 The upper and lower limits of K parameter for different \hat{p} values

\hat{p}	Michaelis-Menten		Bi-bi ordered	
	K^l	K^u	K^l	K^u
0.8	69.7	314	69.7	313
8	69.7	314	69.7	304
80	69.7	312	68.9	233
800	69.5	293	61.8	74.4
8000	68.1	183	No	No

The upper limits of the K parameter in Michaelis-Menten kinetics decreases slower than in bi-bi ordered kinetics. The lower limits in both kinetic are almost constant.

6.2.2 Root Locus for p Parameter

The root locus for p parameter is drawn for both of the acetylation kinetics to determine the effect of the tansacetylase in lac operon model. For Michaelis-Menten kinetics, the characteristic equation is defined for p parameter in Equation (113).

$$1 - \frac{p(K_1 T^3 + K_1 K_{TG} T^2 + T + K_{TG})}{K_1 T^4 + K_1 (K_{TG} + \alpha_{TG} \hat{p}) T^3 + K T^2 + (K K_{TG} + \alpha_{TG} \hat{p}) T} = 0 \quad (113)$$

Again, similar to the bistability analysis of K parameter, the root locus of p parameter is drawn for mathematical model without transacetylase effect to determine the changes in bistability region when $K = 167.1$ and $K_1 = 0.02$ in Figure 6.40.

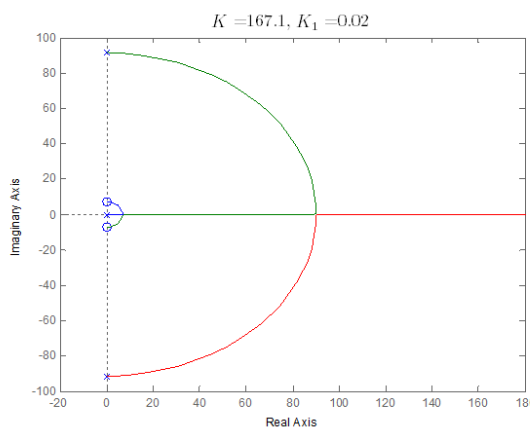


Figure 6.40 The root locus for p parameter when $K = 167.1$ and $K_1 = 0.02$

The root locus of p parameter for the mathematical model with transacetylase effect defined in Michealis-Menten kinetics is also drawn with the nominal values of α_{TG} and K_{TG} in Figure 6.41. The lower and upper limits of the bistability regions for p parameter in both mathematical model are the same as $p \in (182, 594)$. However,

Michaelis-Menten kinetics when parameter values are chosen as $\alpha_{TG} = \widehat{C}_1$ and $K_{TG} = \widehat{C}_3$, construct new lower and upper limits as $p \in (211, 597)$ in Figure 6.42.

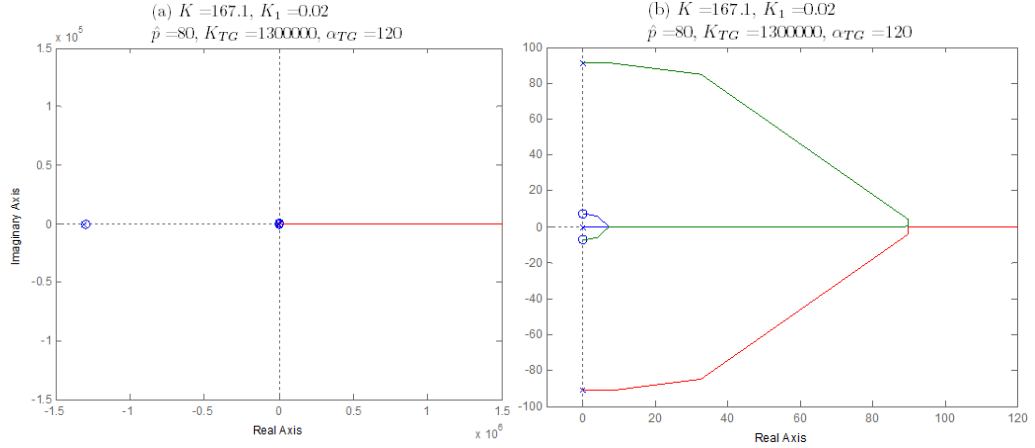


Figure 6.41 a. The root locus for p parameter when $K = 167.1$ and $K_1 = 0.02$ for Michaelis-Menten kinetics with nominal parameter values, b. Zoomed in root locus visualizing the portion of the diagram around the break-away point.

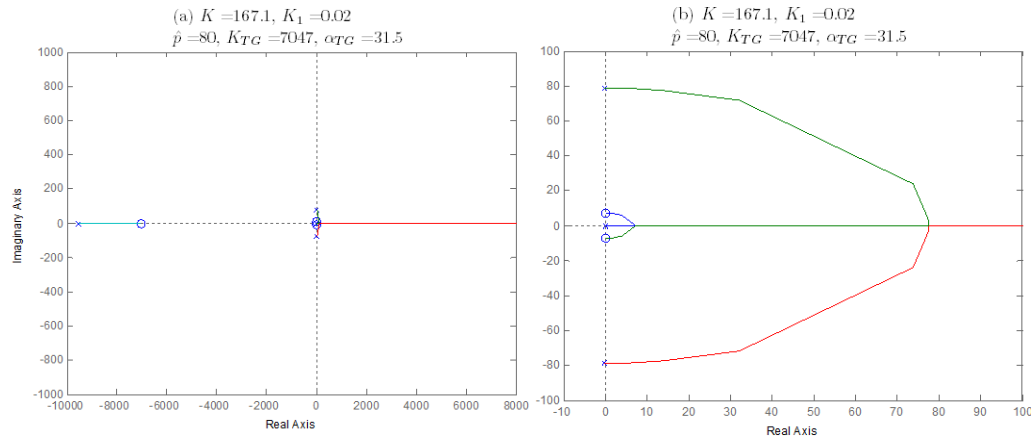


Figure 6.42 a. The root locus for p parameter when $K = 167.1$, $K_1 = 0.02$, $\hat{p} = 80$, $\alpha_{TG} = \widehat{C}_1$ and $K_{TG} = \widehat{C}_3$, b. Zoomed in root locus visualizing the portion of the diagram around the break-away point.

The root locus for bi-bi ordered kinetics, the characteristic equation of p parameter is defined in Equation (114).

$$1 - \frac{p(K_1 T^3 + K_1 \widehat{C}_3 T^2 + T + \widehat{C}_3)}{K_1 T^4 + K_1 (\widehat{C}_3 + \hat{p} \widehat{C}_1) T^3 + (K - \hat{p} K_1 \widehat{C}_2) T^2 + (K \widehat{C}_3 + \hat{p} \widehat{C}_1) T - \hat{p} \widehat{C}_2} = 0 \quad (114)$$

The root locus of p parameter for bi-bi ordered kinetics with nominal parameter values is given in Figure 6.43. The limits of the bistability regions for p parameter when $\widehat{C}_2 = 0.7874$ and $\widehat{C}_2 = 0$ are equal to each other as $p \in (211, 597)$. The bistability region is also the same for Michaelis-Menten kinetics when kinetics parameters are given as $\alpha_{TG} = \widehat{C}_1$ and $K_{TG} = \widehat{C}_3$.

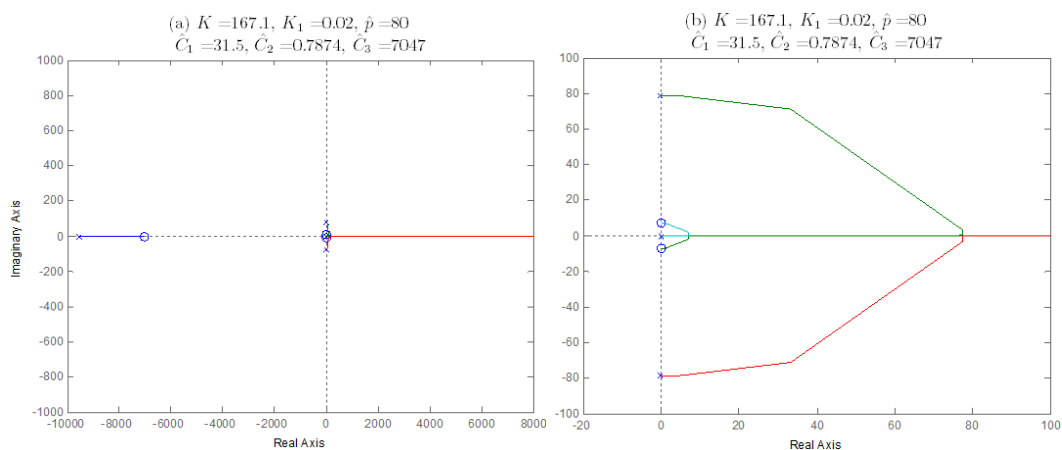


Figure 6.43 a. The root locus for p parameter when $K = 167.1$, $K_1 = 0.02$, $\hat{p} = 80$, $\widehat{C}_1 = 31.5$, $\widehat{C}_2 = 0.7874$ and $\widehat{C}_3 = 7047$, b. Zoomed in root locus visualizing the portion of the diagram around the break-away point.

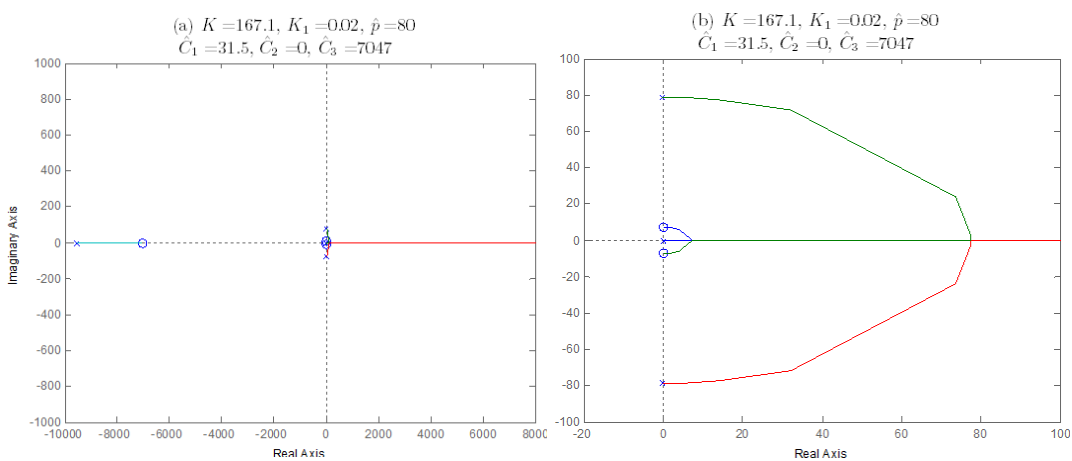


Figure 6.44 a. The root locus for p parameter when $K = 167.1$, $K_1 = 0.02$, $\hat{p} = 80$, $\widehat{C}_1 = 31.5$, $\widehat{C}_2 = 0$ and $\widehat{C}_3 = 7047$, b. Zoomed in root locus visualizing the portion of the diagram around the break-away point.

The root locus plots for five different multiples of each \widehat{C}_1 , \widehat{C}_2 , \widehat{C}_3 , α_{TG} , K_{TG} and \hat{p} parameter are drawn and the bistability region of p parameter (p^l, p^u) is determined as given below.

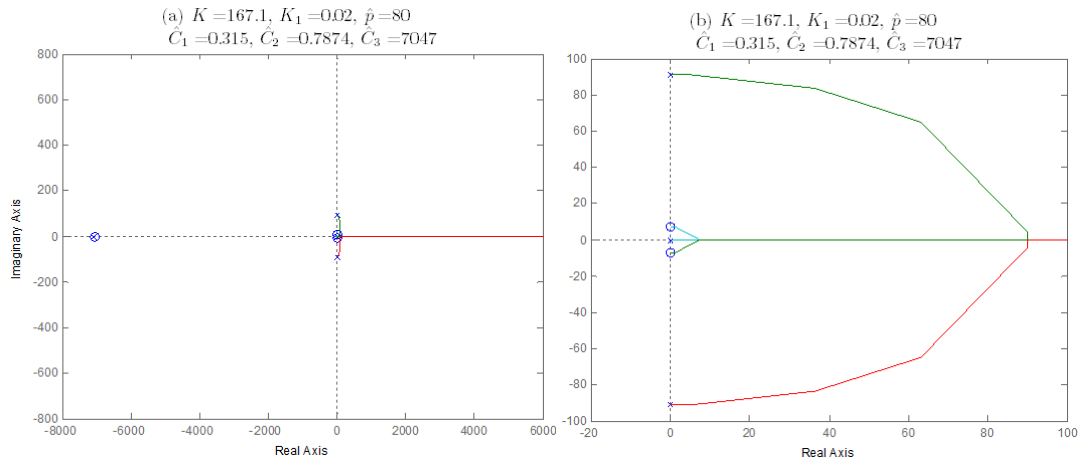


Figure 6.45 a. The root locus for p parameter when $K = 167.1$, $K_1 = 0.02$, $\hat{p} = 80$, $\widehat{C}_1 = 0.315$, $\widehat{C}_2 = 0.7874$ and $\widehat{C}_3 = 7047$, b. Zoomed in root locus visualizing the portion of the diagram around the break-away point.

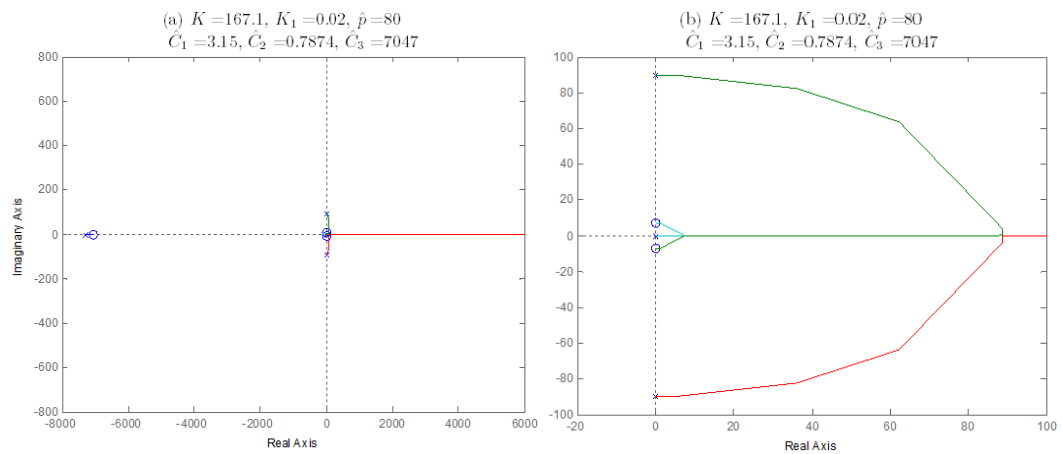


Figure 6.46 a. The root locus for p parameter when $K = 167.1$, $K_1 = 0.02$, $\hat{p} = 80$, $\widehat{C}_1 = 3.15$, $\widehat{C}_2 = 0.7874$ and $\widehat{C}_3 = 7047$, b. Zoomed in root locus visualizing the portion of the diagram around the break-away point.

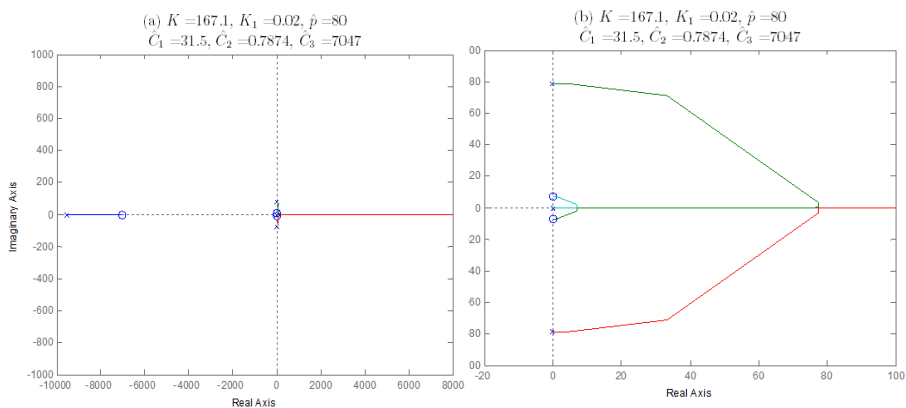


Figure 6.47 a. The root locus for p parameter when $K = 167.1, K_1 = 0.02, \hat{p} = 80, \hat{C}_1 = 31.5, \hat{C}_2 = 0.7874$ and $\hat{C}_3 = 7047$, b. Zoomed in root locus visualizing the portion of the diagram around the break-away point.

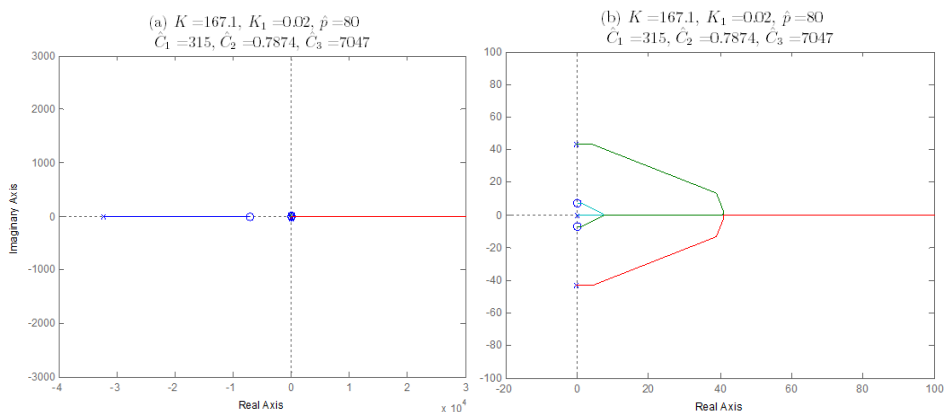


Figure 6.48 a. The root locus for p parameter when $K = 167.1, K_1 = 0.02, \hat{p} = 80, \hat{C}_1 = 315, \hat{C}_2 = 0.7874$ and $\hat{C}_3 = 7047$, b. Zoomed in root locus visualizing the portion of the diagram around the break-away point.

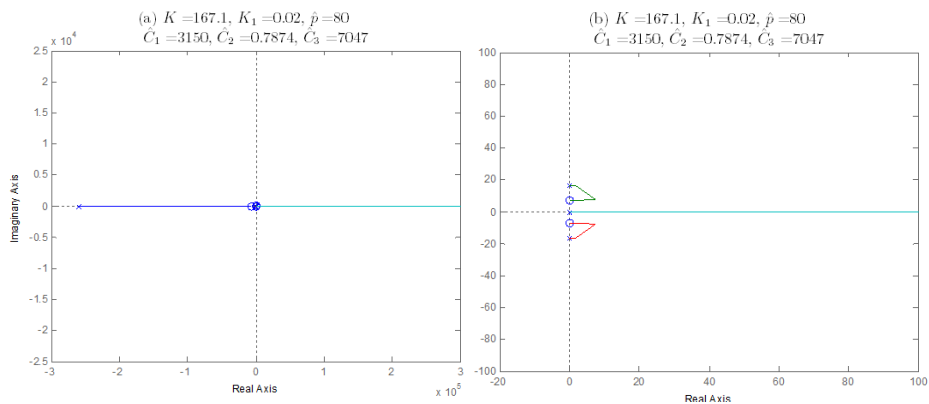


Figure 6.49 a. The root locus for p parameter when $K = 167.1, K_1 = 0.02, \hat{p} = 80, \hat{C}_1 = 3150, \hat{C}_2 = 0.7874$ and $\hat{C}_3 = 7047$, b. Zoomed in root locus visualizing the portion of the diagram around the break-away point.

Table 6.7 The upper and lower limits of p parameter for different \widehat{C}_1 values

\widehat{C}_1	p^l	p^u
0.315	182	594
3.15	185	595
31.5	211	597
315	383	621
3150	No	No

While the lower limit of the p parameter is changing, the upper limit is almost constant.

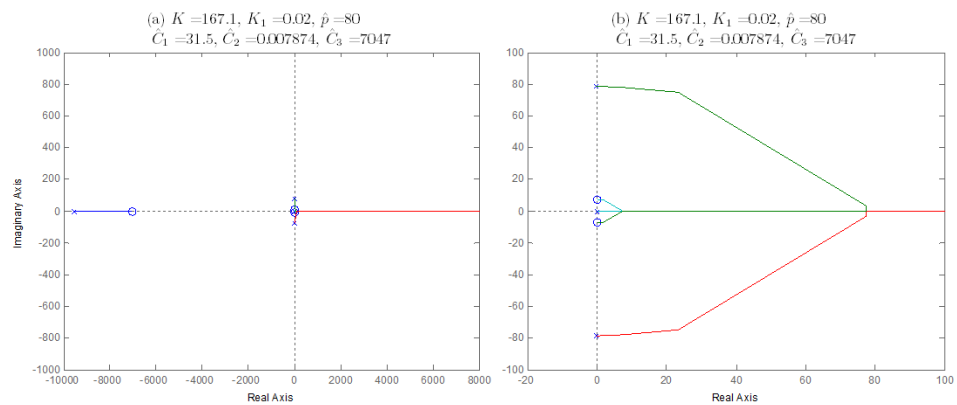


Figure 6.50 a. The root locus for p parameter when $\widehat{C}_2 = 0.007874$ the others are equal to nominal values, b. Zoomed in root locus visualizing the portion of the diagram around the break-away point.

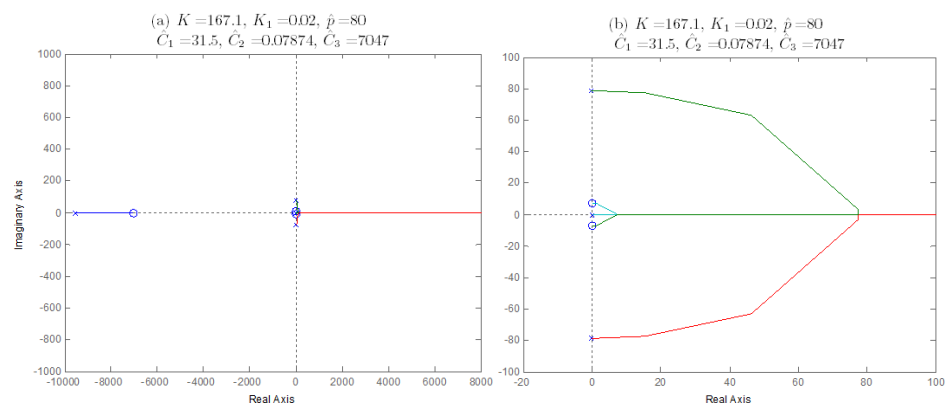


Figure 6.51 a. The root locus for p parameter when $K = 167.1$, $K_1 = 0.02$, $\hat{p} = 80$, $\widehat{C}_1 = 31.5$, $\widehat{C}_2 = 0.07874$ and $\widehat{C}_3 = 7047$, b. Zoomed in root locus visualizing the portion of the diagram around the break-away point.

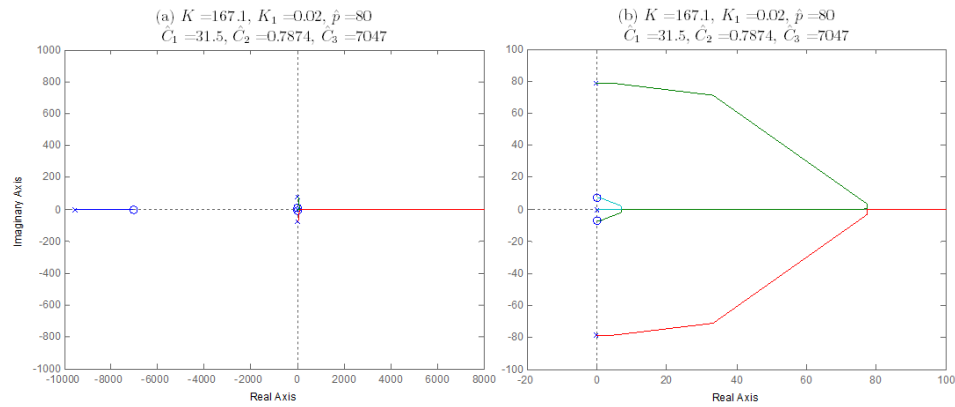


Figure 6.52 a. The root locus for p parameter when $= 167.1, K_1 = 0.02, \hat{p} = 80, \hat{C}_1 = 31.5, \hat{C}_2 = 0.7874$ and $\hat{C}_3 = 7047$, b. Zoomed in root locus visualizing the portion of the diagram around the break-away point.

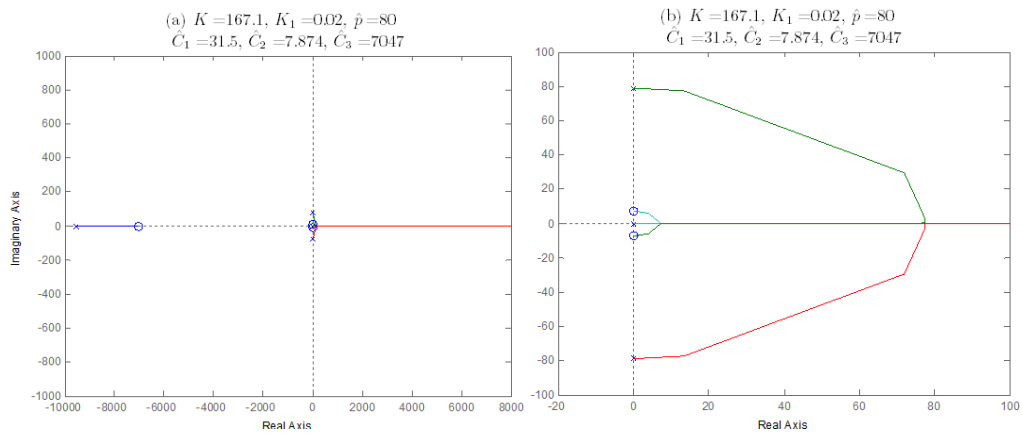


Figure 6.53 a. The root locus for p parameter when $K = 167.1, K_1 = 0.02, \hat{p} = 80, \hat{C}_1 = 31.5, \hat{C}_2 = 7.874$ and $\hat{C}_3 = 7047$, b. Zoomed in root locus visualizing the portion of the diagram around the break-away point.

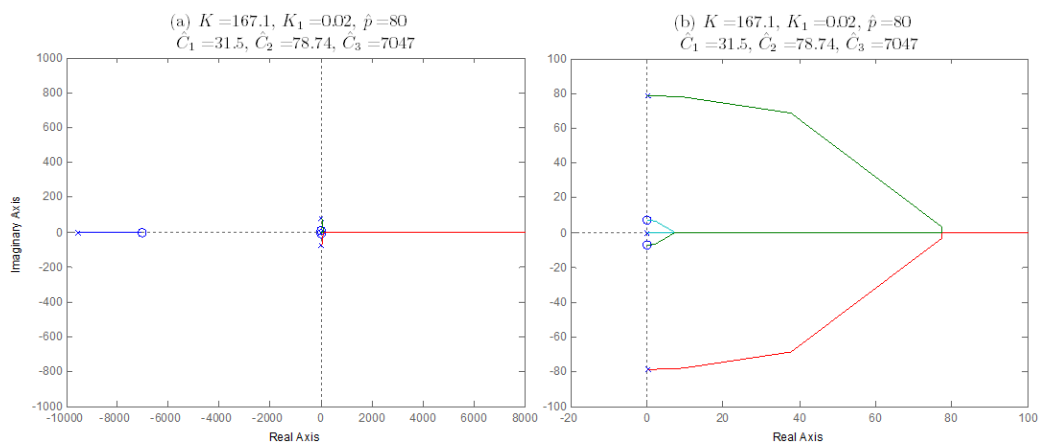


Figure 6.54 a. The root locus for p parameter when $K = 167.1, K_1 = 0.02, \hat{p} = 80, \hat{C}_1 = 31.5, \hat{C}_2 = 78.74$ and $\hat{C}_3 = 7047$, b. Zoomed in root locus visualizing the portion of the diagram around the break-away point.

Table 6.8 The upper and lower limits of p parameter for different \widehat{C}_2 values

\widehat{C}_2	p^l	p^u
0.007874	211	597
0.07874	211	597
0.7874	211	597
7.874	211	597
78.74	210	596

Both the lower and upper limits of the bistability region are constant for different \widehat{C}_2 values.

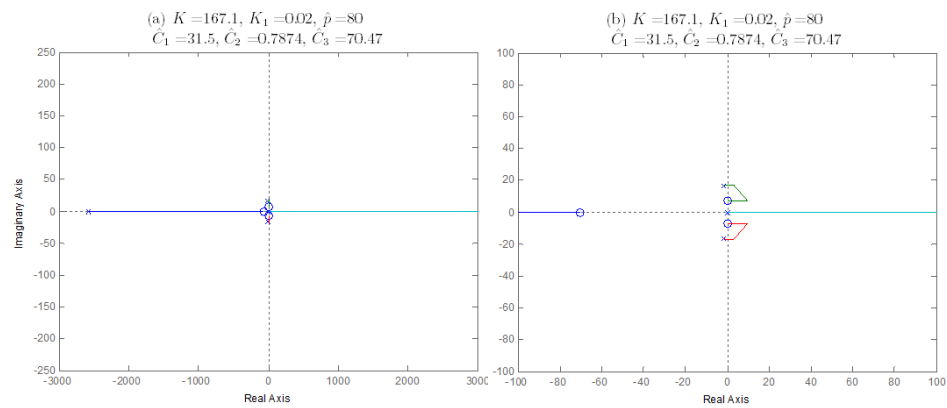


Figure 6.55 a. The root locus for p parameter when $K = 167.1, K_1 = 0.02, \hat{p} = 80, \widehat{C}_1 = 31.5, \widehat{C}_2 = 0.7874$ and $\widehat{C}_3 = 70.47$, b. Zoomed in root locus visualizing the portion of the diagram around the break-away point.

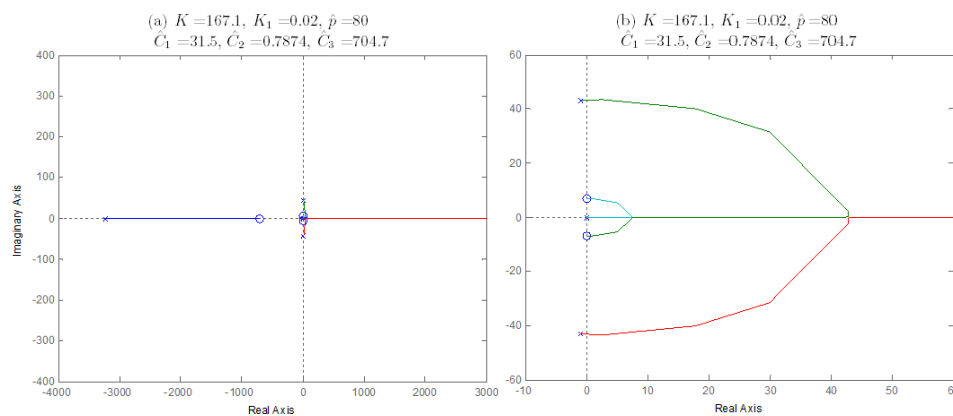


Figure 6.56 a. The root locus for p parameter when $K = 167.1, K_1 = 0.02, \hat{p} = 80, \widehat{C}_1 = 31.5, \widehat{C}_2 = 0.7874$ and $\widehat{C}_3 = 704.7$, b. Zoomed in root locus visualizing the portion of the diagram around the break-away point.

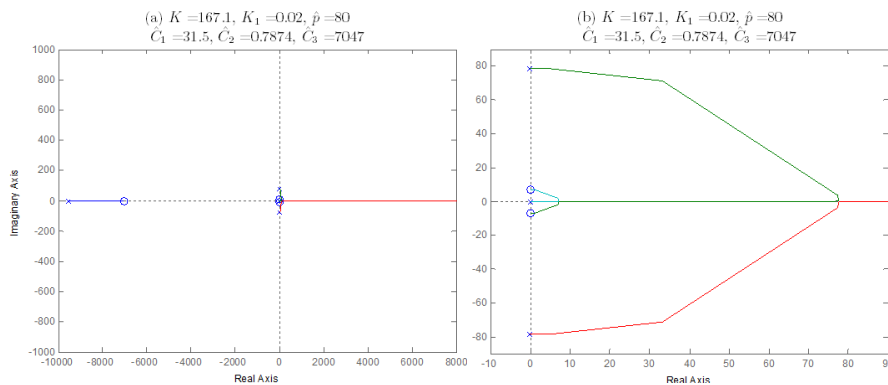


Figure 6.57 a. The root locus for p parameter when $K = 167.1, K_1 = 0.02, \hat{p} = 80, \hat{C}_1 = 31.5, \hat{C}_2 = 0.7874$ and $\hat{C}_3 = 7047$, b. Zoomed in root locus visualizing the portion of the diagram around the break-away point.

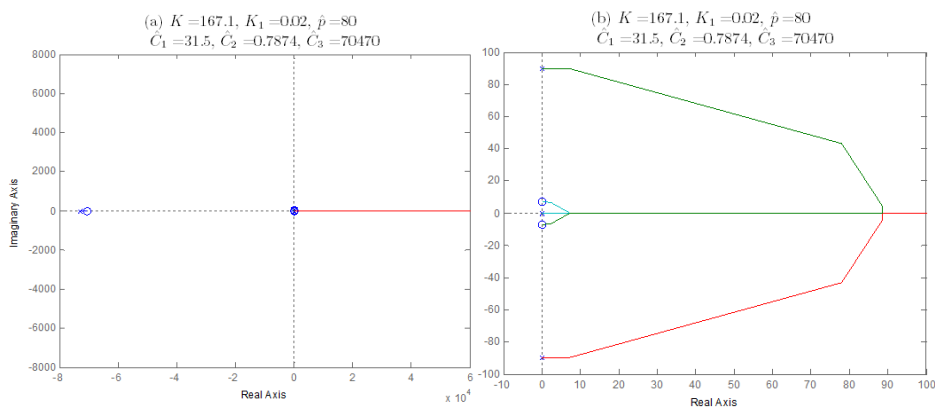


Figure 6.58 a. The root locus for p parameter when $K = 167.1, K_1 = 0.02, \hat{p} = 80, \hat{C}_1 = 31.5, \hat{C}_2 = 0.7874$ and $\hat{C}_3 = 70470$, b. Zoomed in root locus visualizing the portion of the diagram around the break-away point.

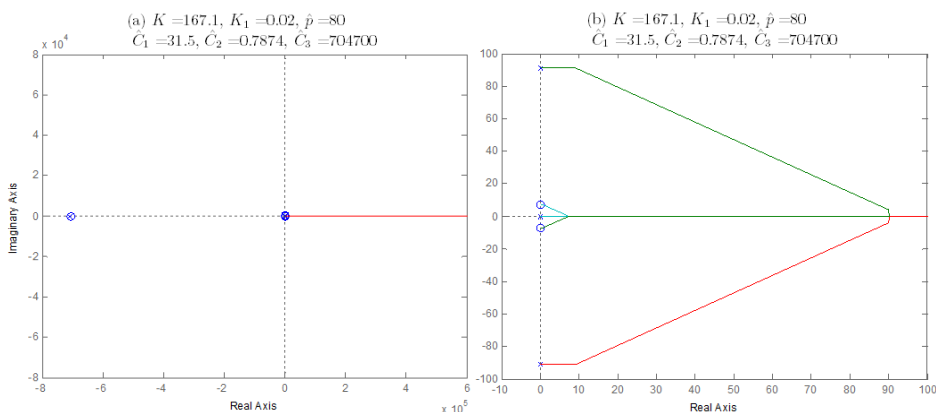


Figure 6.59 a. The root locus for p parameter when $K = 167.1, K_1 = 0.02, \hat{p} = 80, \hat{C}_1 = 31.5, \hat{C}_2 = 0.7874$ and $\hat{C}_3 = 704700$, b. Zoomed in root locus visualizing the portion of the diagram around the break-away point.

Table 6.9 The upper and lower limits of p parameter for different \widehat{C}_3 values

\widehat{C}_3	p^l	p^u
70.47	No	No
704.7	376	620
7047	211	597
70470	185	595
704700	182	594

Similar to \widehat{C}_1 case, the lower limit changes in a large amount while the upper one is almost constant. But in this case, the increase of \widehat{C}_3 values causes a decrease in the lower limit of p parameter.

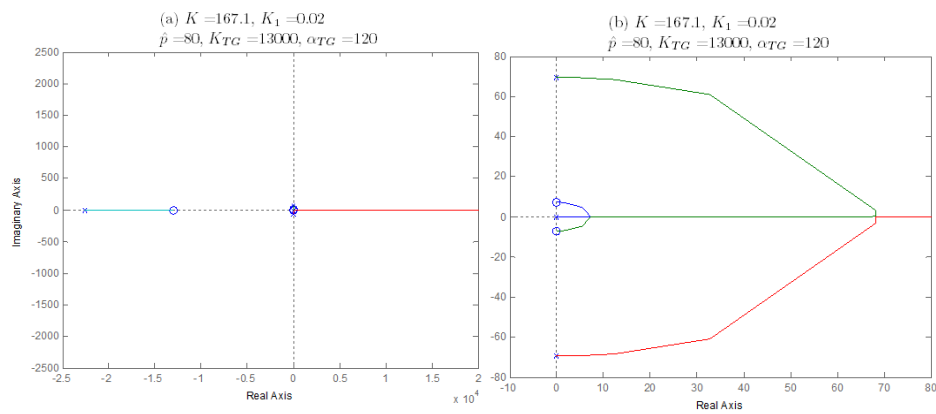


Figure 6.60 a. The root locus for p parameter when $K = 167.1$, $K_1 = 0.02$, $\hat{p} = 80$, $\alpha_{TG} = 120$ and $K_{TG} = 13000$, b. Zoomed in root locus visualizing the portion of the diagram around the break-away point.

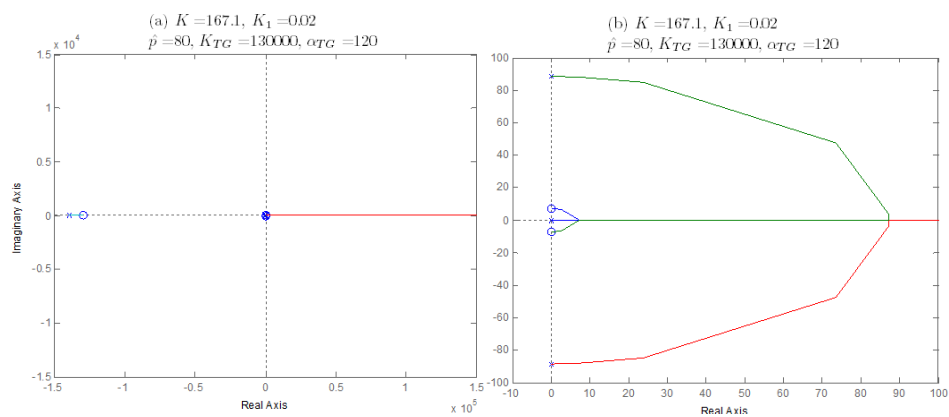


Figure 6.61 a. The root locus for p parameter when $K = 167.1$, $K_1 = 0.02$, $\hat{p} = 80$, $\alpha_{TG} = 120$ and $K_{TG} = 130000$, b. Zoomed in root locus visualizing the portion of the diagram around the break-away point.

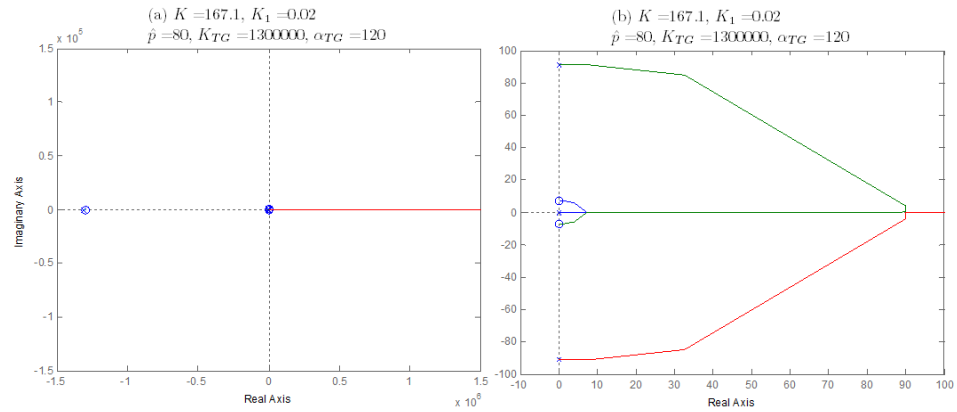


Figure 6.62 a. The root locus for p parameter when $K = 167.1$, $K_1 = 0.02$, $\hat{p} = 80$, $\alpha_{TC} = 120$ and $K_{TC} = 1300000$, b. Zoomed in root locus visualizing the portion of the diagram around the break-away point.

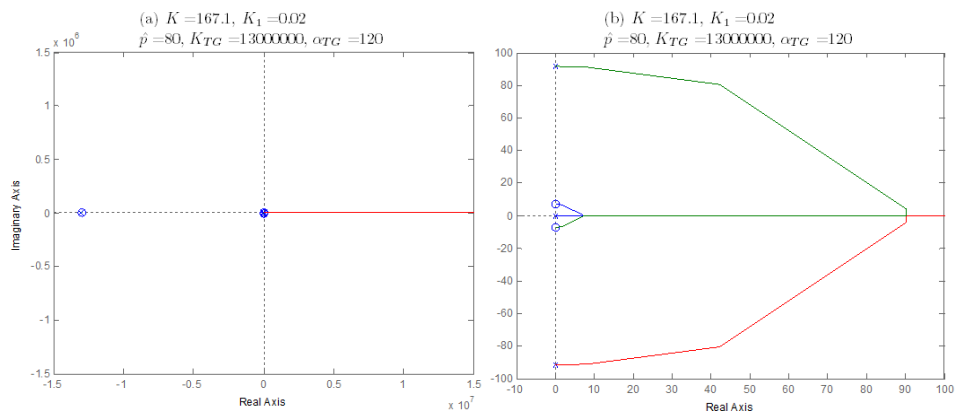


Figure 6.63 a. The root locus for p parameter when $K = 167.1$, $K_1 = 0.02$, $\hat{p} = 80$, $\alpha_{TC} = 120$ and $K_{TC} = 13000000$, b. Zoomed in root locus visualizing the portion of the diagram around the break-away point.

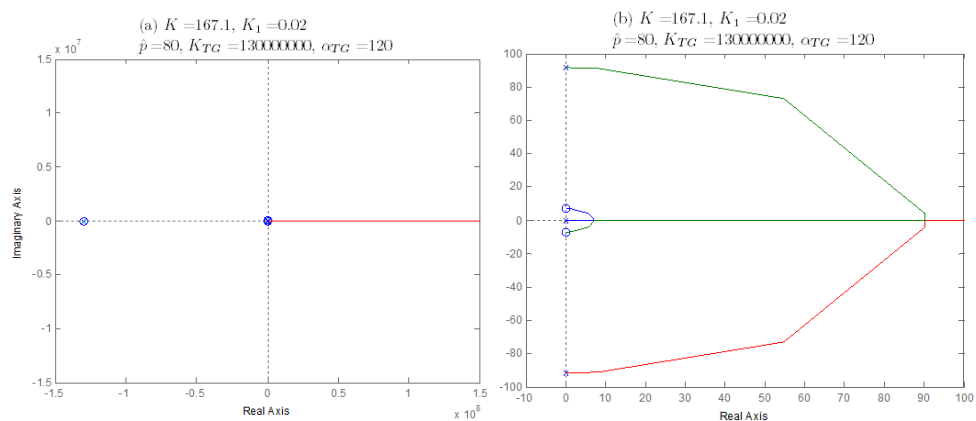


Figure 6.64 a. The root locus for p parameter when $K = 167.1$, $K_1 = 0.02$, $\hat{p} = 80$, $\alpha_{TC} = 120$ and $K_{TC} = 130000000$, b. Zoomed in root locus visualizing the portion of the diagram around the break-away point.

Table 6.10 The upper and lower limits of p parameter for different K_{TG} values

K_{TG}	p^l	p^u
13000	239	600
130000	188	595
1300000	182	594
13000000	182	594
130000000	182	594

The lower limit of the bistability range decreases when K_{TG} increases however the upper limit is almost constant.

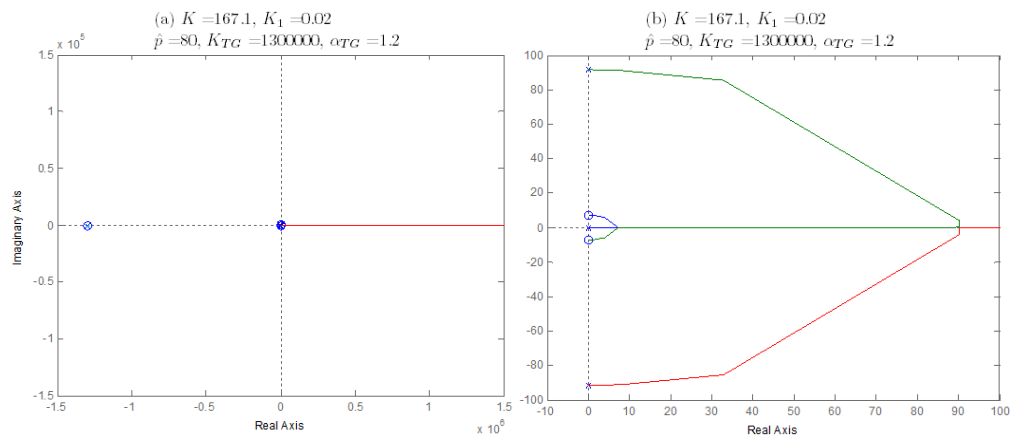


Figure 6.65 a. The root locus for p parameter when $K = 167.1$, $K_1 = 0.02$, $\hat{p} = 80$, $\alpha_{TG} = 1.2$ and $K_{TG} = 1300000$, b. Zoomed in root locus visualizing the portion of the diagram around the break-away point.

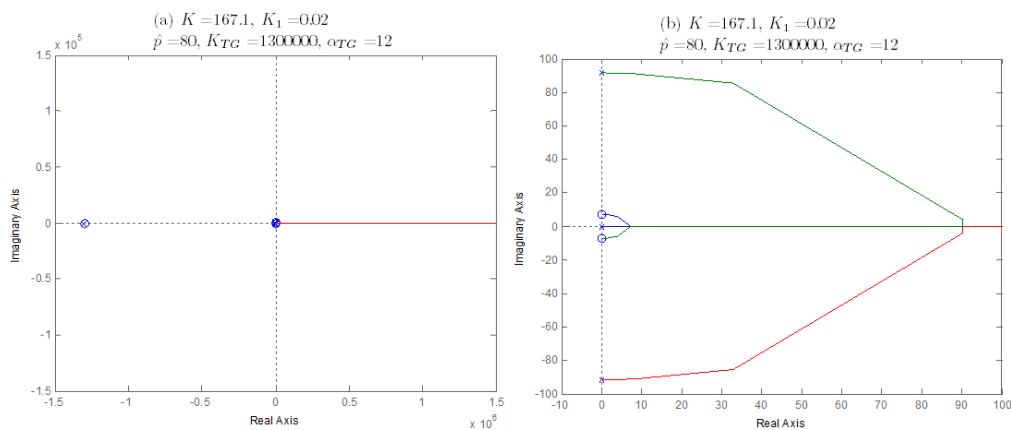


Figure 6.66 a. The root locus for p parameter when $K = 167.1$, $K_1 = 0.02$, $\hat{p} = 80$, $\alpha_{TG} = 12$ and $K_{TG} = 1300000$, b. Zoomed in root locus visualizing the portion of the diagram around the break-away point.

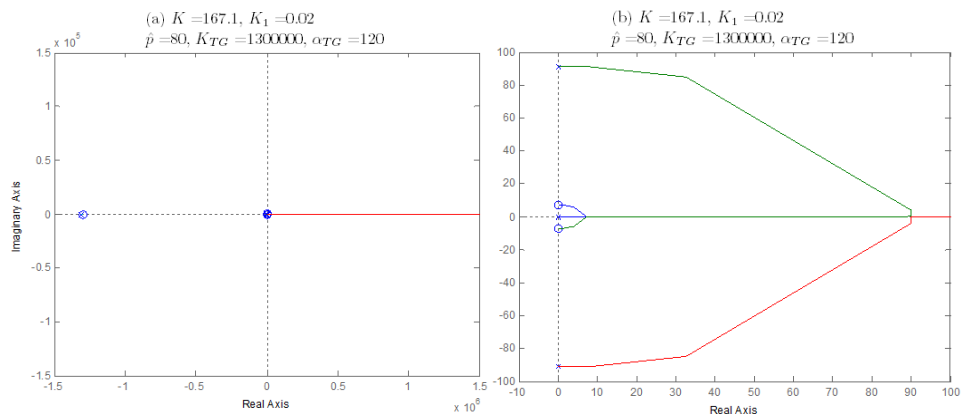


Figure 6.7 a. The root locus for p parameter when $K = 167.1, K_1 = 0.02, \hat{p} = 80, \alpha_{TC} = 120$ and $K_{TC} = 1300000$, b. Zoomed in root locus visualizing the portion of the diagram around the break-away point.

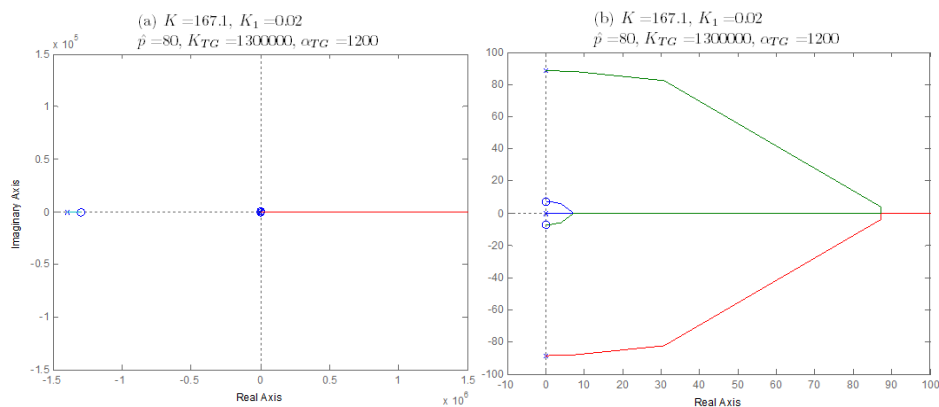


Figure 6.8 a. The root locus for p parameter when $K = 167.1, K_1 = 0.02, \hat{p} = 80, \alpha_{TC} = 1200$ and $K_{TC} = 1300000$, b. Zoomed in root locus visualizing the portion of the diagram around the break-away point.

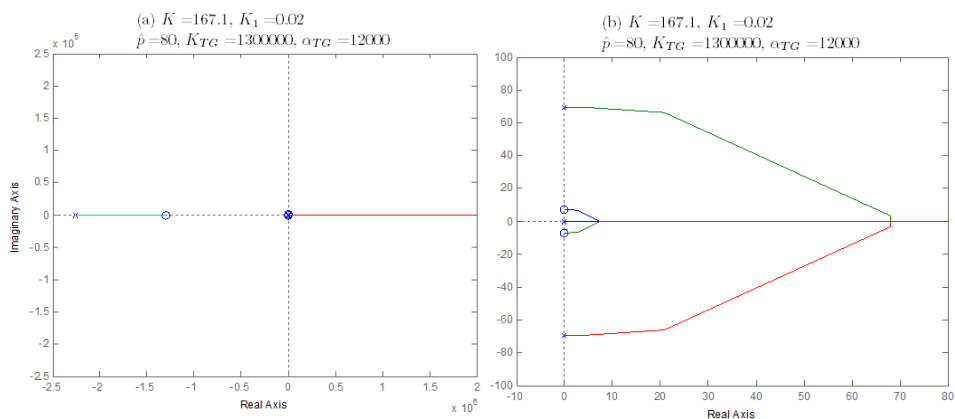


Figure 6.9 a. The root locus for p parameter when $K = 167.1, K_1 = 0.02, \hat{p} = 80, \alpha_{TC} = 12000$ and $K_{TC} = 1300000$, b. Zoomed in root locus visualizing the portion of the diagram around the break-away point.

Table 6.11 The upper and lower limits of p parameter for different α_{TG} values

α_{TG}	p^l	p^u
1.2	182	594
12	182	594
120	182	594
1200	188	595
12000	239	600

The lower limit of bistability region of p parameter increases when α_{TG} gets larger values. But again, the upper limit is almost constant.

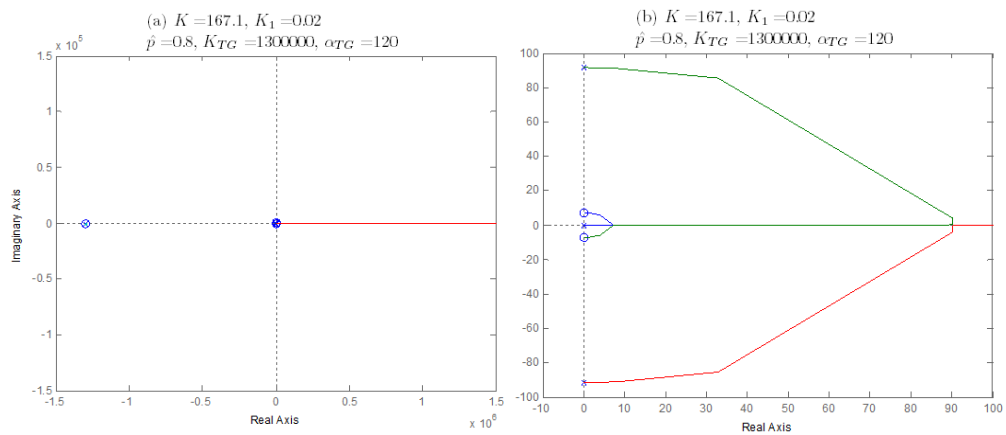


Figure 6.70 a. The root locus of p parameter when $K = 167.1, K_1 = 0.02, \hat{p} = 0.8$ and the nominal values of α_{TG} and K_{TG} in Michaelis-Menten kinetics, b. Zoomed in root locus visualizing the portion of the diagram around the break-away point.

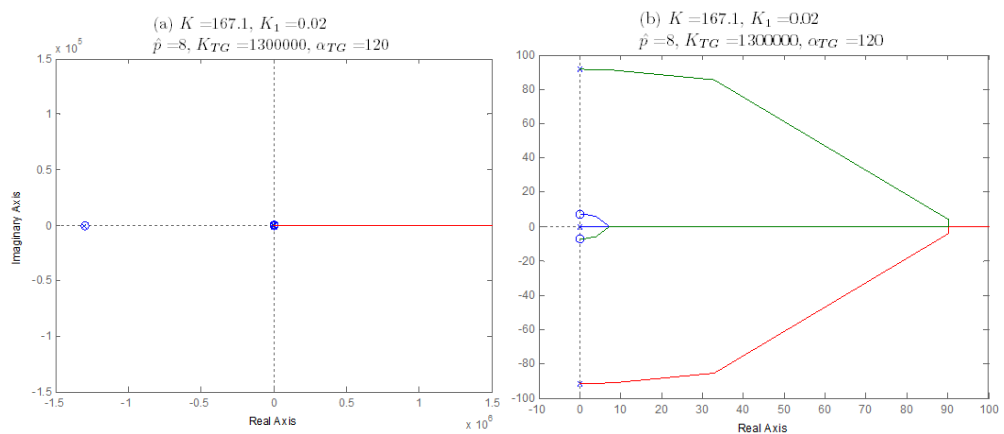


Figure 6.71 a. The root locus of p parameter when $K = 167.1, K_1 = 0.02, \hat{p} = 8$ and the nominal values of α_{TG} and K_{TG} in Michaelis-Menten kinetics, b. Zoomed in root locus visualizing the portion of the diagram around the break-away point.

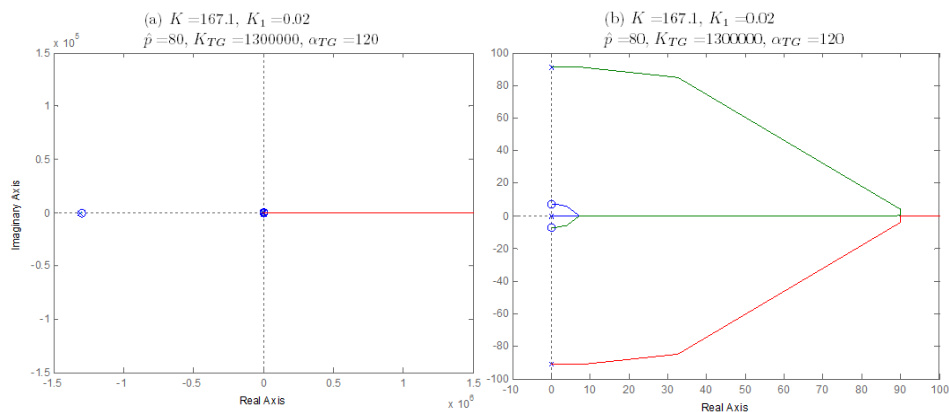


Figure 6.72 a. The root locus of p parameter when $K = 167.1$, $K_1 = 0.02$, $\hat{p} = 80$ and the nominal values of α_{TG} and K_{TG} in Michaelis-Menten kinetics, b. Zoomed in root locus visualizing the portion of the diagram around the break-away point.

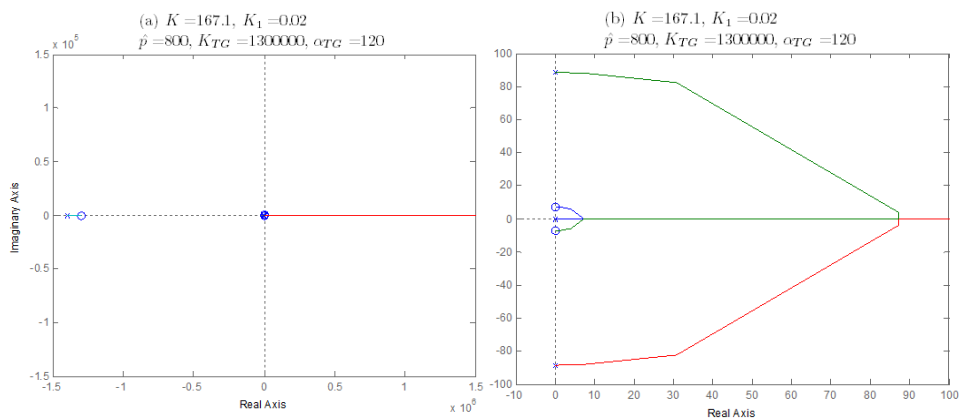


Figure 6.73 a. The root locus of p parameter when $K = 167.1$, $K_1 = 0.02$, $\hat{p} = 800$ and the nominal values of α_{TG} and K_{TG} in Michaelis-Menten kinetics, b. Zoomed in root locus visualizing the portion of the diagram around the break-away point.

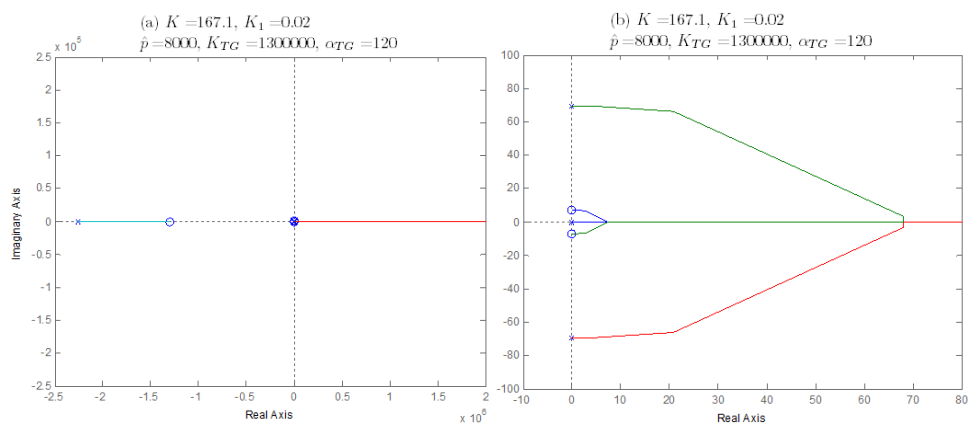


Figure 6.74 a. The root locus of p parameter when $K = 167.1$, $K_1 = 0.02$, $\hat{p} = 8000$ and the nominal values of α_{TG} and K_{TG} in Michaelis-Menten kinetics, b. Zoomed in root locus visualizing the portion of the diagram around the break-away point.

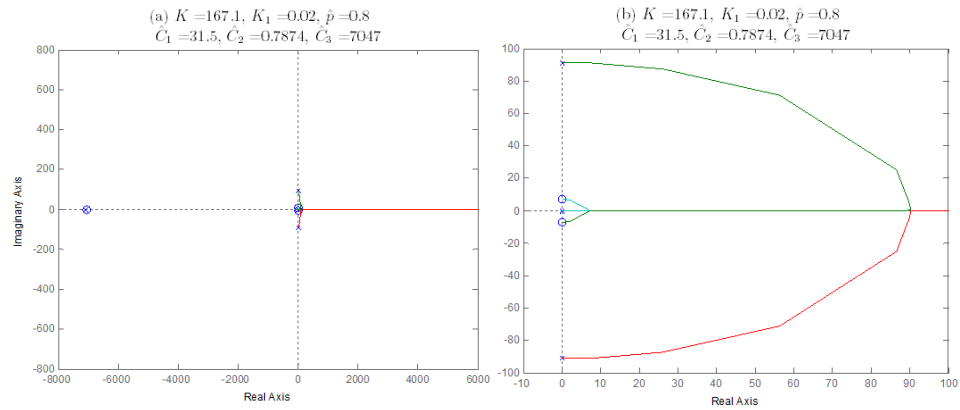


Figure 6.75 a. The root locus of p parameter when $K = 167.1, K_1 = 0.02, \hat{p} = 0.8$ and the nominal values of \hat{C}_1, \hat{C}_2 and \hat{C}_3 in bi-bi ordered kinetics, b. Zoomed in root locus visualizing the portion of the diagram around the break-away point.

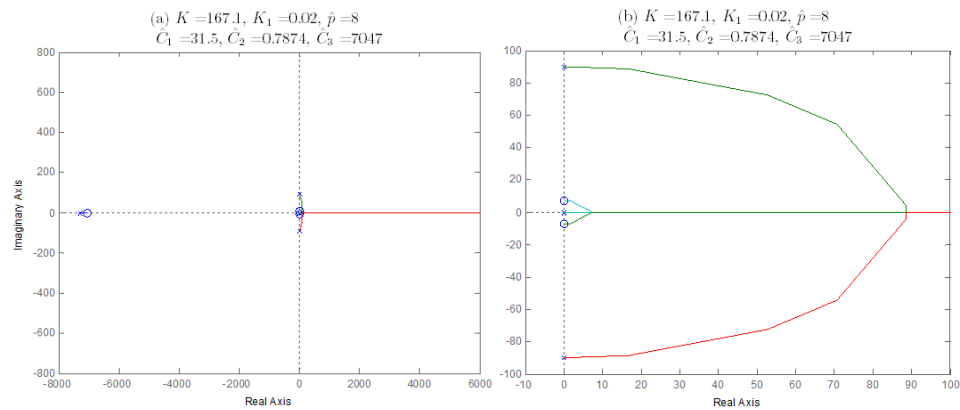


Figure 6.76 a. The root locus of p parameter when $K = 167.1, K_1 = 0.02, \hat{p} = 8$ and the nominal values of \hat{C}_1, \hat{C}_2 and \hat{C}_3 in bi-bi ordered kinetics, b. Zoomed in root locus visualizing the portion of the diagram around the break-away point.

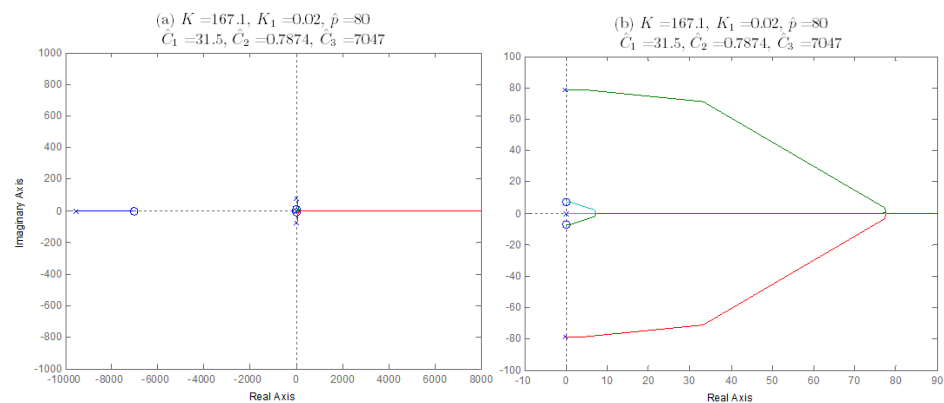


Figure 6.77 a. The root locus of p parameter when $K = 167.1, K_1 = 0.02, \hat{p} = 80$ and the nominal values of \hat{C}_1, \hat{C}_2 and \hat{C}_3 in bi-bi ordered kinetics, b. Zoomed in root locus visualizing the portion of the diagram around the break-away point.

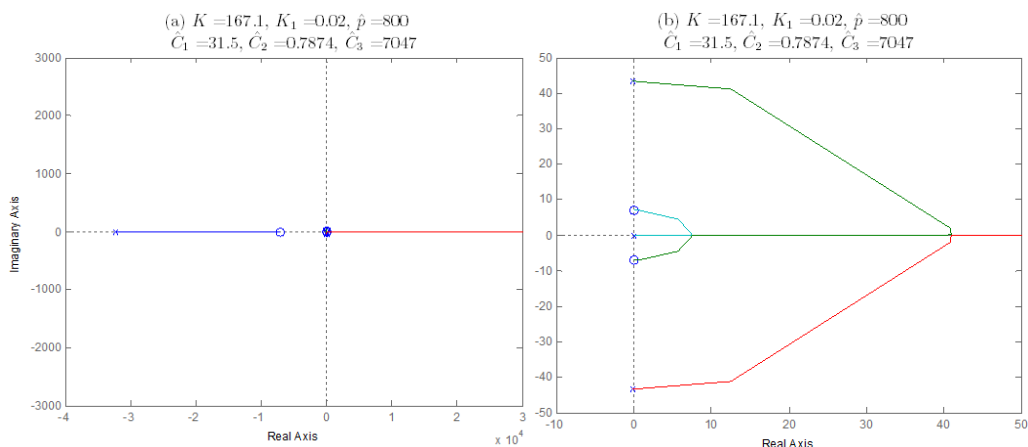


Figure 6.77 a. The root locus of p parameter when $K = 167.1$, $K_1 = 0.02$, $\hat{p} = 800$ and the nominal values of \widehat{C}_1 , \widehat{C}_2 and \widehat{C}_3 in bi-bi ordered kinetics, b. Zoomed in root locus visualizing the portion of the diagram around the break-away point.

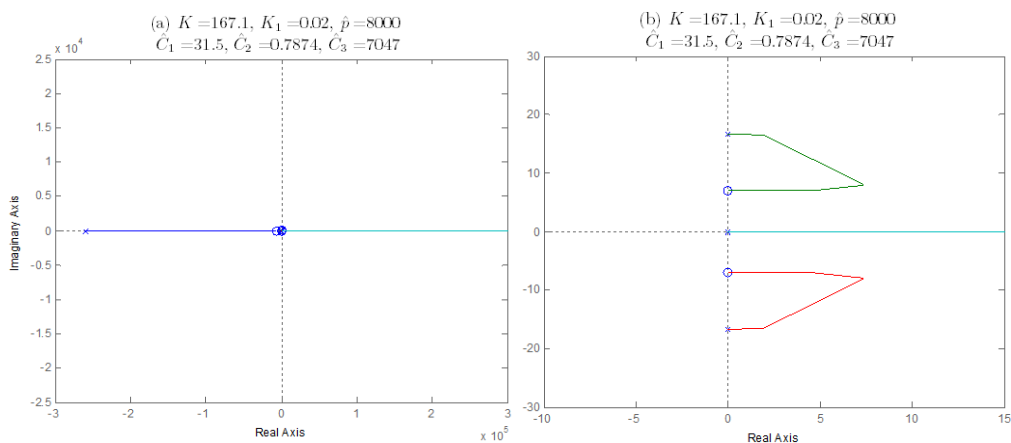


Figure 6.78 a. The root locus of p parameter when $K = 167.1$, $K_1 = 0.02$, $\hat{p} = 8000$ and the nominal values of \widehat{C}_1 , \widehat{C}_2 and \widehat{C}_3 in bi-bi ordered kinetics, b. Zoomed in root locus visualizing the portion of the diagram around the break-away point.

Table 6.12 The upper and lower limits of p parameter for different \hat{p} values

\hat{p}	Michaelis-Menten		Bi-Bi ordered	
	p^l	p^u	p^l	p^u
0.8	182	594	182	594
8	182	594	185	595
80	182	594	211	597
800	188	595	383	620
8000	239	600	No	No

The lower limit of the p parameter in bi-bi ordered kinetic increases faster than in Michaelis-Menten kinetics. The upper limits in both kinetic, are almost constant.

6.2.3 Root locus for K_1 Parameter

The root locus for K_1 parameter is drawn for both of the acetylation kinetics to determine the effect of the tansacetylase in lac operon model to compare the bistability region with the mathematical model without transacetylase. Like K and p parameters, to determine the bistability region of K_1 parameter, the root locus of K_1 is drawn for mathematical model without transacetylase effect $p = 250$ and $K = 167.1$ in Figure 6.79. The lower and upper limits of the bistability region is determined as $K_1 \in (0.0106, 0.113)$ from the root locus graph.

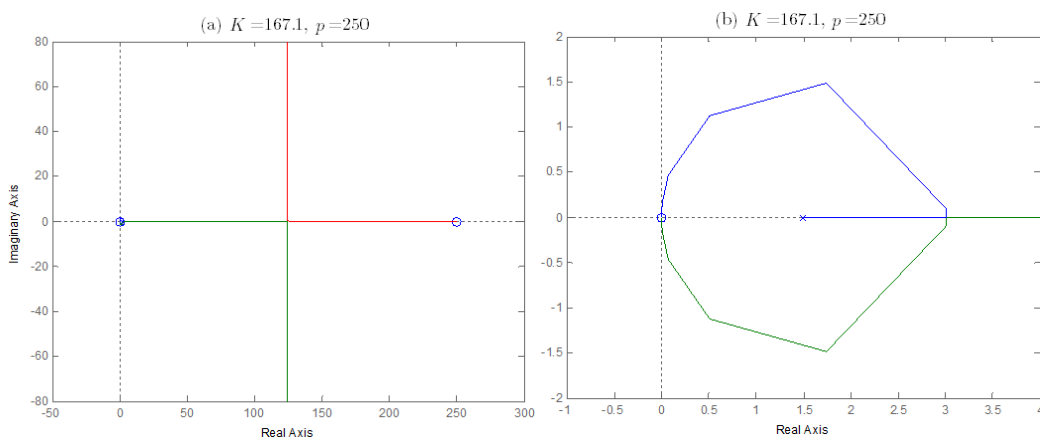


Figure 6.79 a. The root locus of K_1 parameter for the model without transacetylase effect when $K = 167.1$ and $p = 250$ b. Zoomed in root locus visualizing the portion of the diagram around the break-away point.

The root locus for Michaelis-Menten kinetic, the characteristic equation is defined for K_1 parameter in the equation below.

$$1 + \frac{K_1[T^4 + (K_{TG} - p + \alpha_{TG}\hat{p})T^3 - pK_{TG}T^2]}{KT^2 + (KK_{TG} + \alpha_{TG}\hat{p} - p)T - pK_{TG}} = 0 \quad (115)$$

The root locus for K_1 parameter is drawn with default values of the other parameters in Figure 6.80. Similarly, to identify the effects of the acetylation kinetics in the bistability region, another root locus for K_1 parameter when $p = 250$, $\hat{p} = 80$, $\alpha_{TG} = \widehat{C}_1$, $K_{TG} = \widehat{C}_3$ and $K = 167.1$ is given in Figure 6.81. The bistability region for Michaelis-Menten kinetics with the nominal parameter values is determined as $K_1 \in (0.0106, 0.113)$ similar to the mathematical model without tranacetylase effect. For Michaelis-Menten kinetics with $\alpha_{TG} = \widehat{C}_1$, $K_{TG} = \widehat{C}_3$, the bistability region gets narrow and it is obtained from root locus graph as $K_1 \in (0.0143, 0.114)$.

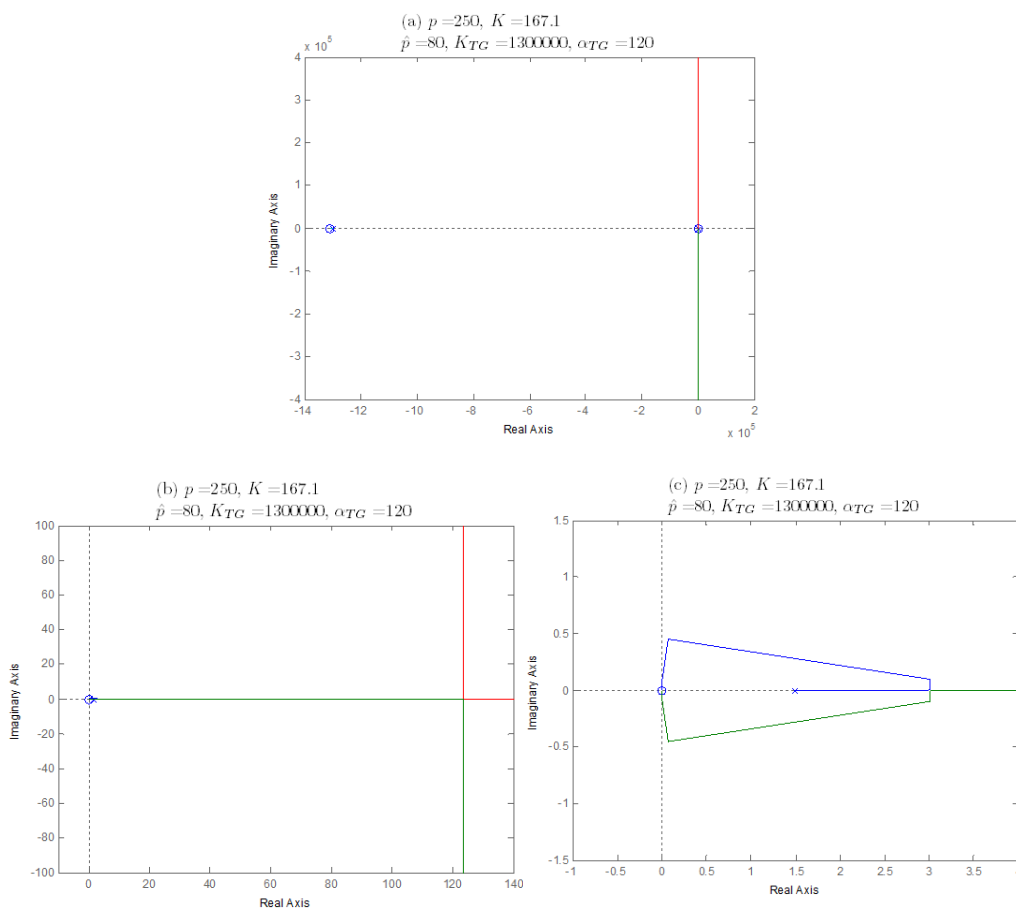


Figure 6.80 a. The root locus for K_1 parameter when $p = 250$ and $K = 167.1$ for Michaelis-Menten kinetics with nominal parameter values, b.-c. Zoomed in root locus visualizing the portion of the diagram around the break-in/away point.

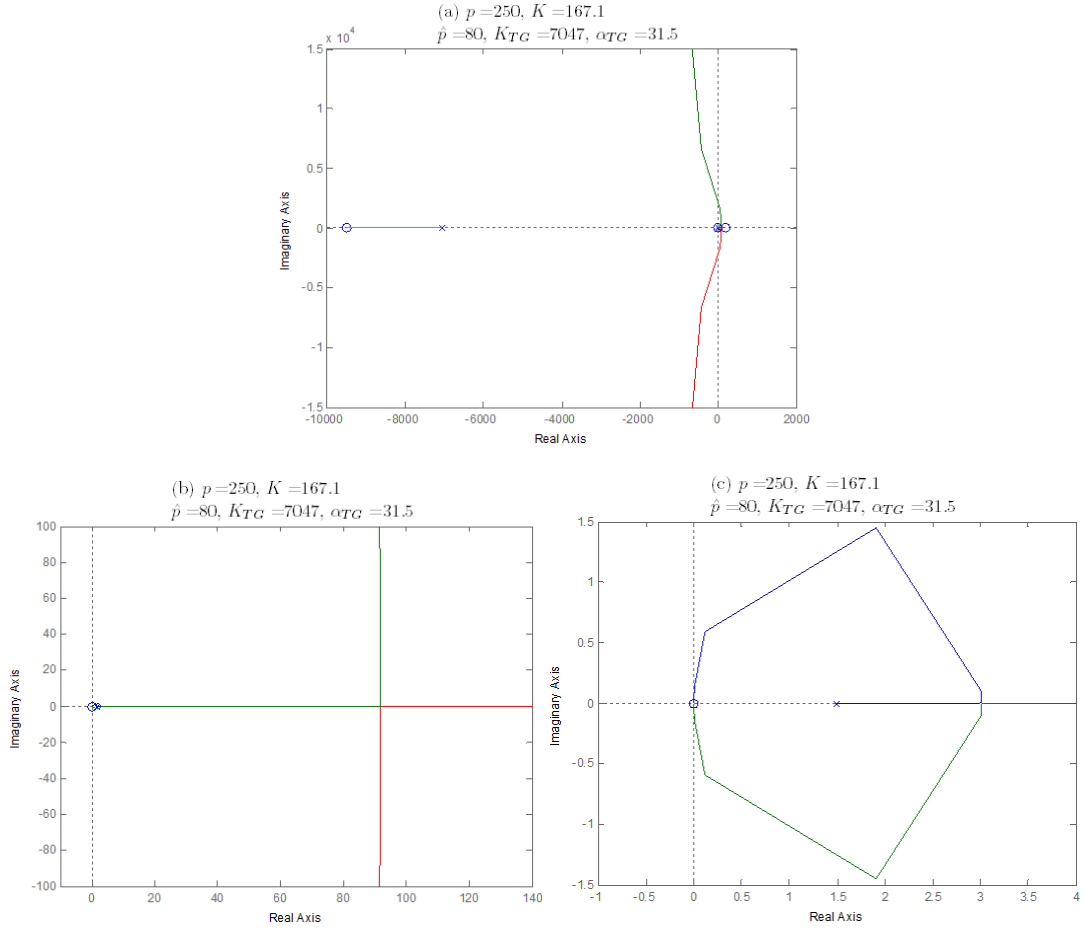


Figure 6.81 a. The root locus for K_1 parameter when $p = 250, K = 167.12, \hat{p} = 80, \alpha_{TG} = \widehat{C}_1$ and $K_{TG} = \widehat{C}_3$, b.-c. Zoomed in root locus visualizing the portion of the diagram around the break-in/away point.

The root locus for bi-bi ordered kinetics, the characteristic equation according to K_1 parameter is defined in Equation (116).

$$1 + \frac{K_1 [T^2 + (\widehat{C}_3 - p + \hat{p}\widehat{C}_1)T - (p\widehat{C}_3 + \hat{p}\widehat{C}_2)]T^2}{KT^2 + (K\widehat{C}_3 - p + \hat{p}\widehat{C}_1)T - (p\widehat{C}_3 + \hat{p}\widehat{C}_2)} = 0 \quad (116)$$

The root locus for K_1 parameter is drawn with nominal parameter values in bi-bi ordered kinetics in Figure 6.82. The root locus for the condition $\widehat{C}_2 = 0$ is given in Figure 6.83 to determine the effect of \widehat{C}_2 parameter in the bistability region. The lower and upper limits are again equal to each other as $K_1 \in (0.0143, 0.114)$.

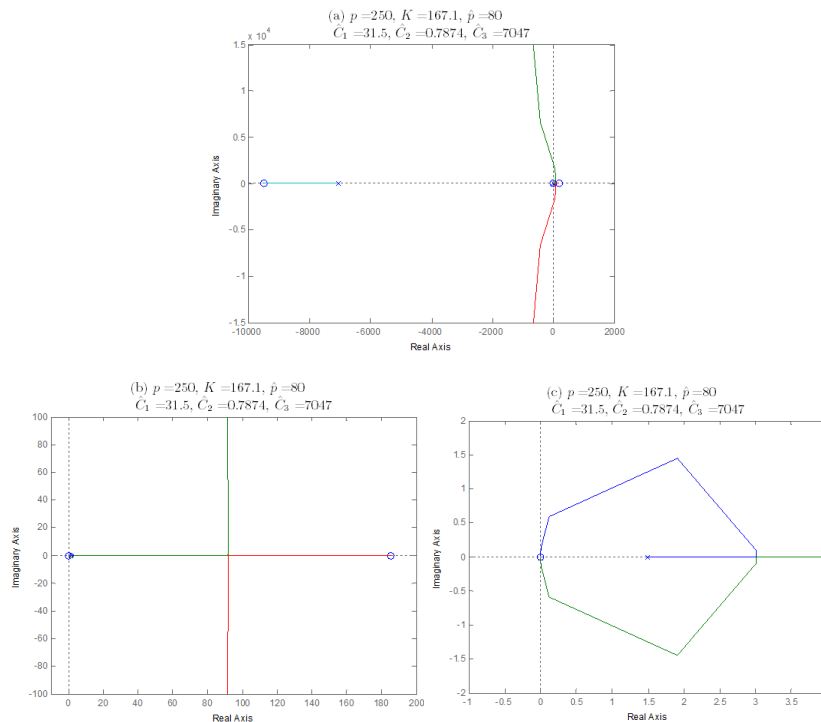


Figure 6.82 a. The root locus for K_1 parameter when $p = 250, K = 167.1, \hat{p} = 80, \widehat{C}_1 = 31.5, \widehat{C}_2 = 0.7874$ and $\widehat{C}_3 = 7047$, b.-c. Zoomed in root locus visualizing the portion of the diagram around the break-in/away point.

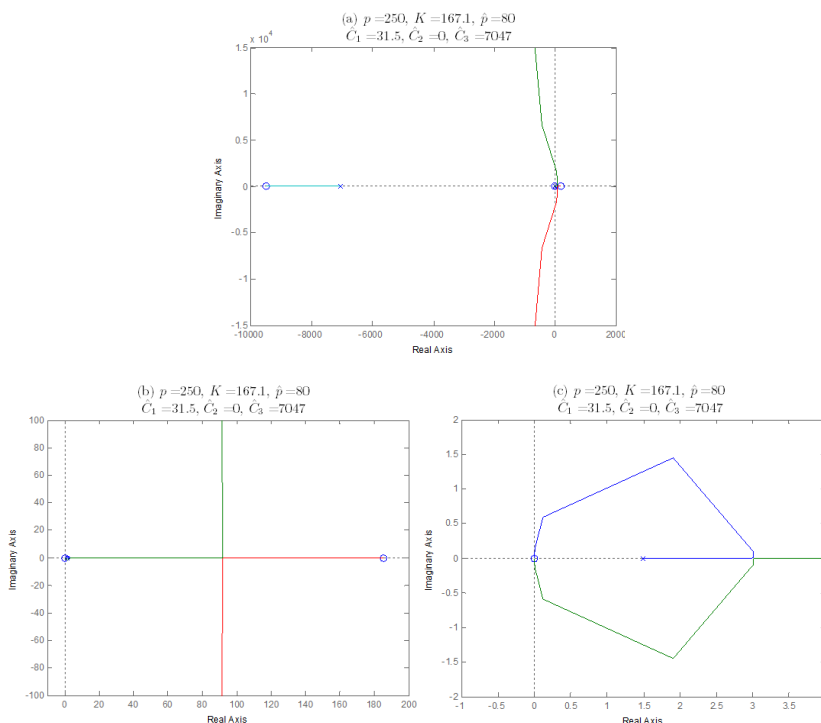


Figure 6.83 a. The root locus for K_1 parameter when $p = 250, K = 167.1, \hat{p} = 80, \widehat{C}_1 = 31.5, \widehat{C}_2 = 0$ and $\widehat{C}_3 = 7047$, b.-c. Zoomed in root locus visualizing the portion of the diagram around the break-in/away point.

The root locus plots for five different multiples of each as $\widehat{C}_1, \widehat{C}_2, \widehat{C}_3, \alpha_{TG}, K_{TG}$ and \hat{p} parameter are drawn and the K_1^l and K_1^u are determined given below.

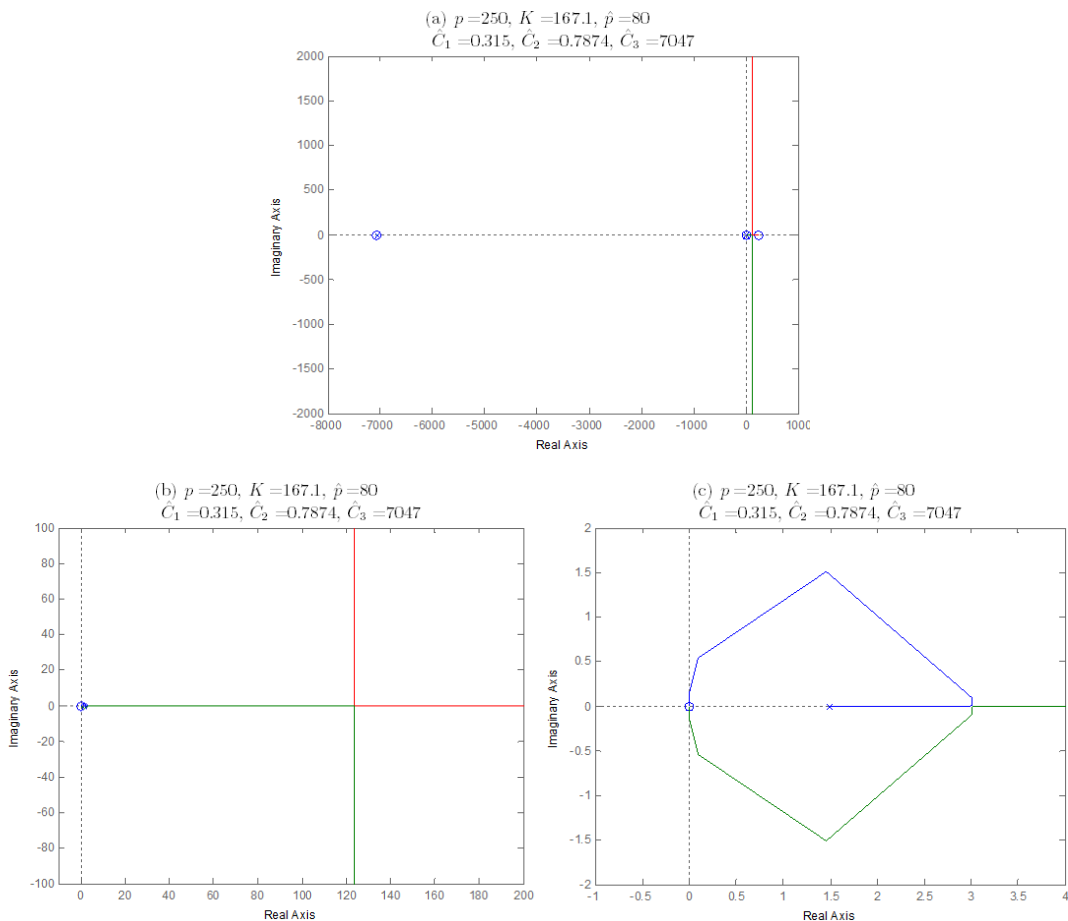


Figure 6.84 a. The root locus for K_1 parameter when $p = 250, K = 167.1, \hat{p} = 80, \widehat{C}_1 = 0.315, \widehat{C}_2 = 0.7874$ and $\widehat{C}_3 = 7047$, b.-c. Zoomed in root locus visualizing the portion of the diagram around the break-in/away point.

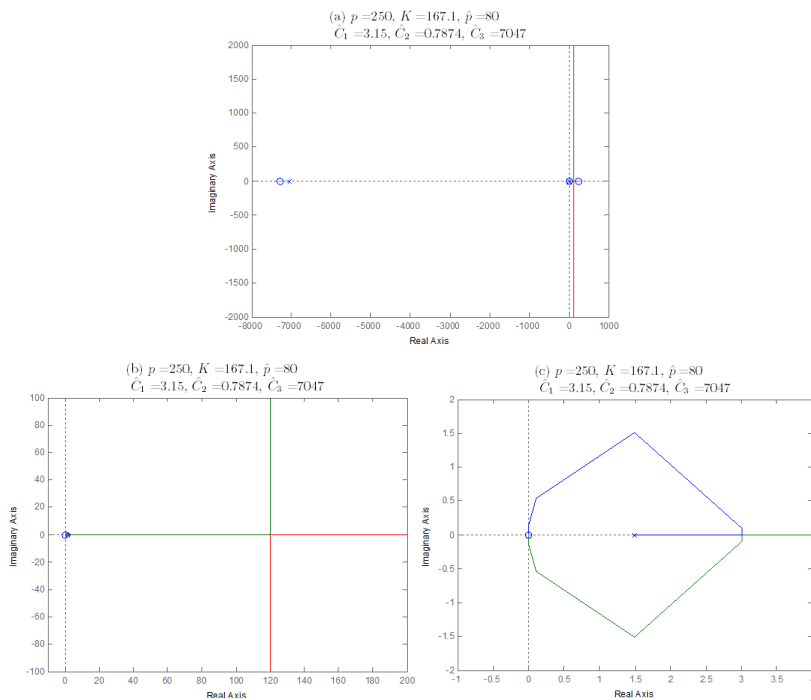


Figure 6.85 a. The root locus for K_1 parameter when $p = 250, K = 167.1, \hat{p} = 80, \hat{C}_1 = 3.15, \hat{C}_2 = 0.7874$ and $\hat{C}_3 = 7047$, b.-c. Zoomed in root locus visualizing the portion of the diagram around the break-in/away point.

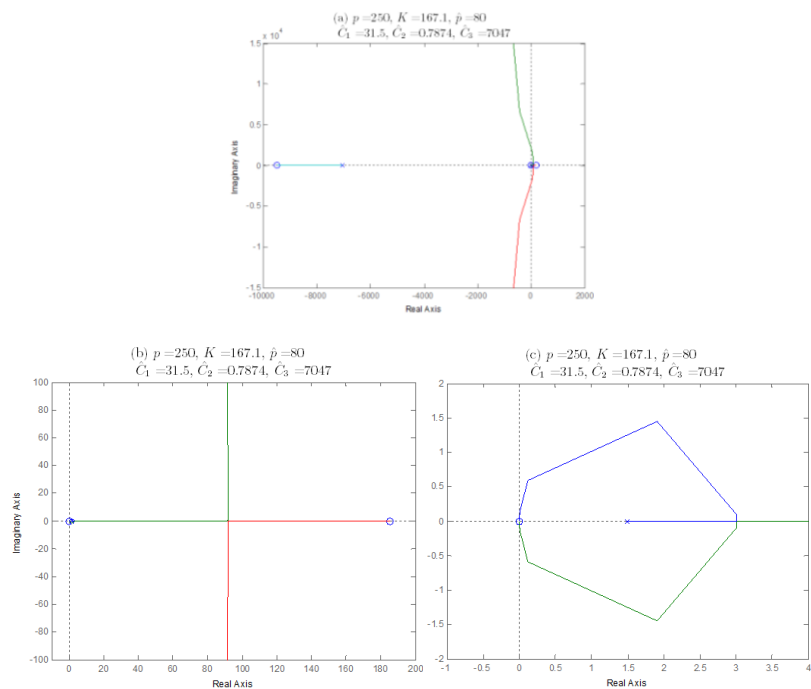


Figure 6.86 a. The root locus for K_1 parameter when $K = 167.1, \hat{p} = 80, \hat{C}_1 = 31.5, \hat{C}_2 = 0.7874$ and $\hat{C}_3 = 7047$, b.-c. Zoomed in root locus visualizing the portion of the diagram around the break-in/away point.

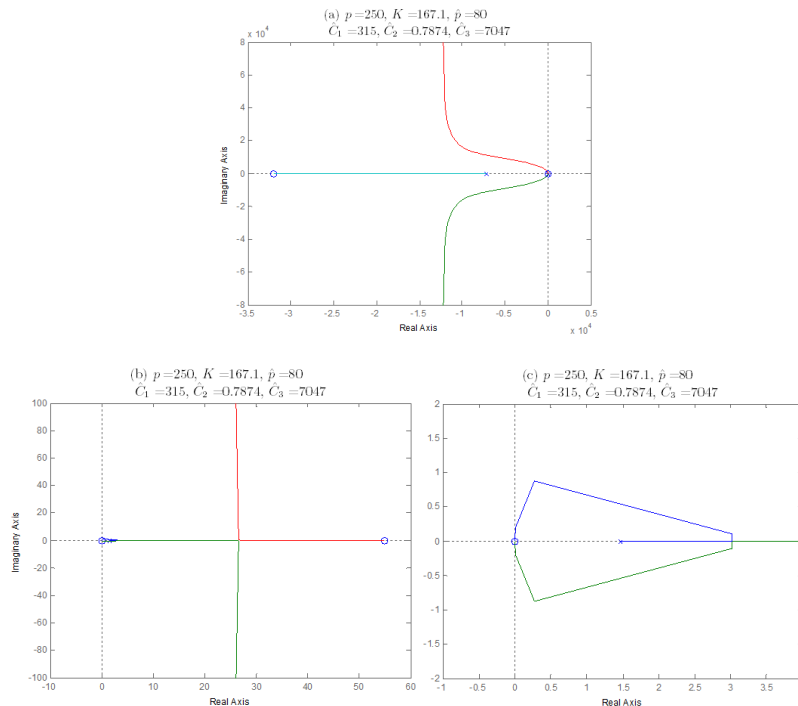


Figure 6.87 a. The root locus for K_1 parameter when $K = 167.1, \hat{p} = 80, \widehat{C}_1 = 315, \widehat{C}_2 = 0.7874$ and $\widehat{C}_3 = 7047$, b.-c. Zoomed in root locus visualizing the portion of the diagram around the break-in/away point.

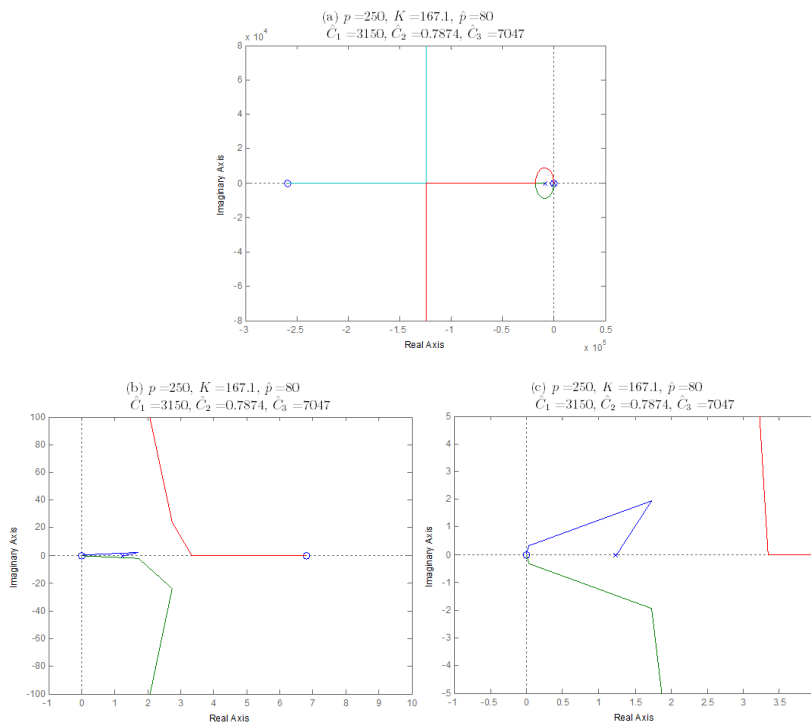


Figure 6.88 a. The root locus for K_1 parameter when $K = 167.1, \hat{p} = 80, \widehat{C}_1 = 3150, \widehat{C}_2 = 0.7874$ and $\widehat{C}_3 = 7047$, b.-c. Zoomed in root locus visualizing the portion of the diagram around the break-in/away point.

Table 6.13 The upper and lower limits of K_1 parameter for different \widehat{C}_1 values

\widehat{C}_1	K_1^l	K_1^u
0.315	0.0106	0.113
3.15	0.0109	0.113
31.5	0.0143	0.114
315	0.0471	0.123
3150	No	No

While the upper limit of the K_1 parameter changes slowly, the lower limit changes more rapidly.

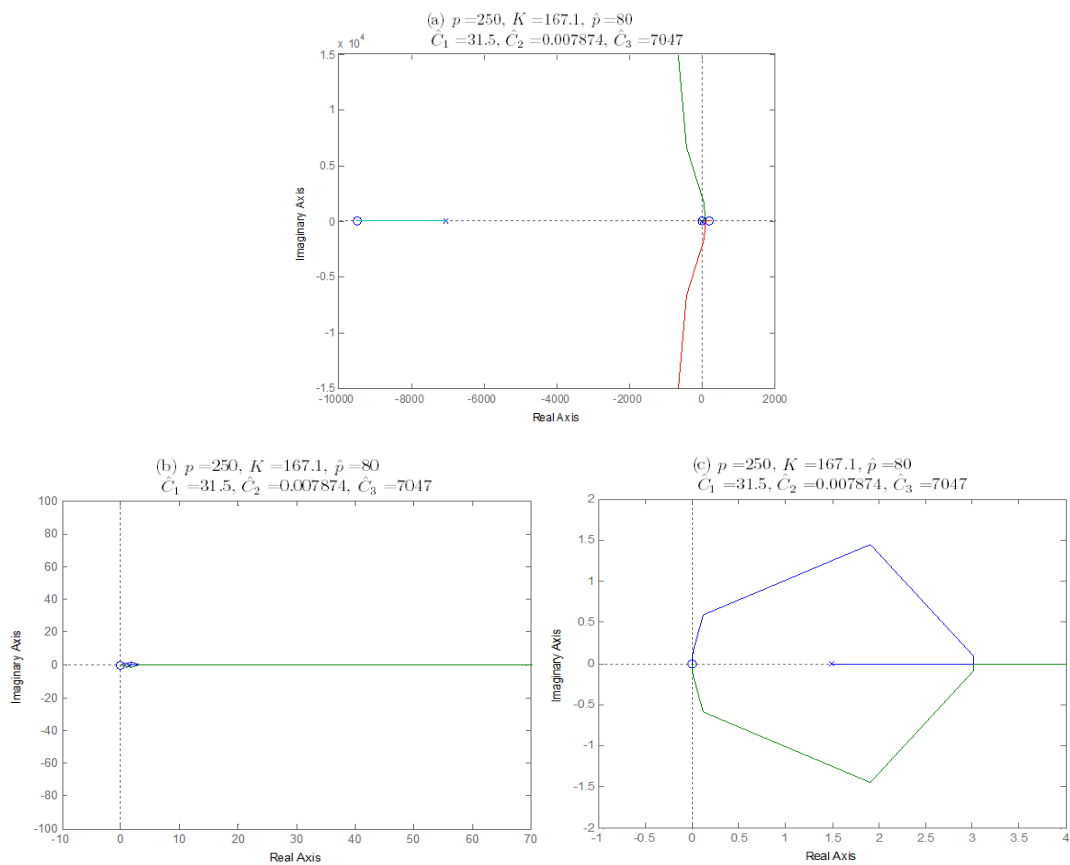


Figure 6.89 a. The root locus for K_1 parameter when $\widehat{C}_2 = 0.007874$ and the others are equal to nominal values, b.-c. Zoomed in root locus visualizing the portion of the diagram around the break-in/away point.

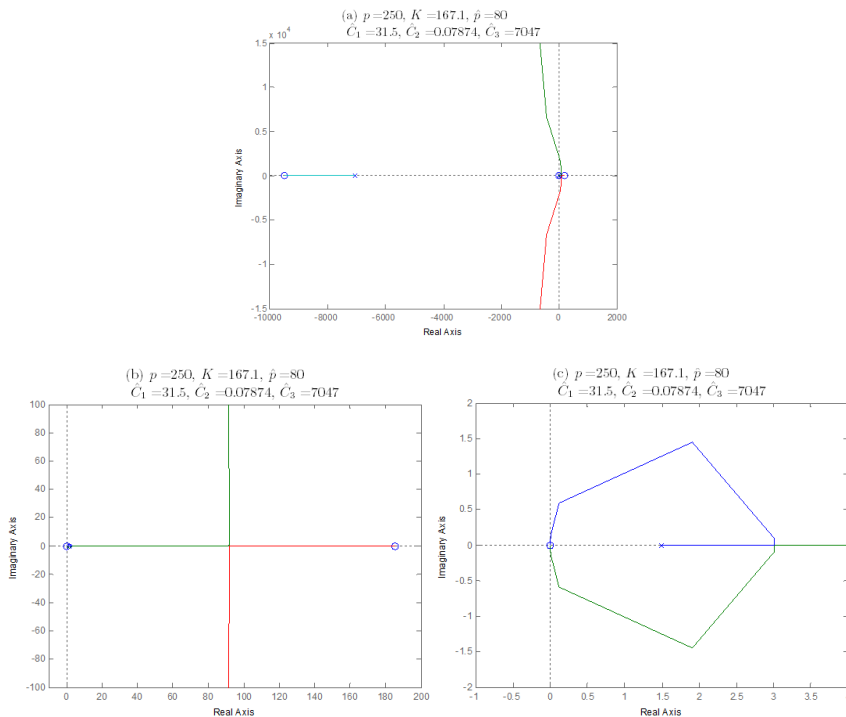


Figure 6.90 a. The root locus for K_1 parameter when $\widehat{C}_2 = 0.07874$ and the others are fixed, b.-c. Zoomed in root locus visualizing the portion of the diagram around the break-in/away point.

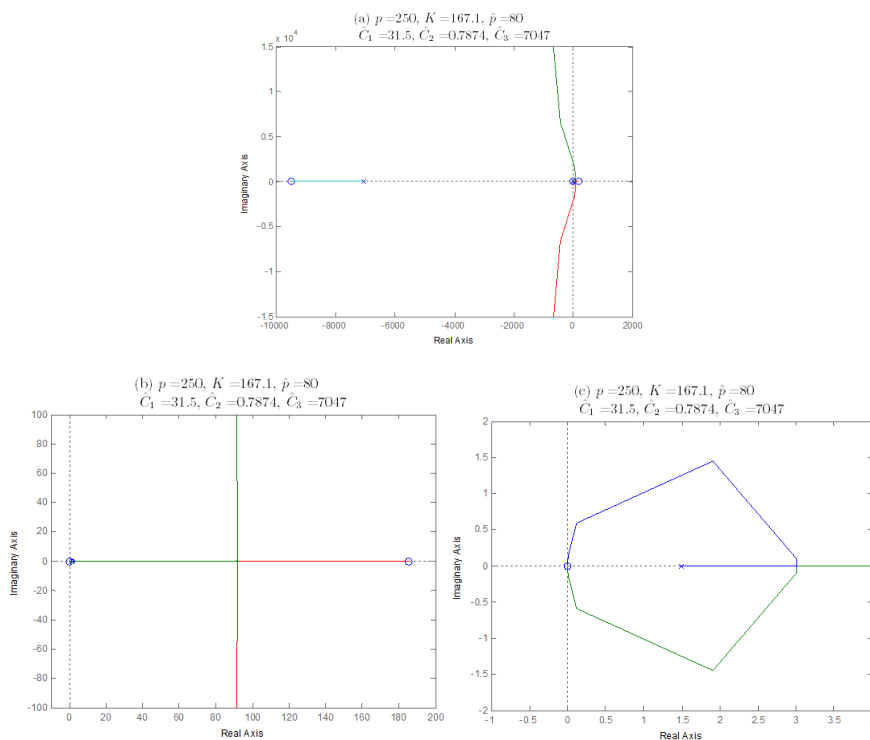


Figure 6.91 a. The root locus for K_1 parameter when $\widehat{C}_2 = 0.7874$ and the others are fixed, b.-c. Zoomed in root locus visualizing the portion of the diagram around the break-in/away point.

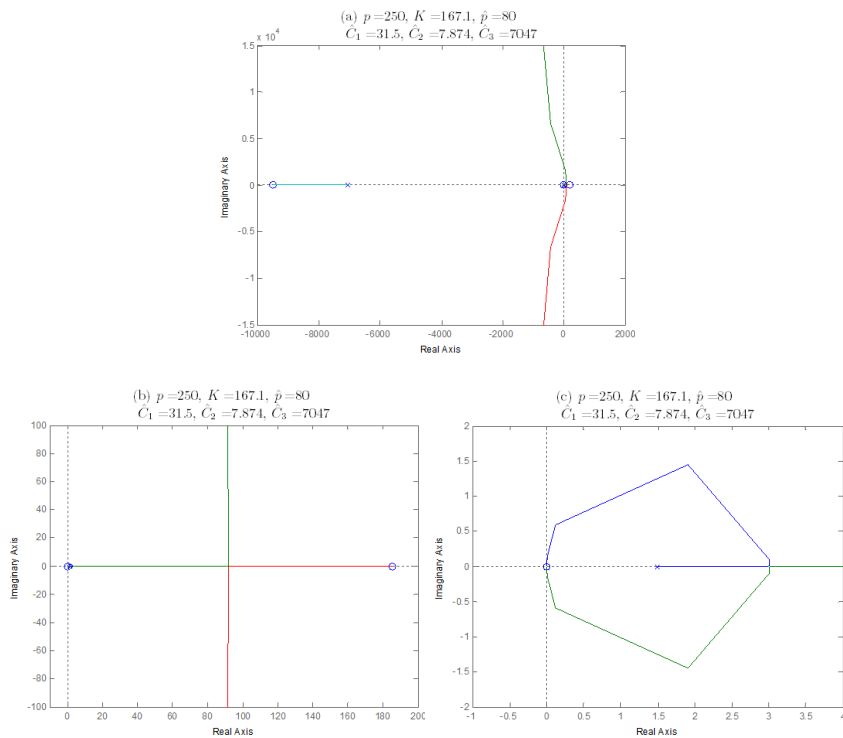


Figure 6.92 a. The root locus for K parameter when $\widehat{C}_2 = 7.874$ and the others are fixed, b.-c. Zoomed in root locus visualizing the portion of the diagram around the break-in/away point.

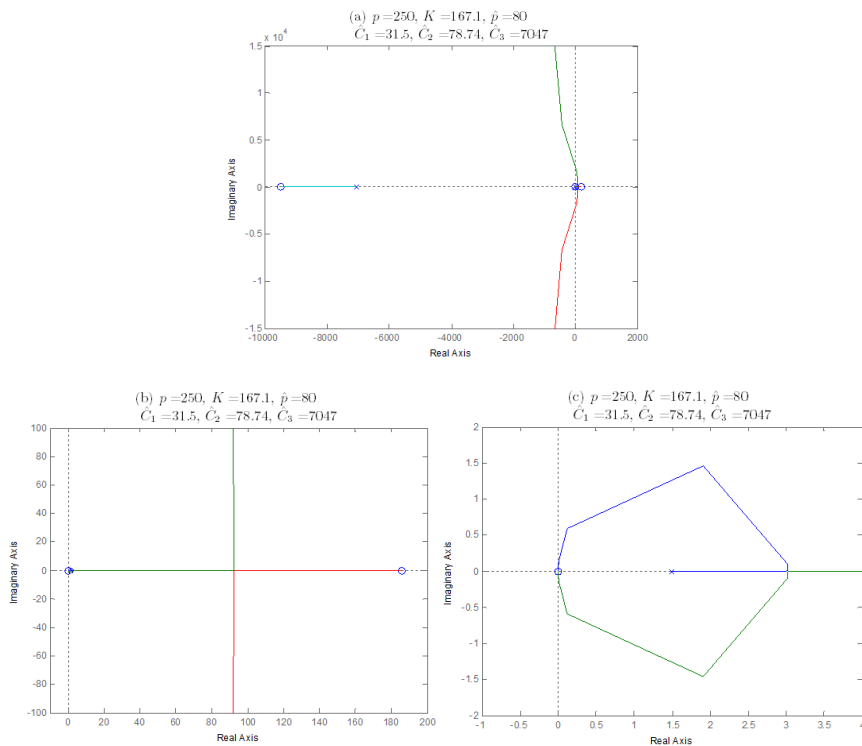


Figure 6.93 a. The root locus for K parameter when $\widehat{C}_2 = 78.74$ and the others are fixed, b.-c. Zoomed in root locus visualizing the portion of the diagram around the break-in/away point.

Table 6.14 The upper and lower limits of K_1 parameter for different \widehat{C}_2 values

\widehat{C}_2	K_1^l	K_1^u
0.007874	0.0143	0.114
0.07874	0.0143	0.114
0.7874	0.0143	0.114
7.874	0.0143	0.114
78.74	0.0142	0.0113

While the upper limit of the K_1 parameter is almost constant, the lower limit changes a small amount for different \widehat{C}_2 values.

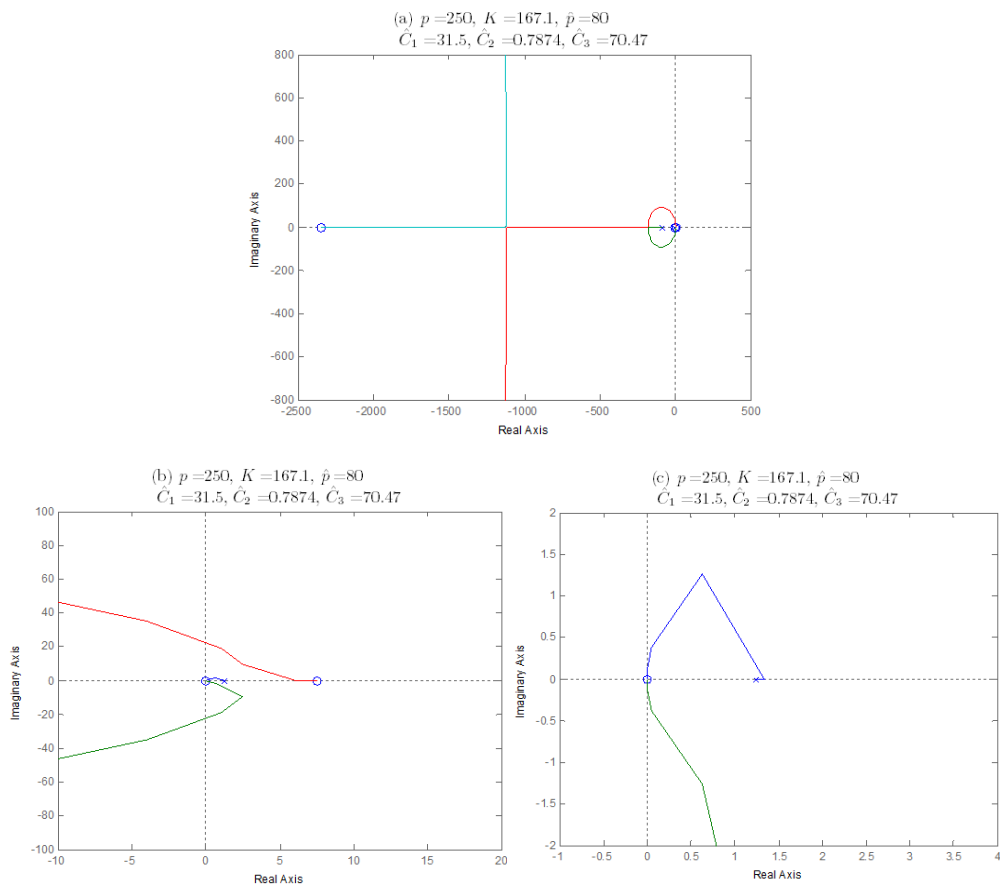


Figure 6.94 a. The root locus for K_1 parameter when $\widehat{C}_3 = 70.47$ and the others are fixed, b.-c. Zoomed in root locus visualizing the portion of the diagram around the break-in/away point.

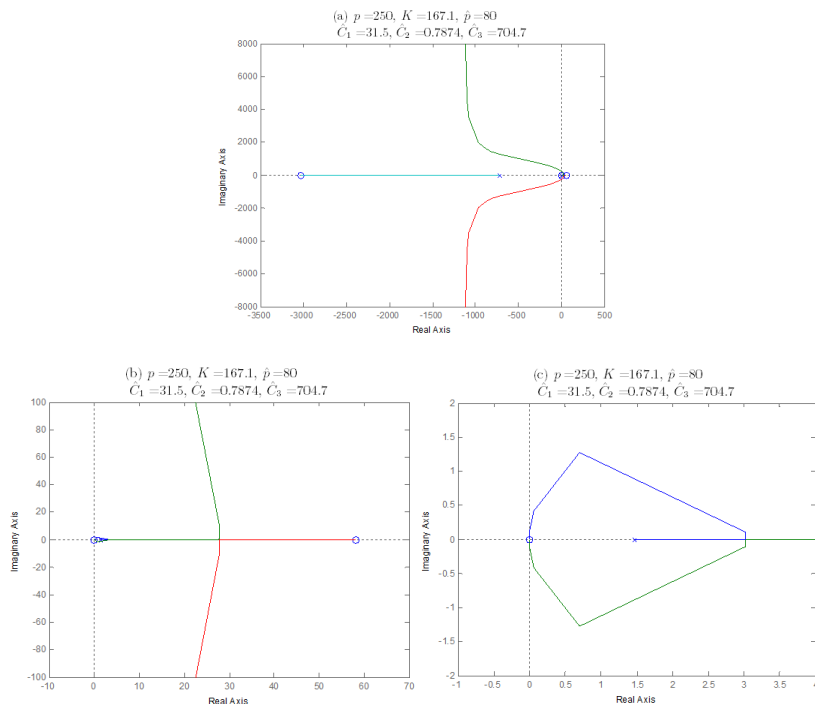


Figure 6.95 a. The root locus for K_1 parameter when $\widehat{C}_3 = 704.7$ and the others are fixed, b.-c. Zoomed in root locus visualizing the portion of the diagram around the break-in/away point.

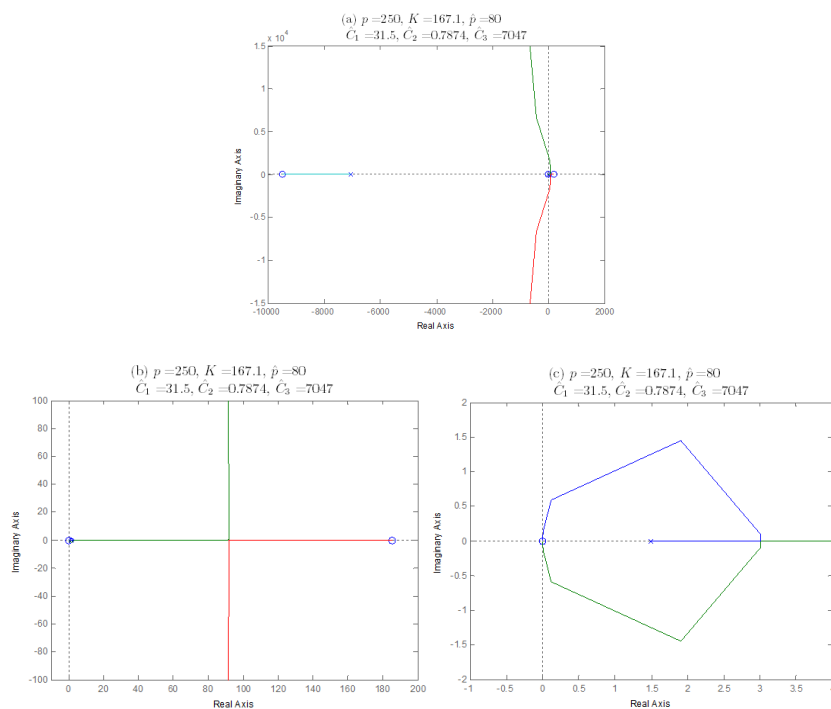


Figure 6.96 a. The root locus for K_1 parameter when $\widehat{C}_3 = 7047$ and the others are fixed, b.-c. Zoomed in root locus visualizing the portion of the diagram around the break-in/away point.

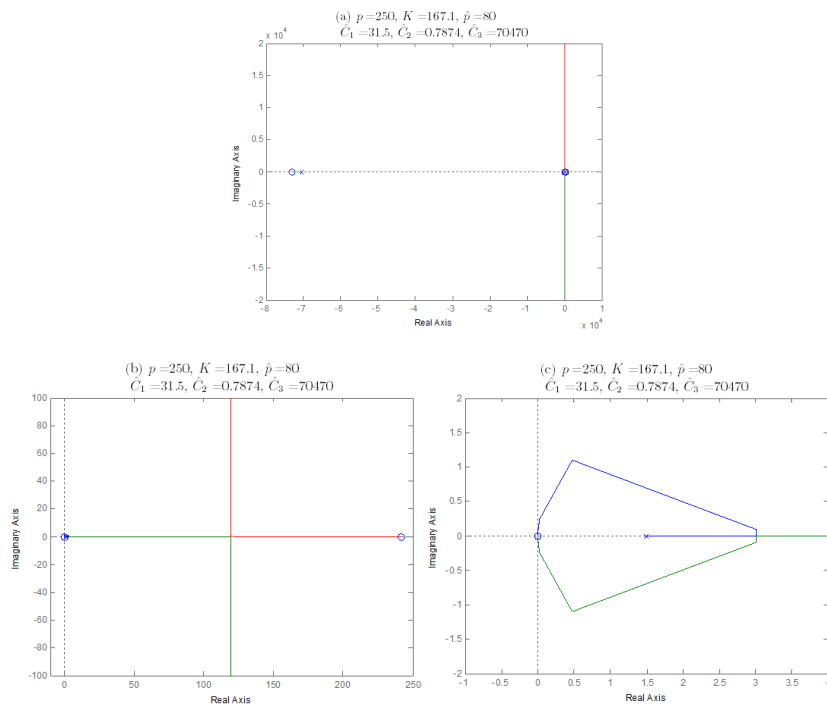


Figure 6.97 a. The root locus for K_1 parameter when $\widehat{C}_3 = 70470$ and the others are fixed, b.-c. Zoomed in root locus visualizing the portion of the diagram around the break-in/away point.

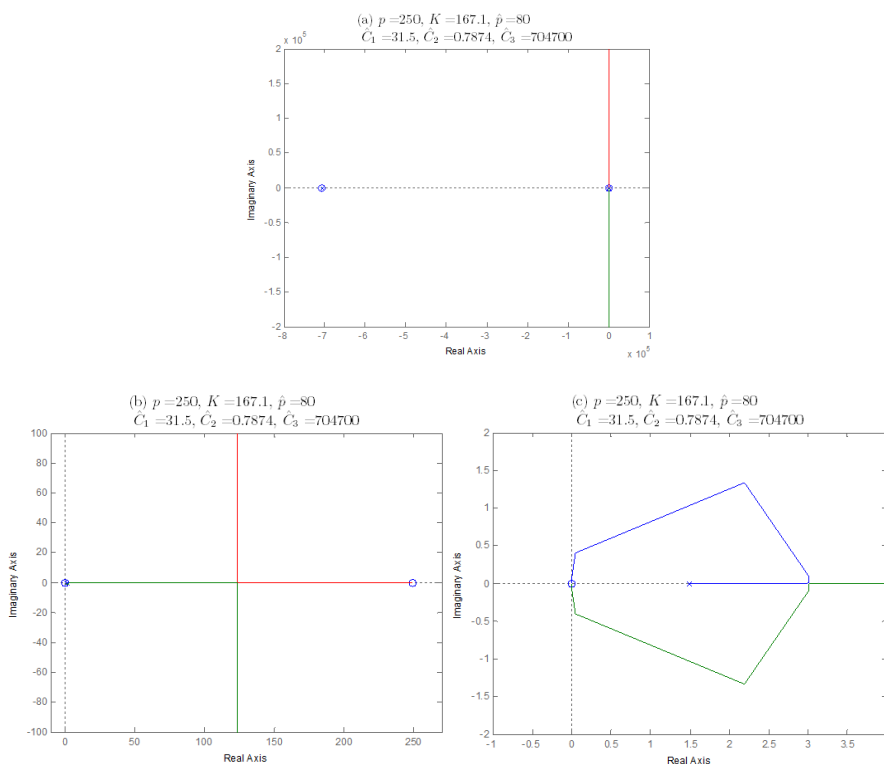


Figure 6.98 a. The root locus for K_1 parameter when $\widehat{C}_3 = 704700$ and the others are fixed, b.-c. Zoomed in root locus visualizing the portion of the diagram around the break-in/away point.

Table 6.15 The upper and lower limits of K_1 parameter for different \widehat{C}_3 values

\widehat{C}_3	K_1^l	K_1^u
70.47	No	No
704.7	0.0459	0.123
7047	0.0143	0.114
70470	0.0109	0.113
704700	0.0106	0.113

Similar to \widehat{C}_1 case, the upper limit changes in a small amount while the lower one is decreasing.

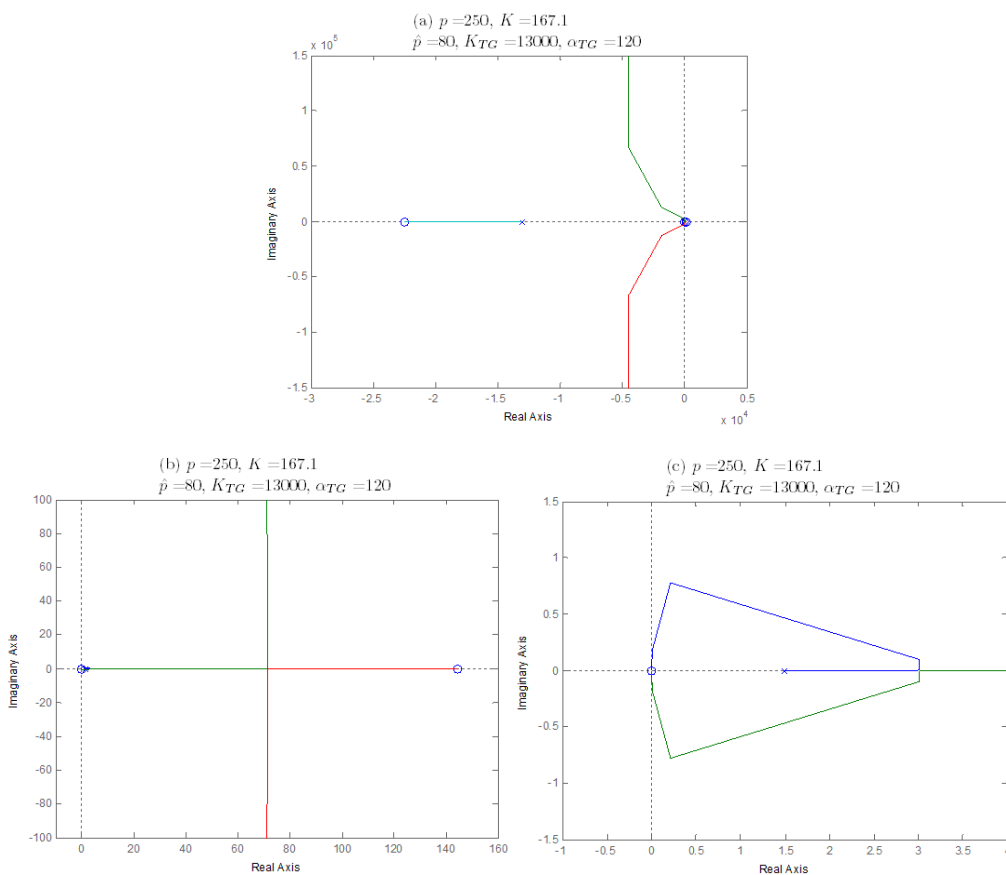


Figure 6.99 a. The root locus for K_1 parameter when $K_{TC} = 13000$, b.-c. Zoomed in root locus visualizing the portion of the diagram around the break-in/away point.

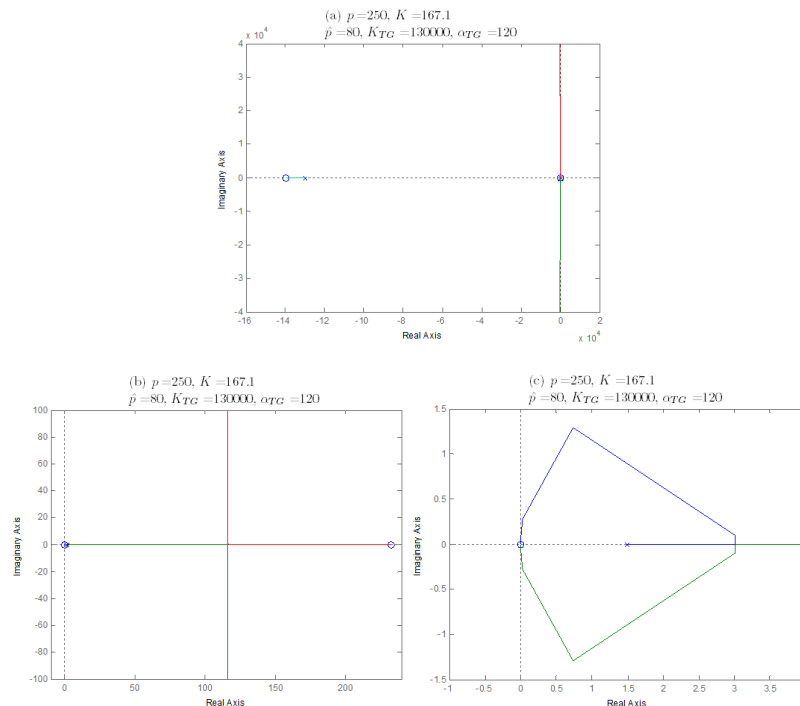


Figure 6.100 a. The root locus for K_1 parameter when $K_{TG} = 130000$, b.-c. Zoomed in root locus visualizing the portion of the diagram around the break-in/away point.

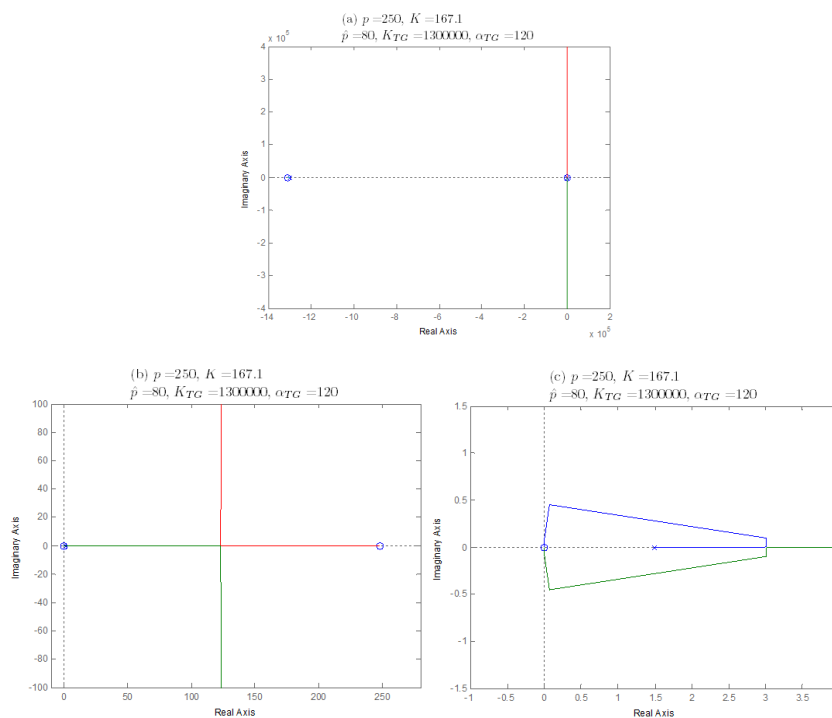


Figure 6.101 a. The root locus for K_1 parameter when $K_{TG} = 1300000$, b.-c. Zoomed in root locus visualizing the portion of the diagram around the break-in/away point.

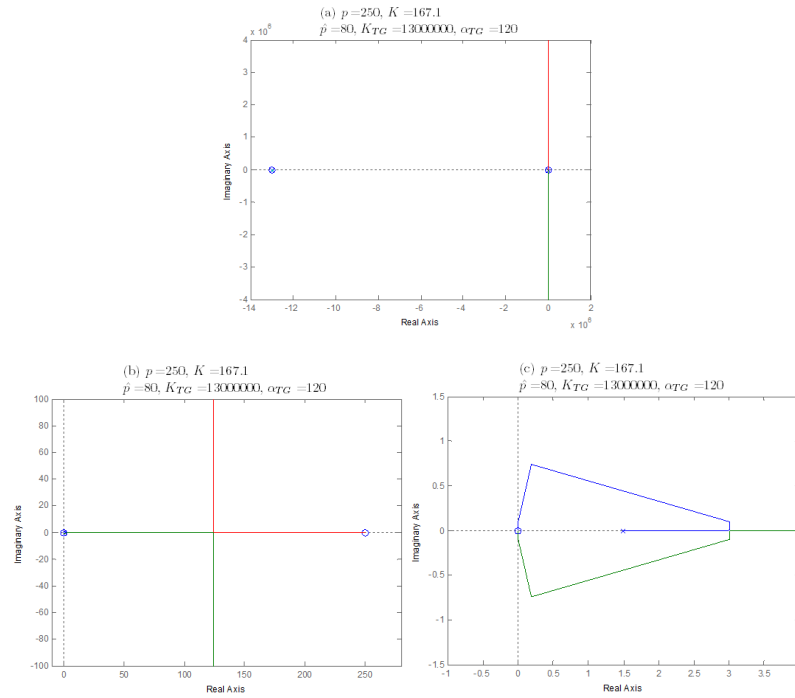


Figure 6.102 a. The root locus for K_1 parameter when $K_{TG} = 13000000$, b.-c. Zoomed in root locus visualizing the portion of the diagram around the break-in/away point.

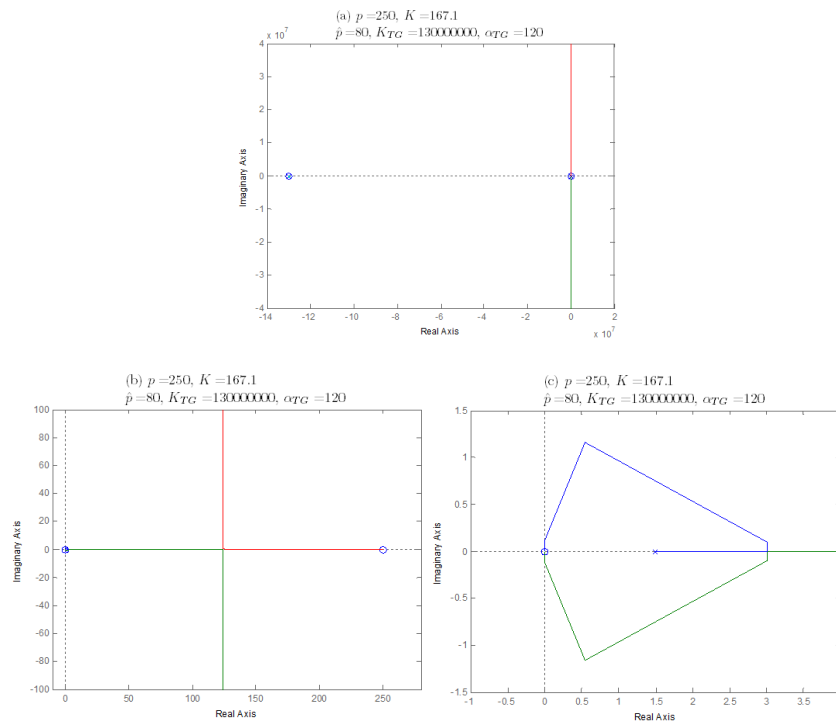


Figure 6.103 a. The root locus for K_1 parameter when $K_{TG} = 130000000$, b.-c. Zoomed in root locus visualizing the portion of the diagram around the break-in/away point.

Table 6.16 The upper and lower limits of K_1 parameter for different K_{TG} values

K_{TG}	K_1^l	K_1^u
13000	0.0182	0.115
130000	0.0113	0.113
1300000	0.0106	0.113
13000000	0.0106	0.113
130000000	0.0106	0.113

The lower limit of the bistability range decreases when K_{TG} increases, however the upper limit is almost constant.

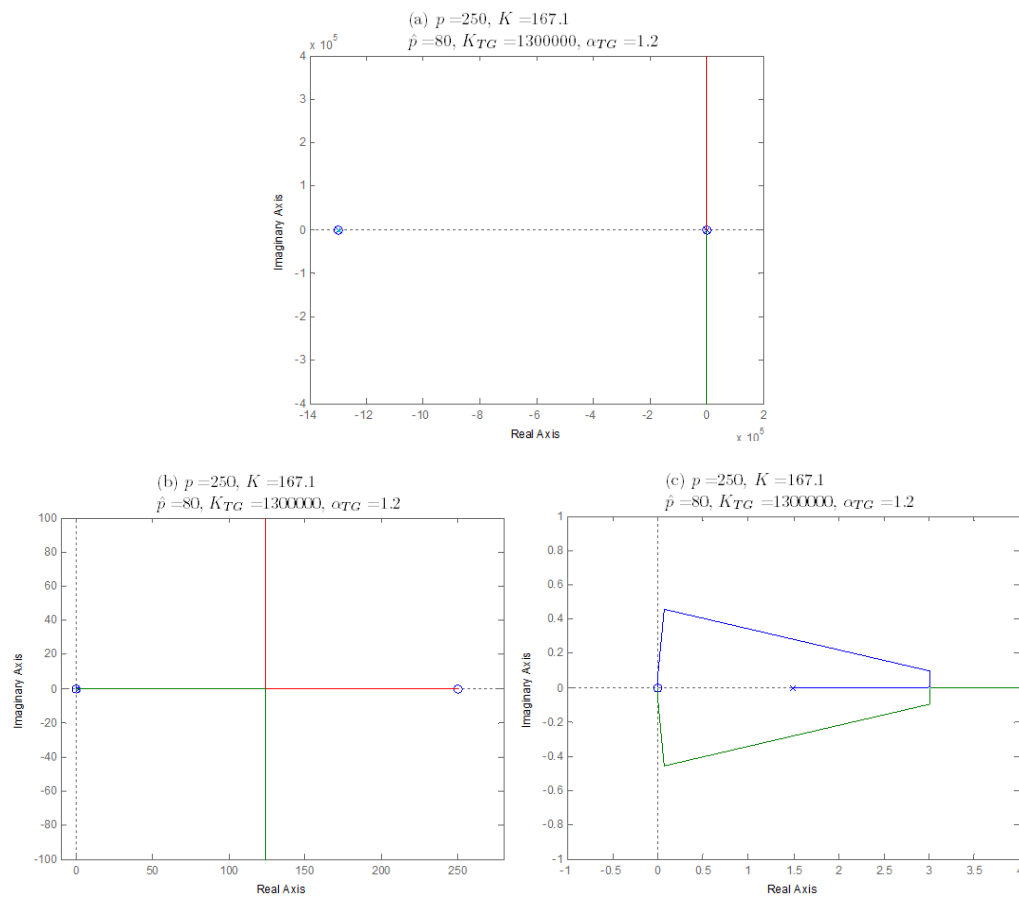


Figure 6.104 a. The root locus for K_1 parameter when $\alpha_{TG} = 1.2$, b.-c. Zoomed in root locus visualizing the portion of the diagram around the break-in/away point.

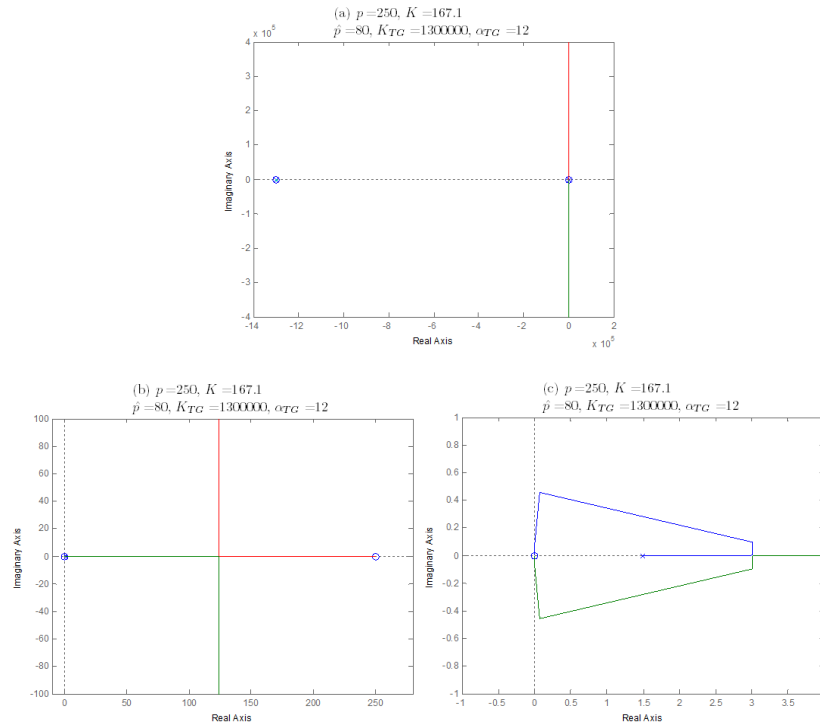


Figure 6.105 a. The root locus for K_1 parameter when $\alpha_{TC} = 12$, b.-c. Zoomed in root locus visualizing the portion of the diagram around the break-in/away point.

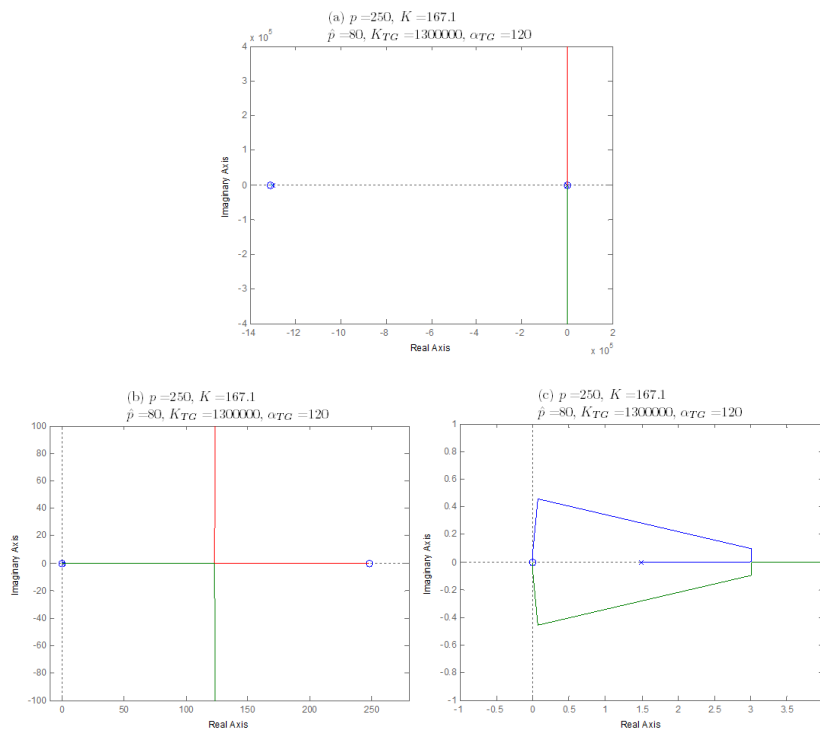


Figure 6.106 a. The root locus for K_1 parameter when $\alpha_{TC} = 120$, b.-c. Zoomed in root locus visualizing the portion of the diagram around the break-in/away point.

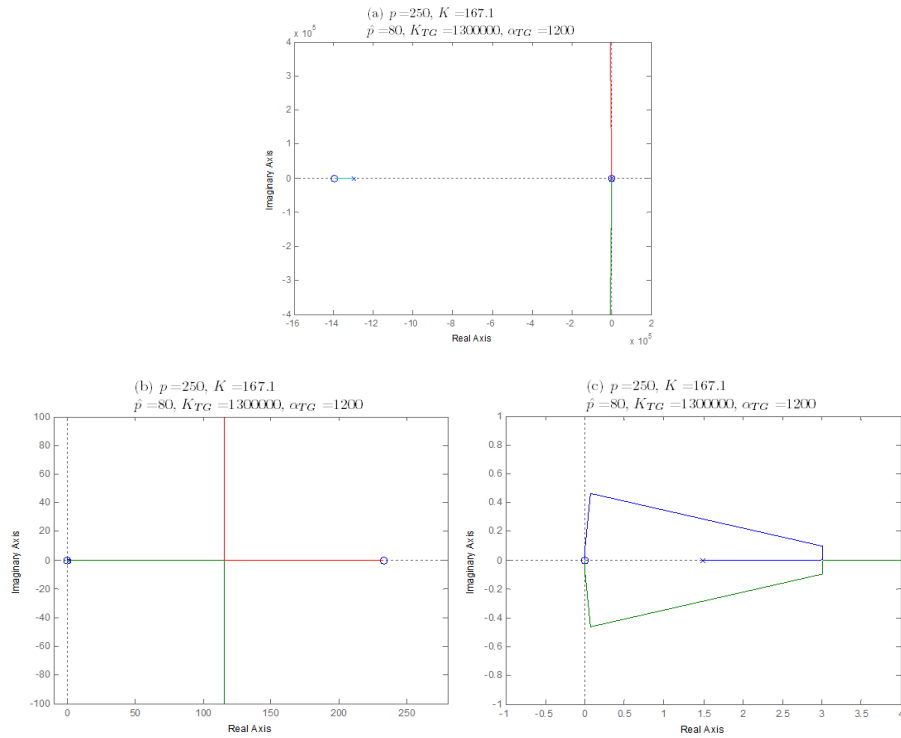


Figure 6.107 a. The root locus for K_1 parameter when $\alpha_{TG} = 1200$, b.-c. Zoomed in root locus visualizing the portion of the diagram around the break-in/away point.

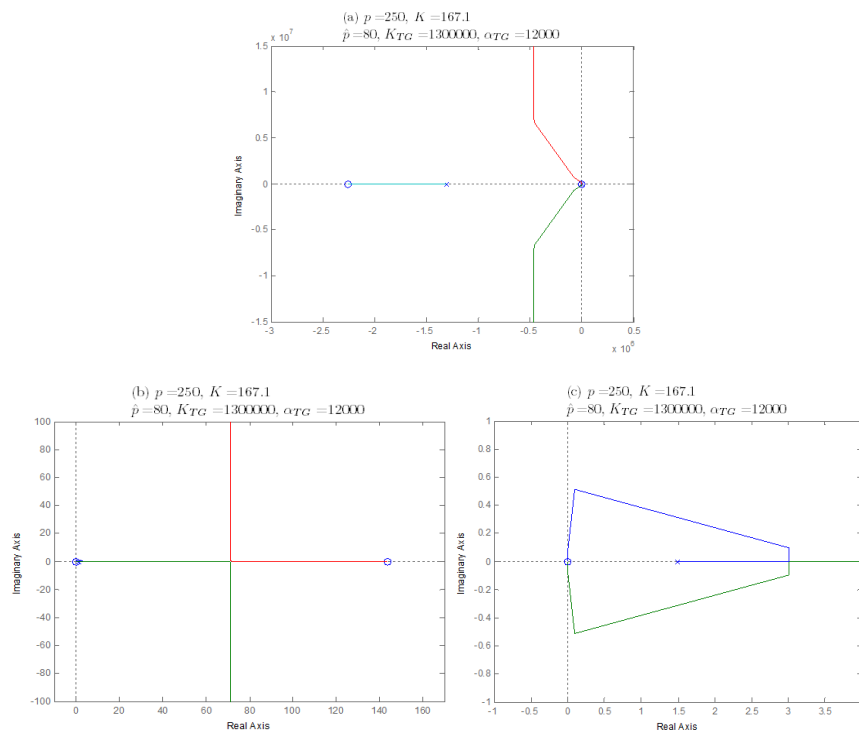


Figure 6.108 a. The root locus for K_1 parameter when $\alpha_{TG} = 12000$, b.-c. Zoomed in root locus visualizing the portion of the diagram around the break-in/away point.

Table 6.17 The upper and lower limits of K_1 parameter for different α_{TG} values

α_{TG}	K_1^l	K_1^u
1.2	0.0106	0.113
12	0.0106	0.113
120	0.0106	0.113
1200	0.0113	0.113
12000	0.0183	0.115

Similar to K_{TG} parameter, the upper limit of bistability region of K parameter changes in a small amount when α_{TG} gets larger values. But this time, the lower limit increases.

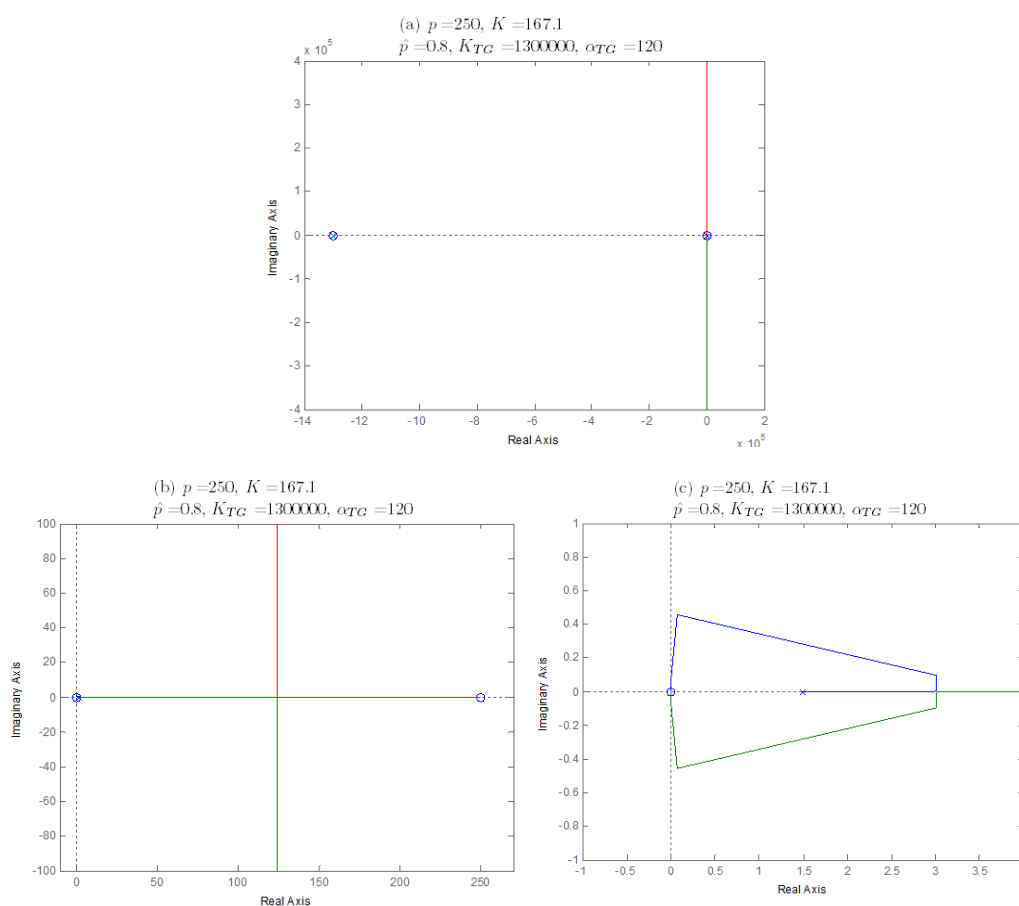


Figure 6.109 a. The root locus of K_1 parameter when $\hat{p} = 0.8$ in Michaelis-Menten kinetics, b.-c. Zoomed in root locus visualizing the portion of the diagram around the break-in/away point.

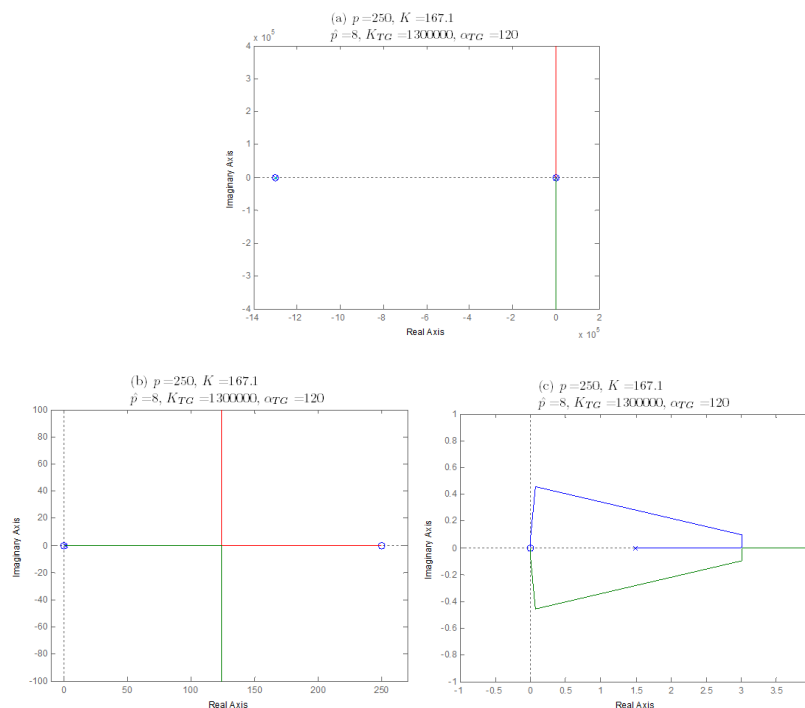


Figure 6.110 a. The root locus of K_1 parameter when $\hat{p} = 8$ in Michaelis-Menten kinetics, b.-c. Zoomed in root locus visualizing the portion of the diagram around the break-in/away point.

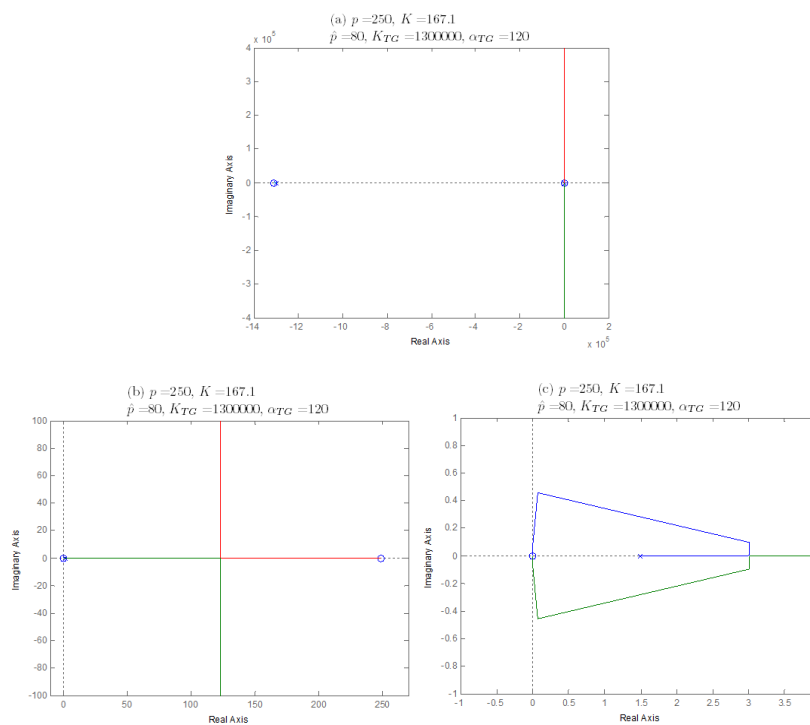


Figure 6.111 a. The root locus of K_1 parameter when $\hat{p} = 80$ in Michaelis-Menten kinetics, b.-c. Zoomed in root locus visualizing the portion of the diagram around the break-in/away point.

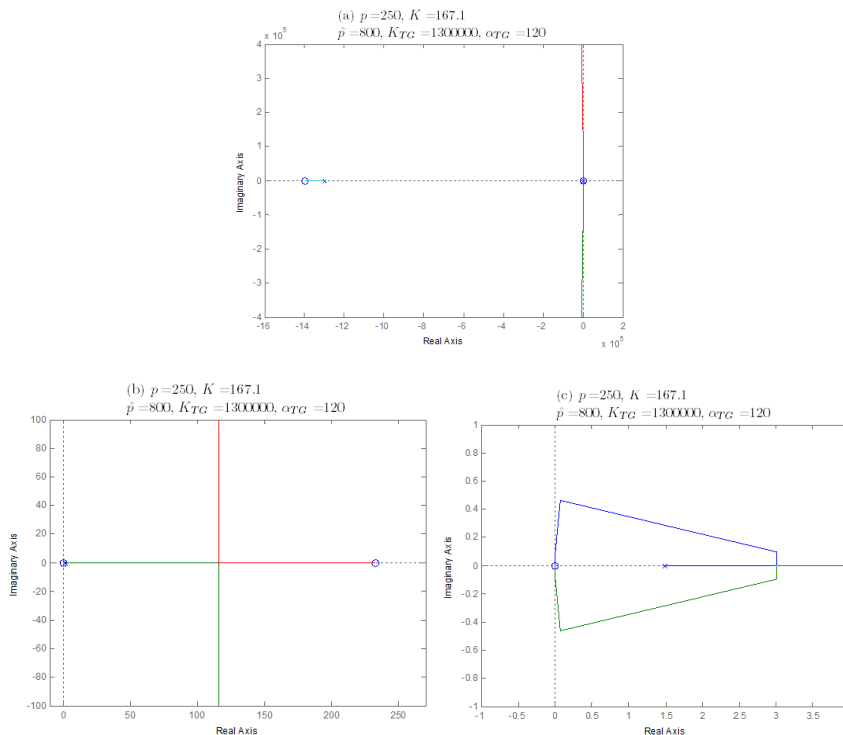


Figure 6.112 a. The root locus of K_1 parameter when $\hat{p} = 800$ in Michaelis-Menten kinetics, b.-c. Zoomed in root locus visualizing the portion of the diagram around the break-in/away point.

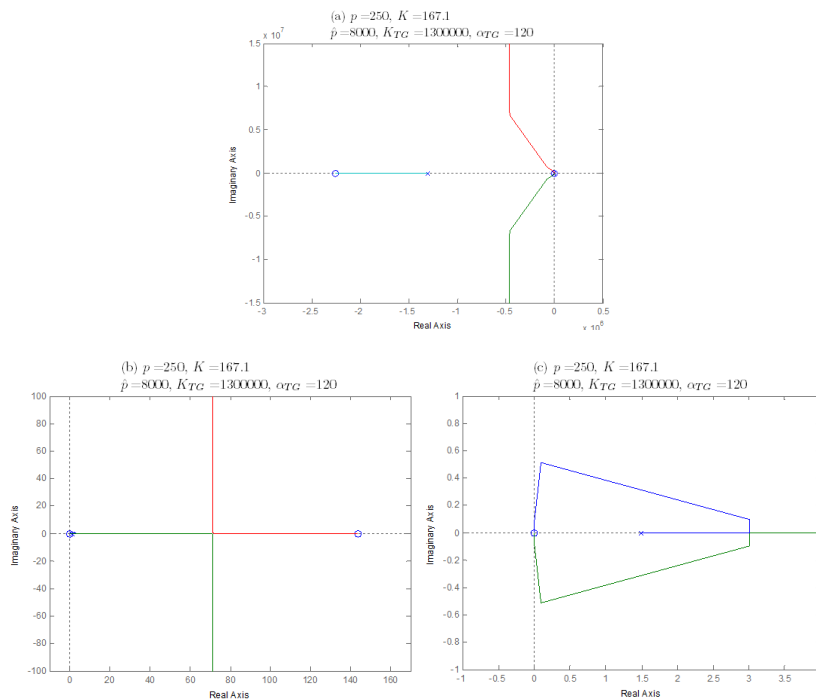


Figure 6.113 a. The root locus of K_1 parameter when $\hat{p} = 8000$ in Michaelis-Menten kinetics, b.-c. Zoomed in root locus visualizing the portion of the diagram around the break-in/away point.

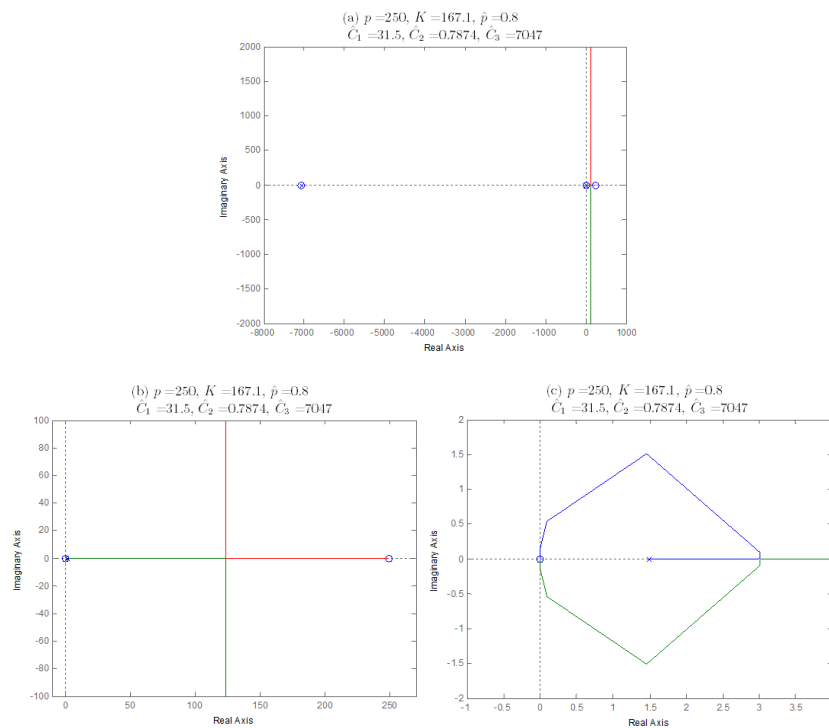


Figure 6.114 a. The root locus of K_1 parameter when $\hat{p} = 0.8$ in bi-bi ordered kinetics, b.-c. Zoomed in root locus visualizing the portion of the diagram around the break-in/away point.

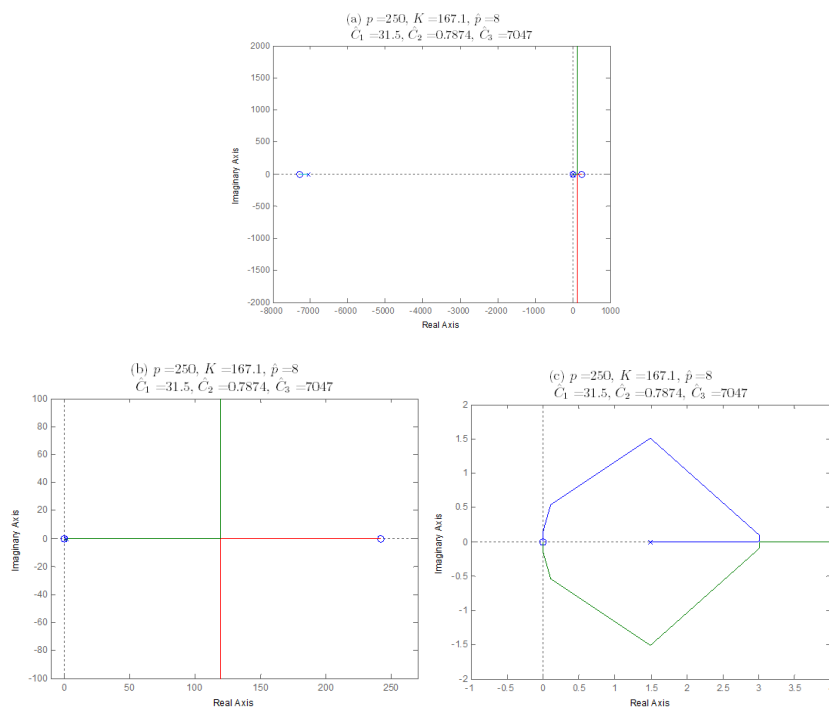


Figure 6.115 a. The root locus of K_1 parameter when $\hat{p} = 8$ in bi-bi ordered kinetics, b.-c. Zoomed in root locus visualizing the portion of the diagram around the break-in/away point.

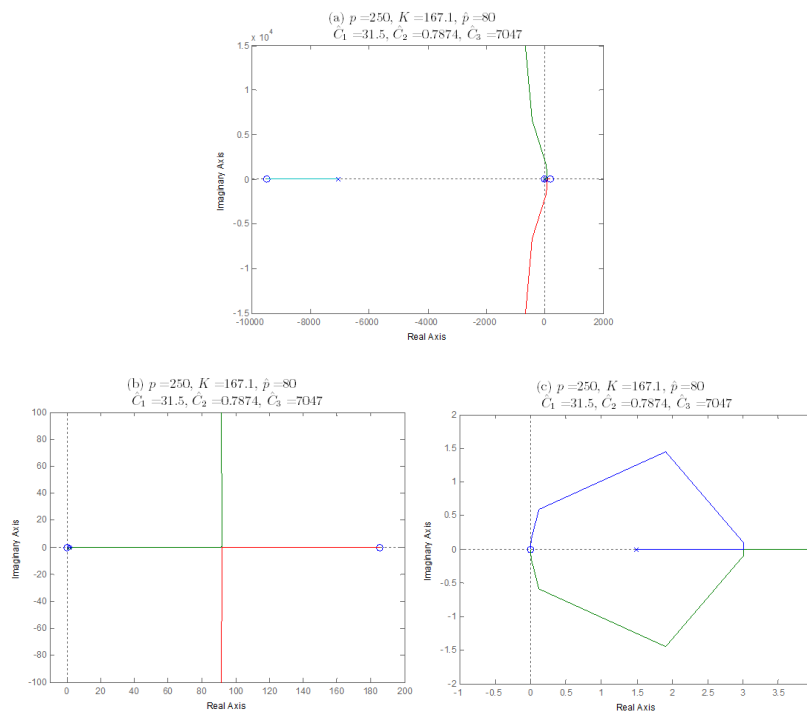


Figure 6.116 a. The root locus of K_1 parameter when $\hat{p} = 80$ in bi-bi ordered kinetics, b.-c. Zoomed in root locus visualizing the portion of the diagram around the break-in/away point.

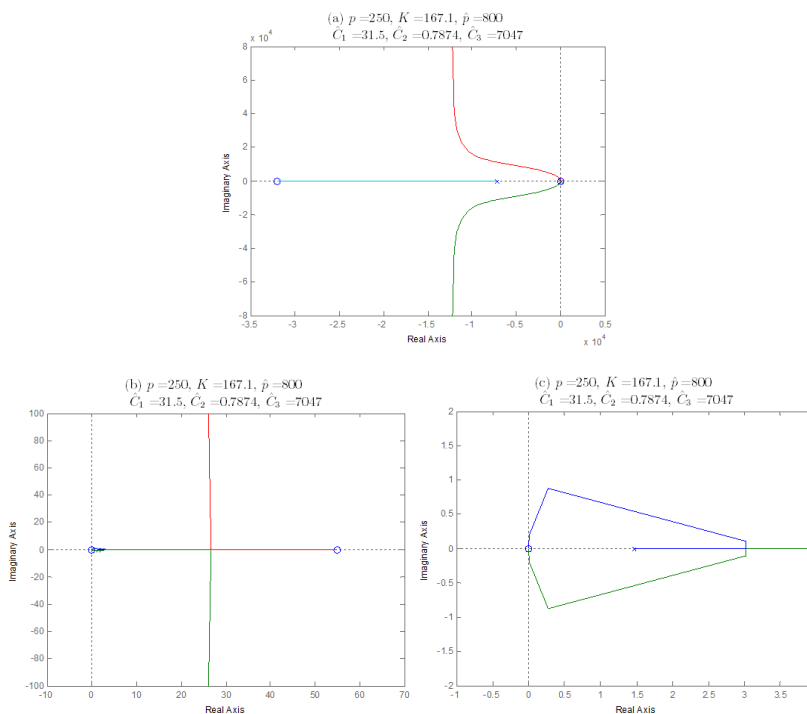


Figure 6.117 a. The root locus of K_1 parameter when $\hat{p} = 800$ in bi-bi ordered kinetics, b.-c. Zoomed in root locus visualizing the portion of the diagram around the break-in/away point.

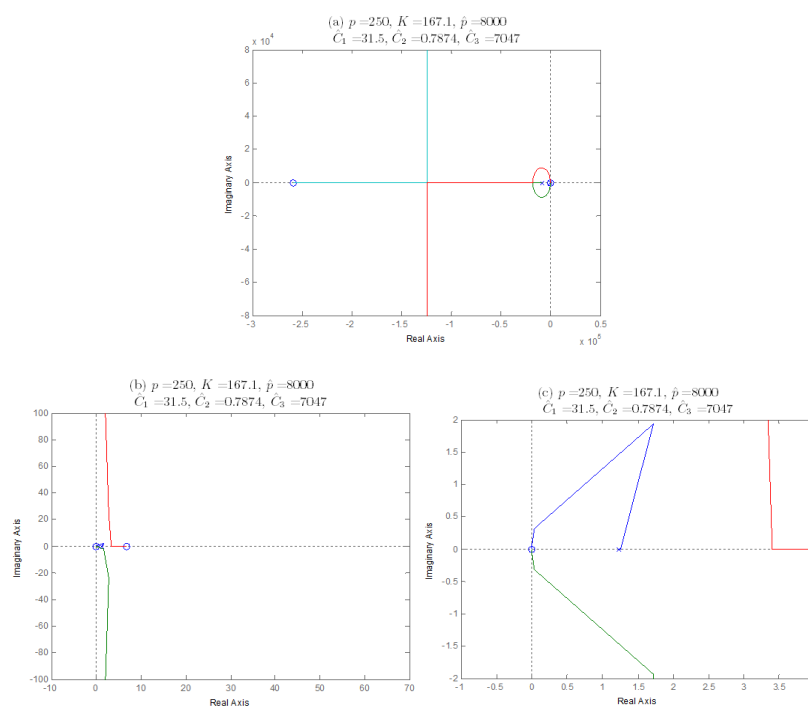


Figure 6.118 a. The root locus of K_1 parameter when $\hat{p} = 8000$ bi-bi ordered kinetics, b.-c. Zoomed in root locus visualizing the portion of the diagram around the break-in/away point.

Table 6.18 The upper and lower limits of K_1 parameter for different \hat{p} values

\hat{p}	Michaelis-Menten		Bi-Bi ordered	
	K_1^l	K_1^u	K_1^l	K_1^u
0.8	0.0106	0.113	0.0106	0.113
8	0.0106	0.113	0.109	0.113
80	0.0106	0.113	0.0143	0.114
800	0.0113	0.113	0.0471	0.123
8000	0.0183	0.115	No	No

Both the upper and lower limits of the K parameter in Michaelis-Menten kinetics increase slower than in bi-bi ordered kinetics.

The result for $p - K - K_1$ parameters are given in Table 6.19.

Table 6.19 The bistability region changes of $p - K - K_1$ parameters

New model Parameters (increase)	K		p		K_1	
	K^l	K^u	p^l	p^u	K_1^u	K_1^u
\widehat{C}_1	Small decrease	Decrease	Increase	Increase	Increase	Small increase
\widehat{C}_2	Constant	Constant	Constant	Constant	Constant	Constant
\widehat{C}_3	Small increase	Increase	Decrease	Decrease	Decrease	Small Decrease
K_{TG}	Constant	Increase	Decrease	Constant	Decrease	Constant
α_{TG}	Constant	Decrease	Increase	Constant	Increase	Constant
\hat{p}	Constant	Decrease	Increase	Constant	Increase	Constant
	Small Decrease	Decrease	Increase	Increase	Increase	Increase

The new parameters cause the same type of changes on the lower and upper limits of the bistability region of p and K_1 parameters and these new parameters have adverse effects on K parameter.

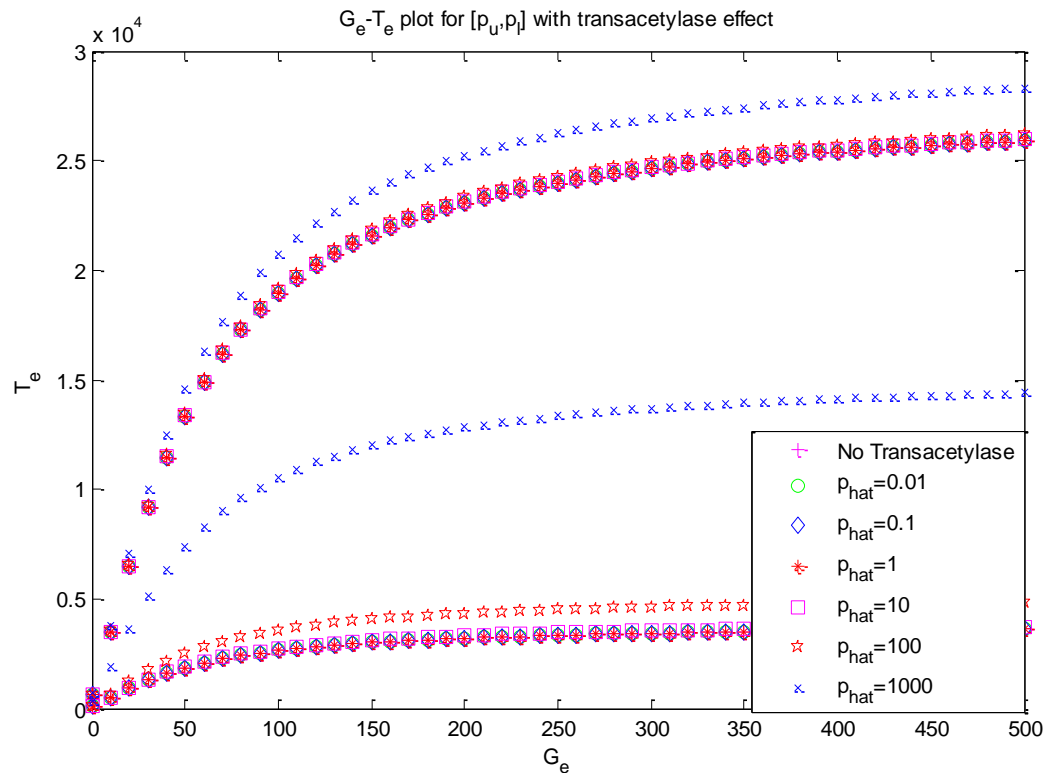
6.3 Interpretation of the Bistability Interval for p with Transacetylase Effect

The evaluations of the change in the bistability range of parameters are made in root locus based bistability analysis parts. The bistability region in the $G_e - T_e$ space is identified by determining the limits T_e^l and T_e^u corresponding to the p^l and p^u limits to determine the changes in the bistability region given in $G_e - T_e$ space. The upper and lower limits of p parameter are calculated for five different multiples of \hat{p} . The calculated values of p parameter are shown in Table 6.20.

Table 6.20 The bistability region for p parameter with different \hat{p} parameter values.

\hat{p}	Bi-bi ordered Kinetics		Michaelis- Menten Kinetics	
	p^l	p^u	p^l	p^u
0.01	182	594	182	594
0.1	182	594	182	594
1	182	594	182	594
10	186	595	182	594
100	218	598	183	594
1000	418	627	190	595

Again, the $G_e - T_e$ plot obtained by using Equations (82)-(83) is drawn in Figure 6.119 and Figure 6.120 (Özbudak et al., 2004; Yıldırım et al., 2004).

Figure 6.119 The bistability region in $G_e - T_e$ space for bi-bi ordered kinetics.

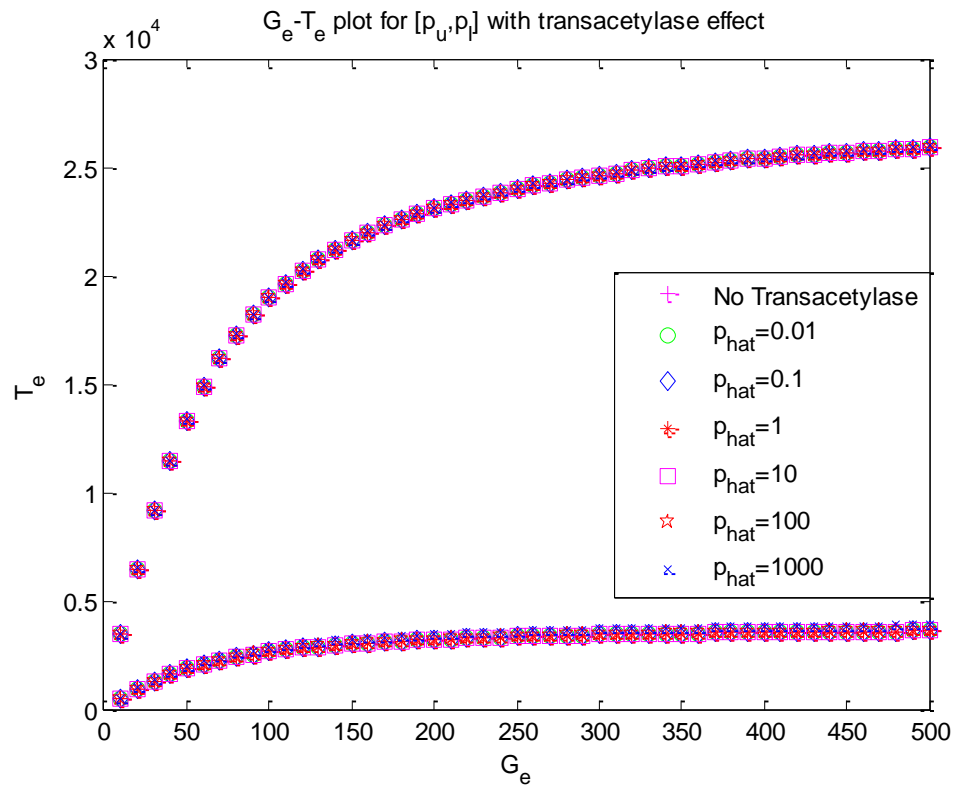


Figure 6.120 The bistability region in $G_e - T_e$ space for Michaelis-Menten kinetics.

CHAPTER SEVEN

CONCLUSION

This thesis presents theoretical and numerical results on the analysis of bistable behavior of TMG induced lac operon with ignoring and also with taking into account the transacetylase effect. Two methods, one is based on discriminant and the other is based on a well known control theoretical tool, i.e. the root locus, are introduced in the thesis for determining the bistability regions in the space of model parameters.

In addition to the bistability analysis, the boundedness of the state variables and local stability of the equilibria are studied in the thesis only for the lac operon model with no GAT effect. These two analyses can be said to be valid also for the second model considering transacetylase effect since the second model is also derived based on the enzyme kinetics by employing Hill and Micheales-Menten approaches and the application of the analyses are straightforward.

The discriminant and root locus based bistability analyses for the lac operon model with no transacetylase effect are performed in algebraic, graphical, and numerical ways all supporting to each other. It is observed along the studies that the algebraic and graphical methods may get stuck for models possessing high order polynomial equilibrium equations. It is also concluded that the developed root locus based method provides an efficient numerical tool for any kind and arbitrary order of gene regulatory and metabolic networks model when it is defined in a state equation form with rational right hand sides as in the models derived based on enzyme kinetics employing Hill and Michealis-Menten approaches.

The developed discriminant and root locus based methods for the parametric equilibrium analysis of the lac operon models provide also a solution to the problem of analysis of the gene regulatory network models under parameter uncertainties. The determined bistability ranges for the lac operon model parameters may be helpful for understanding the variations in the appearance of the bistable behavior of the biological lac operon which is observed to show differences from one species to

another and even from one experiment to another. The determined bistability ranges may also lead to derive new efficient feedback and/or optimal control methods for the regulation of the behavior of lac operon while optimizing some performance measure.

REFERENCES

- Avcu, N., Demir, G. K., Pekergin, F., Alyürük, H., Çavaş, L., & Güzeliş, C. (2012). TMG uyarımlı bir lak operon modeli için sınırlılık ve yerel kararlılık analizi. *In Proc. Eleco2012 Elektrik-Elektronik ve Bilgisayar Mühendisliği Sempozyumu*, 420-425
- Batt, G., Belta, C., & Weiss, R. (2008). Temporal logic analysis of gene networks under parameter uncertainty. *IEEE Trans. Automatic Control, Special issue on Systems Biology*, 53, 215-229.
- Cohn, M., & Horibata, K. (1959). Analysis of the differentiation and of the heterogeneity within a population of *Escherichia coli* undergoing induced B galactosidase synthesis. *J. Bacteriol.*, 78, 613-623.
- Danchin, A. (2009). Cells need safety valves. *Bioessays*, 31(7), 769-773.
- de Jong, H. (2002). Modeling and simulation of genetic regulatory systems: A literature review. *Journal of Computational Biology*, 9(1), 67-103.
- de Jong, H., Geiselman, J., Hernandez, C., & Page, M. (2003). Genetic network analyzer: Qualitative simulation of genetic regulatory networks. *Bioinformatics*, 19(3), 336-344.
- de Jong, H., Gouze, J. L., Hernandez, C., Page, M., Sari, T., & Geiselman, J. (2004). Qualitative simulation of genetic regulatory networks using piecewise-linear models. *Bull. Math. Biol.*, 66(2), 301-340.
- Fell, A. (1992). Metabolic control analysis: A survey of its theoretical and experimental development. *Biochemistry J.*, 286, 313-330.
- Jacob, F., Perrin, D., Sanchez, C., & Monod, J. (1960). L'operon: groupe de gene a expression par un operateur. *C. R. Acad. Sci.*, 250, 1727-1729.

- Julius, A., Halasz, A., Sakar, S., Harvey, R., & Pappas, G. J. (2008). Stochastic modeling and control of biological systems: The lactose regulation system of *E. coli*. *IEEE Trans. Auto. Cont.*, 51-65.
- Kitano, H. (2004). Cancer as a robust system: Implications for anticancer therapy. *Nature Reviews Cancer*, 4, 227–235.
- Kitano, H. (2007). A robustness-based approach to systems-oriented drug design. *Nature Reviews Drug Discovery*, 6, 202-210.
- Murray, J. D. (2002). *Mathematical Biology: I An Introduction and II Spatial Models and Biomedical Applications*. (3rd ed.), NY: Springer.
- Musso, R. E., & Zabin, I. (1973). Substrate specificity and kinetic studies on thiogalactoside transacetylase. *Biochemistry*, 12, 553-557.
- Novick, A., & Wiener, M. (1957). Enzyme induction as an all-or-none phenomenon. *Proc. Natl. Acad. Sci.*, 43, 553-566.
- Özbudak, M., Thattai, M., Lim, H. N., Shraiman, B. I., & Van Oudenaarden, A. (2004). Multistability in the lactose utilization network of *Escherichia coli*. *Nature*, 427, 737-740.
- Ropers, D., de Jong, H., Page, M., Schneider, D., Geiselmann, J. (2006). Qualitative simulation of the carbon starvation response in *Escherichia coli*. *BioSystems*, 84, 124–152.
- Santillan, M., & Mackey, M. C. (2004). Influence of catabolite repression and inducer exclusion on the bistable behavior of the lac operon. *Biophysical Journal*, 86, 1282-1292.
- Santillan, M., Mackey, M. C., & Zeron, E. S. (2007). Origin of bistability in the lac operon. *Biophys. J.*, 92, 3830-3842.

- Santillan, M. & Mackey, M. C. (2008). Quantitative approach to the study of bistability in the lac operon of *Escherichia coli*. *Journal of the Royal Society*, 5, 29-39
- Van Hoek, M. J., & Hogeweg P. (2006). In silico evolved lac operons exhibit bistability for artificial inducers, but not for lactose. *Biophys. J.*, 91, 2833-2843.
- Vidyasagar, M. (1972). *Nonlinear System Analysis*. New Jersey: Prentice Hall.
- Wong, P., Gladney, S., & Keasling, J. D. (1997). Mathematical model of the lac operon: Inducer exclusion, catabolite repression, and diauxic growth on glucose and lactose. *Biotechnol. Prog.*, 13, 132-143.
- Yagil, G., & Yagil, E. (1971). On the relation between effector concentration and the rate of induced enzyme synthesis. *Biophys. J.*, 11, 11-27.
- Yıldırım, N., & Mackey, M. C. (2003). Feedback regulation in the lactose operon: A mathematical modeling study and comparison with experimental data. *Biophysical Journal*, 84, 2841-2851.
- Yıldırım, N., Santillan, M., Horike D., & Mackey M. C. (2004). Dynamics and bistability in a reduced model of the lac operon. *Chaos*, 4(2), 279-92.